AD-A087 480 DUKE UNIV DURHAM NC DEPT OF PHYSICS F/G 7/4
MICROWAVE INVESTIGATIONS OF MATTER.(U)
JUN 80 F C DE LUCIA DAAG29-77-G-0007
UNCLASSIFIED ARO-14150.7-P NL

| OF |
AD-
A087480

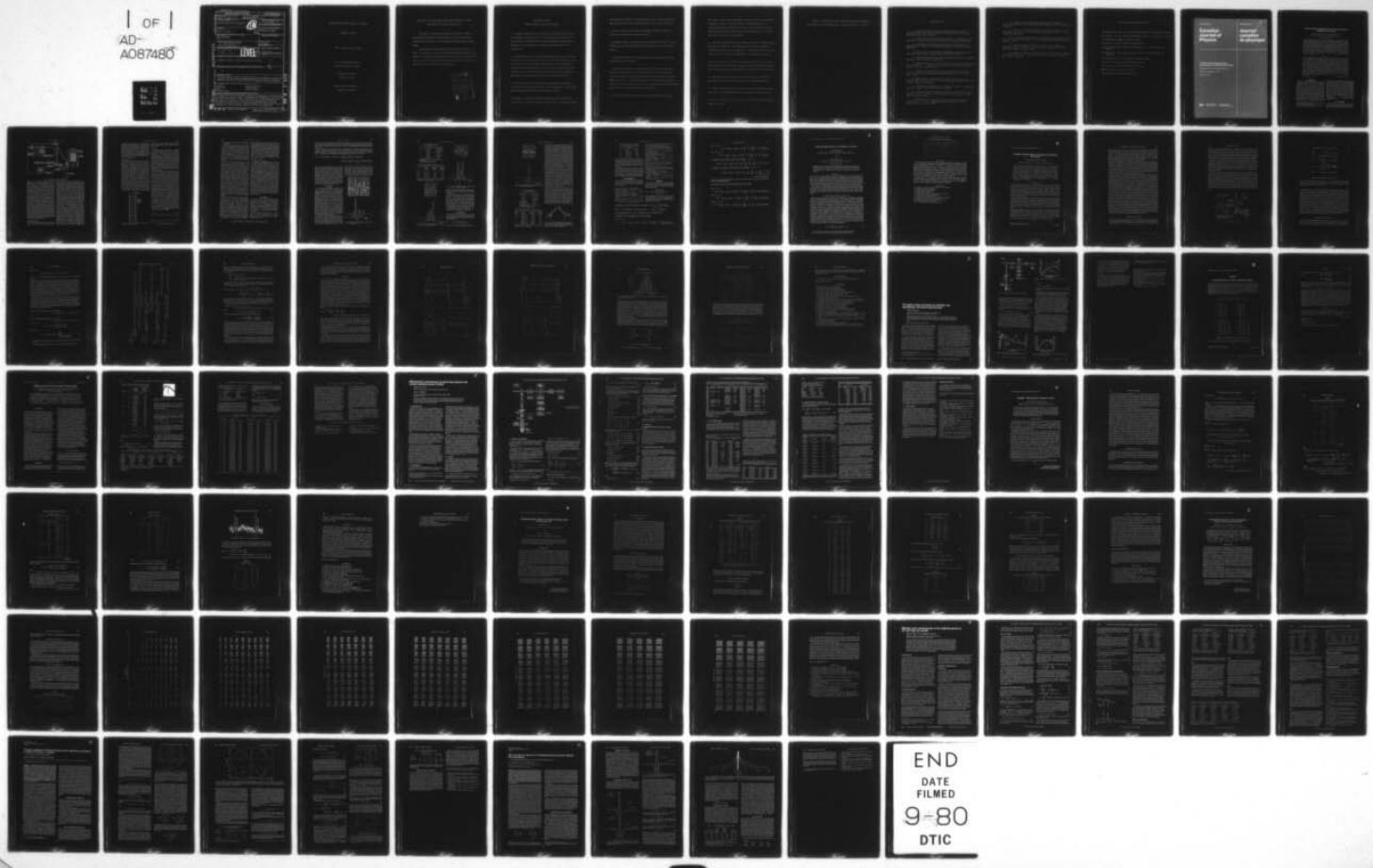

END
DATE
FILMED
9-80
DTIC

UNCLASSIFIED

SECURITY CLASSIFICATION OF THIS PAGE (When Data Entered)

REPORT DOCUMENTATION PAGE

READ INSTRUCTIONS BEFORE COMPLETING FORM

1. REPORT NUMBER: 14150.7-P	2. GOVT ACCESSION NO.: AD-A087480
3. RECIPIENT'S CATALOG NUMBER:	
4. TITLE (and Subtitle): MICROWAVE INVESTIGATIONS OF MATTER.	5. TYPE OF REPORT & PERIOD COVERED: Final Report: 15 Oct 76 — 30 Nov 79
	6. PERFORMING ORG. REPORT NUMBER:
7. AUTHOR(s): Frank C. De Lucia	8. CONTRACT OR GRANT NUMBER(s): DAAG29-77-G-0007
9. PERFORMING ORGANIZATION NAME AND ADDRESS: Duke University, Durham, NC 27706	10. PROGRAM ELEMENT, PROJECT, TASK AREA & WORK UNIT NUMBERS:
11. CONTROLLING OFFICE NAME AND ADDRESS: U. S. Army Research Office, Post Office Box 12211, Research Triangle Park, NC 27709	12. REPORT DATE: Jun 80
	13. NUMBER OF PAGES:
14. MONITORING AGENCY NAME & ADDRESS (if different from Controlling Office): 93	15. SECURITY CLASS. (of this report): Unclassified
	15a. DECLASSIFICATION/DOWNGRADING SCHEDULE:

LEVEL II

16. DISTRIBUTION STATEMENT (of this Report)

Approved for public release; distribution unlimited.

17. DISTRIBUTION STATEMENT (of the abstract entered in Block 20, if different from Report)

NA

18. SUPPLEMENTARY NOTES

The view, opinions, and/or findings contained in this report are those of the author(s) and should not be construed as an official Department of the Army position, policy, or decision, unless so designated by other documentation.

19. KEY WORDS (Continue on reverse side if necessary and identify by block number)

microwaves
spectroscopy
masers
millimeter waves
submillimeter waves
silicon oxides
molecular lasers

20. ABSTRACT (Continue on reverse side if necessary and identify by block number)

The project "Microwave Investigations of Matter" represented a broad attack on a wide variety of scientific topics and technological developments in the millimeter and submillimeter spectral region. Attached are the journal publications and a brief summary of our work. In addition to the cited journal publications, approximately an equal number of invited and contributed papers have been presented at scientific meetings. Because the material in these talks is highly correlated with journal articles, they will not be listed separately.

DD FORM 1 JAN 73 1473 EDITION OF 1 NOV 65 IS OBSOLETE

UNCLASSIFIED 118245

MICROWAVE INVESTIGATIONS OF MATTER

Frank C. De Lucia

Oct. 15, 1976 to Oct. 15, 1979

U. S. Army Research Office

Grant No. DAAG 29 77 G 0007

Department of Physics

Duke University

SUMMARY OF WORK UNDER ARO GRANT DAAG 29 77 G 0007

15 October 1976 through 15 October 1979

The project, "Microwave Investigations of Matter", 14150-P, represented a broad attack on a wide variety of scientific topics and technological developments in the millimeter and submillimeter spectral region.

Attached are the journal publications and a brief summary of our work. In addition to the cited journal publications, approximately an equal number of invited and contributed papers have been presented at scientific meetings. Because the material in these talks is highly correlated with the journal articles, they will not be listed separately.

Summary of Results

(keyed according to list of publications)

1. This paper represents the first operation of a molecular beam maser in the submillimeter spectral region. The extremely high resolution of this device makes it an especially powerful spectroscopic tool and presents the possibility of the construction of a primary frequency standard in the submillimeter.

2. This paper reports the first pressure broadening study on H_2S. Because of a paucity (none) of transitions at conventional microwave frequencies, this important species had not been previously studied. More importantly our theoretical calculations (Anderson theory) show that the theory was in fact generally valid (to $\sim$ 10%) and that previous inconsistencies ($\sim$ 100%) were due to inaccurate infrared data rather than theoretical shortcomings.

3. This paper reports the first observation of symmetric top forbidden transitions in the NMMW spectral region. The results lead to a substantially improved knowledge of the energy level structure of PH_3

4. This paper demonstrates the power of millimeter and submillimeter spectroscopy as a diagnostic probe of molecular lasers. Several conventional

wisdoms about the HCN laser were shown to be untrue. This project and its spin offs will become a major part of our effort in the next contract period.

5. This is a short note that relates centrifugal distortions to changes in molecular constants and is a spin off of paper 1.

6. This paper reports the results of a high temperature ($\sim 1500^{\circ}C$) study of SiO and represents the first laboratory observation of one of the interstellar masers.

7. This is an invited review of the applications and techniques of millimeter and submillimeter spectroscopy.

8. Molecular laser plasmas are rich sources of excited vibrational states. This paper reports the use of the HCN laser plasma as a source for these excited state studies. An interesting symbiosis between this project and that reported in 4) exists. So little is known about the excited states of molecules in the millimeter and submillimeter that one ordinarily must do the spectroscopic project first so that you know what you are diagnosing.

9. This paper represents an extension of the work reported in 3 to AsH_3.

10. Because of its extreme centrifugal distortion, water is the most difficult $^1\Sigma$ molecule to model. This paper reports a combined analysis of our millimeter and submillimeter microwave data, new FIR Fourier transform data, and energy levels derived from IR combination differences to upgrade the energy levels of AFGL spectral table.

11. This paper reports the results of an extensive project to model the HNO_3 spectrum from 0-300 GHz. The primary result is a model that predicts $\sim$ 5000 transitions in this region $\leq$ 1 MHz. I understand that this work is of some interest to BMD for their modeling of the "disturbed" atmosphere.

12. This work has been the subject of two papers delivered at the Columbus Meeting and is being finalized for inclusion in a thesis and journal publication. Again, I understand that this work (especially HO_2) relates to BMD interests.

13. This is a spectroscopic project on the millimeter and submillimeter spectrum of the extremely reactive and unstable mixed diatomic halides.

14. This is a paper that reports an interesting and potentially very valuable approach to the theoretical modeling of the absorptions of hot water vapor.

15. and 16. These papers represent the last papers from Professor Gordy's biophysics program.

With the exception of 12. (which has shared support with NASA) the work reported here was supported by no other federal agency than ARO.

Publication List

1. "Extension of High-resolution Beam Maser Spectroscopy into the Submillimeter Wave Region," Michael Garvey and Frank C. De Lucia, Canadian J. Phys. 55, 1115 (1977).

2. "Pressure Broadening of Hydrogen Sulfide," Paul Helminger and Frank C. De Lucia, J. Quant. Spectrosc. Radiat. Transfer 17, 751 (1977).

3. "'Forbidden' Rotational Spectra of Symmetric-top Molecules: PH_3 and PD_3," David A. Helms and Walter Gordy, J. Mol. Spectrosc. 66, 206 (1977).

4. "The Study of Laser Processes by Millimeter and Submillimeter Microwave Spectroscopy," Applied Physics Letter 31, 606 (1977).

5. "Centrifugal Distortion in Water and Hydrogen Sulfide," R. Michael Garvey, J. Mol. Spectrosc. 65, 330 (1977).

6. "Millimeter Spectrum and Molecular Constants of Silicon Monoxide," E. Lowry Manson, Jr., William W. Clark, Frank C. De Lucia, and Walter Gordy, Phys. Rev. A 15, 223 (1977).

7. "Millimeter and Submillimeter-wave Spectroscopy," Frank C. De Lucia in Molecular Spectroscopy: Modern Research, Vol. II, Academic Press (1976).

8. "Millimeterwave Spectroscopy of Active Laser Plasmas: The Excited Vibrational States of HCN," Paul A. Helminger and Frank C. De Lucia, J. Chem. Phys. 67, 4262 (1977).

9. "'Forbidden' Millimeter-wave Transitions in Arsine," David Helms and Walter Gordy, J. Mol. Spectrosc. 69, 473 (1978).

10. "Centrifugal Distortion Analysis of the Ground Vibrational States of $H_2{}^{17}O$ and $H_2{}^{18}O$," Paul A. Helminger and Frank C. De Lucia, J. Mol. Spectrosc. 70, 263 (1978).

11. "Millimeter-wave Spectrum, Centrifugal Distortion Analysis, and Energy Levels of HNO_3," Gabriele Cazzoli and Frank C. De Lucia, J. Mol. Spectrosc. 76, 131 (1979).

12. "Millimeter-wave Studies of Unstable Molecular Species," Arthur Charo and Frank C. De Lucia (presented in part at the 1977 Ohio State Symposium).

13. "Millimeter Wave Measurements of the Rotational Spectra of ClF, BrF, BrCl, ICl, and IBr," Robert E. Willis and William W. Clark, J. Chem. Physics 72, 4946 (1980).

14. "A Modified Centrifugal Distortion Hamiltonian for Light Asymmetric Rotors," John Kolena and Frank C. De Lucia (presented at AAS San Francisco, January, 1980).

15. "Nuclear Coupling of ^{33}S and the Nature of Free Radicals in Irradiated Crystals of N-Acetyl-L-Cysteine," J. H. Hadley and W. Gordy, Proc. Natl. Acad. Sci. 74, 216 (1977).

16. "Electron Spin Resonance of ^{17}O-labeled Protein-Peroxide Radicals: Zein and Edestin," Louis J. Dimmey and Walter Gordy, Proc. Natl. Acad. Sci. USA 77, 343 (1980).

Participating Scientific Personnel

(1) Walter Gordy, James B. Duke Professor of Physics: Principal Investigator

(2) Frank C. De Lucia, Associate Professor of Physics: Co-principal Investigator

(3) John Kolena, Visiting Assistant Professor

(4) Paul A. Helminger, Senior Visiting Scientist

(5) R. Michael Garvey, Research Assistant, Ph. D. , Instructor/Research Associate

(6) William W. Clark, Research Assistant, Ph. D. , Instructor/Research Associate

(7) Gabriele Cazzoli , Nato Senior Postdoctoral Fellow

(8) David A. Helms, Research Assistant, Ph. D.

(9) Robert E. Willis, Research Assistant, Ph. D.

(10) Arthur Charo, Research Assistant

(11) William Matteson, Research Assistant

Reprinted from

Canadian Journal of Physics

Réimpression du

Journal canadien de physique

Extension of high resolution beam maser spectroscopy into the submillimetre wave region

R. Michael Garvey and Frank C. De Lucia

Volume 55 • Number 12 • 1977

Pages 1115–1123

National Research Council Canada

Conseil national de recherches Canada

Extension of high resolution beam maser spectroscopy into the submillimetre wave region[1]

R. Michael Garvey[2] and Frank C. De Lucia

Department of Physics, Duke University, Durham, NC 27706, U.S.A.

Received December 20, 1976

High resolution molecular beam maser spectroscopy has been extended into the submillimetre wave region of the spectrum. The maser spectrometer consists of a multiple beam source, stacked quadrupole state selector, and Fabry–Perot cavity. The submillimetre wave stimulating signal is produced by harmonic generation from a millimetre-wave klystron, directly referenced to WWVB. The maser signal is detected in a cryogenic photodetector. Linewidths 50–100 times narrower than the Doppler width and good signal-to-noise ratios were obtained. This system has been used to resolve the small deuterium hyperfine splittings of both the $1_{10} \rightarrow 1_{01}$ transition of D_2O at 317 GHz and the $J = 1 \rightarrow 0$ transition of ND_3 at 309 GHz. The relevance of the D_2O quadrupole interaction data to the electric field gradient in water is discussed. The spectroscopic constants in kilohertz for D_2O in the states 1_{10} and 1_{01} are, respectively, $(eQq_J)_D = 34.81 \pm 0.32$, $C_D = -2.661$, and $(eQq_J)_D = -29.60 \pm 0.55$, $C_D = -2.532$. The constants for ND_3 are, in kilohertz: $(eQq_J)_N = 816.2 \pm 1.1$, $C_N = 2.0 \pm 1.5$, $(eQq_J)_D = 19.9 \pm 0.8$, and $C_D = -2.2 \pm 0.8$.

La spectroscopie à haute résolution par maser et faisceau moléculaire a été étendue à la région des longueurs d'onde inframillimétriques. Le spectromètre maser est constitué par une source à multiples faisceaux, un sélecteur d'états quadrupolaire et une cavité Fabry–Pérot. Le signal stimulant les ondes inframillimétriques est produit, par génération d'harmoniques, à partir d'un klystron fonctionnant dans la région millimétrique, avec référence directe aux signaux WWVB. Le signal maser est détecté dans un photodétecteur cryogénique. On a obtenu des raies ayant des largeurs de 50 à 100 fois inférieures à la largeur Doppler et de bonnes valeurs du rapport signal-bruit. Le système a été utilisé pour résoudre les faibles séparations de structure hyperfine du deutérium dans les deux transitions $1_{10} \rightarrow 1_{01}$ de D_2O, à 317 GHz, et $J = 1 \rightarrow 0$ de ND_3, à 309 GHz. La portée des données concernant l'interaction quadrupolaire de D_2O sur la question du gradient du champ électrique dans l'eau est discutée. Les valeurs en kilohertz des constantes spectroscopiques de D_2O, pour les états 1_{10} et 1_{01}, sont respectivement $(eQq_J)_D = 34.81 \pm 0.32$, $C_D = -2.661$ et $(eQq_J)_D = -29.60 \pm 0.55$, $C_D = -2.532$. Les constantes pour ND_3 sont, en kilohertz: $(eQq_J)_N = 816.2 \pm 1.1$, $C_N = 2.0 \pm 1.5$, $(eQq_J)_D = 19.9 \pm 0.8$ et $C_D = -2.2 \pm 0.8$.

[Traduit par le journal]

Can. J. Phys., 55, 1115 (1977)

I. Introduction

Molecular beam maser spectroscopy was first reported by Gordon (1955) in the centimetre microwave region and the high resolution capabilities of this technique have now been used to study numerous molecular species in this spectral region. A number of proposals have been made to extend beam maser spectroscopy into the submillimetre wavelength region and beam absorption spectroscopy has been reported in this region by van Dijk and Dymanus (1970). These proposals have been motivated by the general desire to extend the capabilities of these devices as well as by the need for studies of specific transitions. For many of the fundamental and interesting molecules, these submillimetre transitions are either the only ones available or are more advantageous to study than the higher J transitions which fall at longer wavelengths. Low J transitions exhibit the largest hyperfine splittings and are least affected by centrifugal distortion. In this paper we report the extension of high resolution molecular beam maser spectroscopy into the submillimetre region and the study of the $J = 1 \rightarrow 0$ transition of ND_3 at 309 GHz and the $1_{10} \rightarrow 1_{01}$ transition of D_2O at 317 GHz.

II. Experimental

Numerous articles which describe centimetre wave molecular beam maser spectrometers have appeared in the literature (Gordon *et al.* 1955;

[1]This work supported by the U.S. Army Research Office, Grant DAAG29-77-G-0007.

[2]Present address: National Bureau of Standards, 325 Broadway, Boulder, CO 80302, U.S.A.

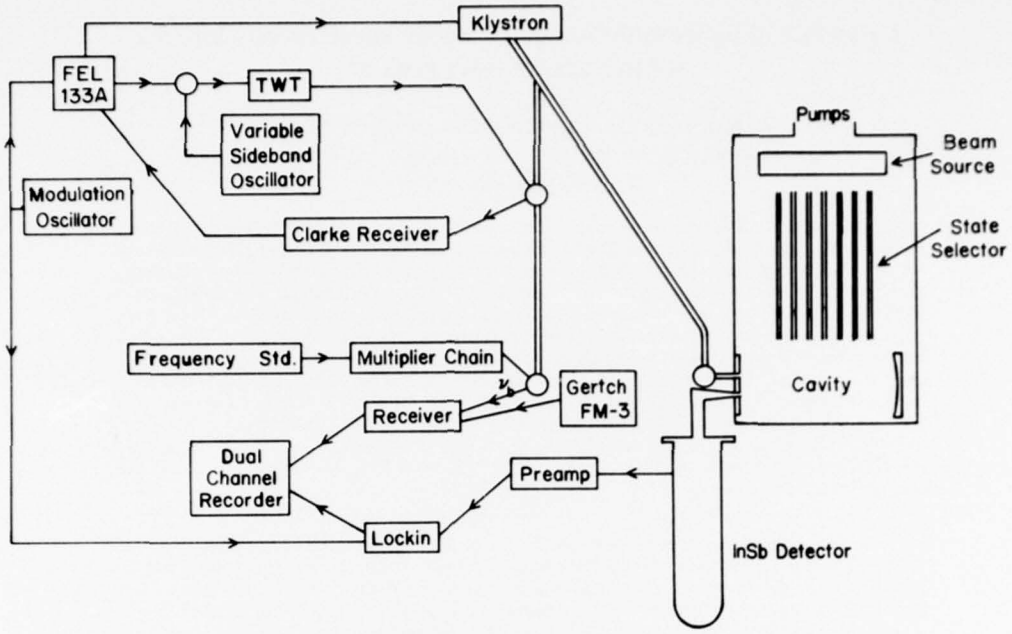

FIG. 1. Submillimetre beam maser spectrometer.

Thaddeus *et al.* 1964). In addition, molecular beam masers for 88 GHz (Marcuse 1961), 72 GHz (Krupnov *et al.* 1964), and various frequencies between 50 and 200 GHz (De Lucia and Gordy 1969; De Lucia and Cederberg 1971; Garvey and De Lucia 1974; Garvey *et al.* 1976) have been described. Because of the difference in wavelength between the more common centimetre wave devices and the one described here, a simple scaling down of dimensions is not a satisfactory design approach. The operation of a molecular beam maser may be divided as follows: (*1*) beam formation, (*2*) state selection, (*3*) microwave cavity, (*4*) generation and detection of submillimetre-wave energy, (*5*) frequency measurement. Figure 1 shows a diagram of the experimental apparatus. Multiple molecular beams are formed in the beam source, pass through a stacked quadrupole electrostatic state selector, and interact with the microwave field of a tunable Fabry–Perot cavity. The microwave field in this cavity is produced by harmonic generation from a millimetre wave klystron. The maser output signal is detected by a helium temperature (1.6 K) InSb photoconducting detector.

A. Beam Formation

Molecular beam masers have ordinarily used effusive beam sources. Kantrowitz and Grey (1951) proposed the use of supersonic jets to obtain beams with greater forward directivity and intensity. Until recently these sources have not been used in beam masers. These supersonic nozzles produce increased forward beam intensities compared to effusive sources, but for beam spectroscopy the greatest gains result from the cooling effects of the supersonic expansion (Dyke *et al.* 1972). Rotational cooling results in partition functions which are substantially smaller than can be obtained in a bulk gas sample before condensation. The increase in population which results is largest for low J transitions. This is fortuitous because of the previously discussed spectroscopic advantages of low J transitions.

Because of the large frontal area of Fabry–Perot cavities, it is advantageous to employ multiple beams to increase the filling factor of the cavity. We have used a seven by nine array of nozzles, each beam having its own electrostatic quadrupole state selector. Collimation of each beam is accomplished by an arrangement of cryogenically cooled channels. It has been found that the complex and precise nozzle geometries originally used in studies of supersonic jet phenomena may be replaced by small holes in a thin metal sheet. To take full advantage of the nozzle source, it is desirable to expand the molecules into the maser vacuum chamber from

as high a source pressure as is feasible. Ultimately, the gas load presented to the collimation structure limits the maximum source pressure that may be used. With holes of 0.34 mm diameter, approximately 10 Torr source pressure was found to be appropriate in our experiment. Although this design is an order of magnitude from the source pressures used in single beam systems, we have realized gains of approximately five over a similar effusive source.

B. State Selection

Population inversion may produce intensity gains of the order of $kT/h\nu$ for transitions of frequency ν. Although this factor is inversely proportional to the frequency, gains of 20 may be realized at 300 GHz. The process of state selection with inhomogeneous electric fields has been the subject of extensive discussion (Becker and Angew 1963; Mednikov and Parygin 1963). A number of different state selectors have been successfully employed, but the multiple beam arrangement allowed by the submillimetre wave Fabry–Perot cavity places constraints upon the state selector geometries which can be used efficiently. Figure 2 shows an end view (beam flow perpendicular to figure) of the state selector used for this experiment (De Lucia and Gordy 1969). The poles of the quadrupole are fabricated from copper rods of 3/16-in. diameter, spaced 3/8-in. on centers. The structure is 12 in. long and is cryogenically pumped from within by cooled copper fins. Arcing within the state selector places an upper limit on the applied voltage of about 35 kV.

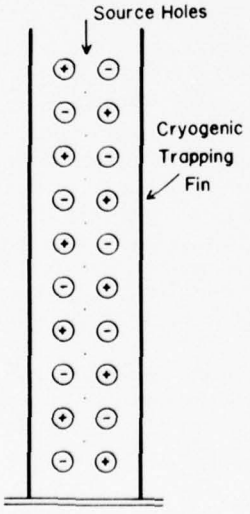

FIG. 2. End view of one vertical bay of state selector with beam source holes indicated.

C. Cavity

At millimetre and submillimetre wavelengths the closed cylindrical cavities used as resonant structures for centimetre wave masers become significantly less advantageous than quasi-optical Fabry–Perot cavities. Because the molecular time-of-flight in the microwave field is the ultimate limit to maser resolution, the diameter of the microwave mode in the cavity should be maximized. For Fabry–Perot cavities made with the usual spherical mirrors, large mode diameters are difficult to obtain at submillimetre wavelengths and the modes themselves are sensitive to imperfections in the long focal length mirrors which are required.

We have developed a Fabry–Perot mirror, shown in Fig. 3, which overcomes the submillimetre-wave mode size problem. The center of the mirror is flat; the edges are curved to confine the microwave mode in a manner analogous to that of conventional spherical mirrors. This mirror may be cut in a stepwise fashion and polished to the final curve as illustrated in Fig. 3. The cavity is formed from this curved mirror and an opposing plane mirror, both fabricated from copper. Diffraction losses are insignificant, Q's approaching the limit imposed by copper losses are attainable, and high order modes are effectively suppressed. This new mirror design has the added advantage that the mode diameter is only a very slow function of wavelength (essentially filling the cavity to the curved edges) and is thereby usable over a wide wavelength range. Power is coupled into and out of the cavity through small holes in the plane mirror. Tuning is accomplished by translation of one of the mirrors.

For the cavity used in this work (the mirror of Fig. 3 and a plane mirror separated by about 20 cm) a mode of approximately 10 cm diameter results. The Q is approximately proportional to $\nu^{1/2}$ and at 1 mm, $Q \approx 500\,000$.

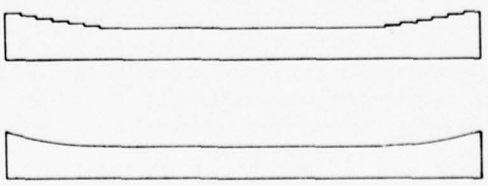

FIG. 3. Fabry–Perot mirror fabrication.

D. Generation and Detection of Submillimetre Radiation

Harmonic generation (King and Gordy 1953) is a proven technique for production of modest amounts of submillimetre radiation and is particularly attractive for beam maser spectroscopy; relaxation rates in a molecular beam are slow and saturation occurs at relatively low power levels. With the high Q cavity used, we have found it possible to generate enough power to saturate the $1_{10} \rightarrow 1_{01}$ transition of D_2O at 317 GHz from a 300 mW 53 GHz klystron (OKI-55V11).

Since the observed linewidth depends upon spectral purity of the stimulating source, it is important that this source be as stable as possible. Free running klystron oscillators are too unstable and it is necessary to lock the signal source to a stable crystal oscillator. A diagram of this stabilization system is included in Fig. 1. The Frequency Engineering Labs 133A Synchronizer contains a variable crystal oscillator and multiplier–amplifier chain which produces a 48 MHz frequency comb extending to several gigahertz. A variable sideband is added and the comb with sidebands is amplified in a traveling wave tube and applied to a crystal mixer (1N26) coupled to the klystron. One of the resulting beat frequencies is down-converted to 27 MHz in a modified Clarke Instruments receiver. Tnis 27 MHz signal is returned to the synchronizer where it is phase compared to a crystal reference oscillator. An error signal is generated and used to stabilize the klystron. The klystron is swept in frequency by means of the variable sideband oscillator.

The very low power levels at which saturation of maser levels occur make superheterodyne linear detectors, which are almost universally used in centimetre wave masers, more attractive than square-law detectors. However, at submillimetre wavelengths, local oscillators and mixers for superheterodyne detection are either unavailable or prohibitively expensive. We have found that the square-law InSb photodetector cooled to 1.6 K has adequate sensitivity for these experiments in the submillimetre region (Helminger *et al.* 1971). This results partly from the increased power output and saturation threshold of submillimetre masers compared to centimetre masers and partly from the increased sensitivity of the cryogenic detector compared to the room temperature detectors more commonly employed. This detector is broadbanded, requires no local oscillator, and is extremely reliable; it has proven to be very satisfactory for our experiments. The output signals are recovered by means of phase sensitive detection (at 3 kHz) of the signal produced as a result of the demodulation by the maser line of a small 1.5 kHz frequency modulation of the klystron.

E. Frequency Measurement

A frequency measurement system, separate from the frequency stabilization system, is used to avoid errors that might be introduced either by inexact loop locks or by instabilities or inaccuracies in the several oscillators. For the frequency measurement system, a 5 MHz crystal oscillator (General Radio 1115-B), phase compared to WWVB (HP117A), generates a standard reference signal which is amplified and multiplied to provide a 60 MHz comb extending to several GHz. This comb is mixed with a sampled portion of the stabilized klystron signal and the beat frequency ν_b is amplified and mixed with a counted reference oscillator (Gertch FM-3) in a communications receiver. As ν_b is swept (as the stabilized klystron is swept) the resulting zero beat is recorded simultaneously with the spectra on a dual channel chart recorder. Ten kilohertz sidebands may be added to the reference oscillator signal to provide a lattice of zero beats which serves as a frequency dispersion calibration on the chart paper.

III. Theory

The theory of molecular hyperfine structure has been extensively discussed in the literature (Thaddeus *et al.* 1964; Garvey *et al.* 1976; Cook and De Lucia 1971; Cederberg 1972). Powerful techniques have been developed which make the calculation of transition frequencies and intensities straightforward. We use the results and notation of Garvey *et al.* (1976) and Cook and De Lucia (1971).

The two identical deuterium nuclei of D_2O make the only contributions to the nuclear hyperfine structure. The Hamiltonian for the relevant interactions is:

$$[1] \qquad \mathcal{H} = \sum_{i=1}^{2} \frac{1}{6} \boldsymbol{V}(D_i)\cdot\boldsymbol{Q}(D_i) + \boldsymbol{I}(D_i)\cdot\boldsymbol{C}(D_i)\cdot\boldsymbol{J} + \boldsymbol{I}(D_1)\cdot\boldsymbol{D}(D_1D_2)\cdot\boldsymbol{I}(D_2)$$

where the terms included represent the electric quadrupole, magnetic dipole, and spin–spin interactions, respectively. This problem is identical in form to the D_2S investigation reported by De Lucia and Cederberg (1971) and the matrix elements for the D_2O hyperfine interactions may be found in that work.

Analysis of the hyperfine structure of ND_3 is considerably more complex, partially because of the increased number of interactions but more significantly because of the three identical particle problem. Application of the techniques of Cederberg (1972) circumvents ambiguities which may occur in such an analysis. The appropriate Hamiltonian for the spectrum observed is:

$$[2]\quad \mathscr{H} = \frac{1}{6}\boldsymbol{V}(N)\cdot\boldsymbol{Q}(N) + \boldsymbol{I}(N)\cdot\boldsymbol{C}(N)\cdot\boldsymbol{J} + \sum_{i=1}^{3}\left[\frac{1}{6}\boldsymbol{V}(D_i)\cdot\boldsymbol{Q}(D_i) + \boldsymbol{I}(D_i)\cdot\boldsymbol{C}(D_i)\cdot\boldsymbol{J} + \boldsymbol{I}(N)\cdot\boldsymbol{D}(ND_i)\cdot\boldsymbol{I}(D_i)\right] + \frac{1}{2}\sum_{\substack{i,j=1\\ i\neq j}}^{3}[\boldsymbol{I}(D_i)\cdot\boldsymbol{D}(D_iD_j)\cdot\boldsymbol{I}(D_j)]$$

where the terms included represent the nitrogen electric quadrupole and magnetic dipole interactions, the deuterium electric quadrupole and magnetic dipole interactions, the nitrogen–deuterium spin–spin interaction, and the deuterium–deuterium spin–spin interaction, respectively. The matrix elements of these terms are included in the Appendix of this paper. The expressions which result lend themselves to machine computation and the energy levels and transition frequencies are obtained by numerical diagonalization of the resulting Hamiltonian matrix.

IV. Results

The experimental beam maser spectrum of the $1_{10} \rightarrow 1_{01}$ transition of D_2O is shown in Fig. 4 along with a theoretical spectrum calculated from the hyperfine constants of Table 1. Table 2 shows both the observed and calculated transition frequencies. The spin–spin interaction constant may be calculated from the molecular geometry. Because of the small size of the nuclear g-factor for deuterium compared to that of hydrogen, the spin rotation constants $C_{1_{10}}$ and $C_{1_{01}}$ can be calculated from previous beam maser work on H_2O and HDO (Bluyssen *et al.* 1967*a*,*b*) with higher accuracy than they can be determined from the D_2O spectrum. The deuterium quadrupole constants of Table 1 were calculated from the observed spectrum. Comparison of the experimental and theoretical data shows agreement well within the experimental error.

The large nitrogen quadrupole interaction in ND_3 produces a triplet which may be resolved in a conventional absorption spectrometer, but the much smaller splittings which result from the deuterium quadrupole interaction are obscured by the Doppler broadening. Figures 5–7 show the resolution of this structure obtained in this experiment. As in the case of D_2O ,the spin–spin interactions may be calculated from the molecular geometry. The remaining hyperfine constants have been evaluated from the beam maser spectrum and appear in Table 3. Table 4 shows a com-

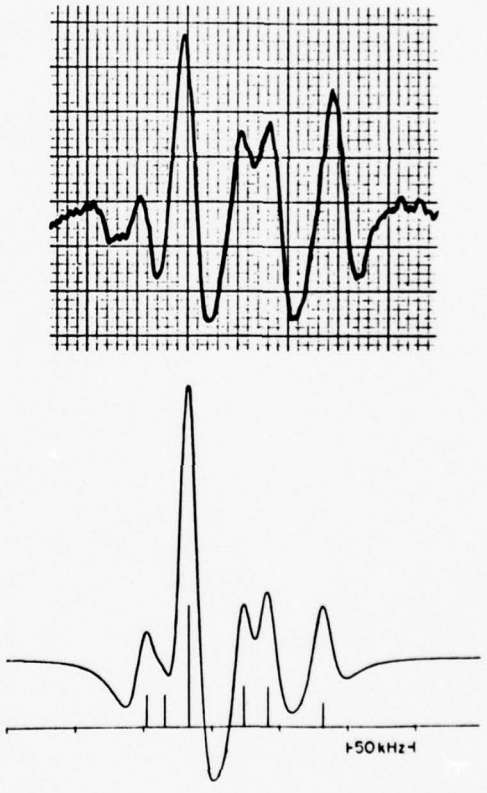

FIG. 4. Experimental and theoretical spectra of the $1_{10} \rightarrow 1_{01}$ transition in D_2O.

TABLE 1. Hyperfine constants of D_2O for $1_{10} \rightarrow 1_{01}$

	Constant	Value (kHz)
1_{10}	$(eQq_J)_D$	34.81 ± 0.32^a
	C_D	-2.661^b
	$\langle 11\|D_{zz}\|11\rangle$	-0.163^c
1_{01}	$(eQq_J)_D$	-29.60 ± 0.55
	C_D	-2.532^b
	$\langle 11\|D_{zz}\|11\rangle$	0.325^c

[a]Uncertainties represent one standard deviation of the experimental data.
[b]Calculated from Bluyssen *et al.* (1967*a*).
[c]Calculated from molecular geometry.

TABLE 2. Hyperfine spectrum of D_2O for $1_{10} \rightarrow 1_{01}$

F	Measured[a] (kHz)	Calculated (kHz)	Difference (kHz)
$0 \rightarrow 1$			
$1 \rightarrow 0$	-46.6 ± 1.8	-46.9	0.3
$2 \rightarrow 2$	-16.3 ± 1.4	-16.5	0.2
$2 \rightarrow 1$	23.3 ± 1.2	24.4	-1.1
$1 \rightarrow 2$	41.5 ± 1.2	41.5	0.0
$1 \rightarrow 1$	82.4 ± 1.2	82.1	0.3

[a]Measured relative to 316 799 845 kHz. Uncertainties represent one standard deviation of the experimental data.

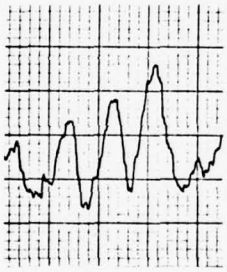

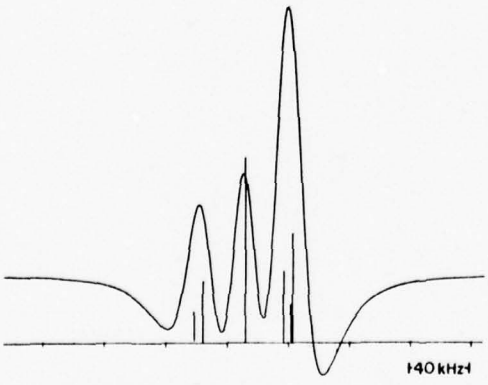

FIG. 5. Experimental and theoretical spectra of the $J = 1 \rightarrow 0$, $F_N = 1$ transition in ND_3.

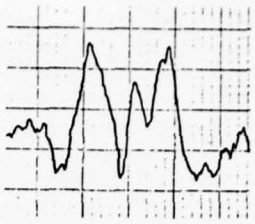

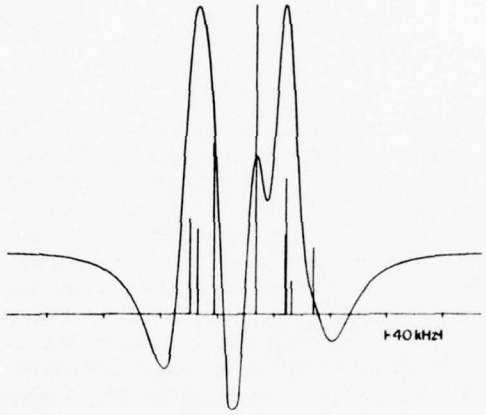

FIG. 6. Experimental and theoretical spectra of the $J = 1 \rightarrow 0$, $F_N = 2$ transition in ND_3.

parison between the experimental hyperfine frequencies and those calculated from the constants of Table 3.

Although there has been considerable experimental and theoretical work on the hyperfine spectra of the isotopic species of ammonia, numerous uncertainties and inconsistencies remain. These problems and the relation of new experimental work to them have been discussed recently by Garvey *et al.* (1976). The submillimetre capabilities of the spectrometer discussed in this paper allow the observation of the $J = 1 \rightarrow 0$ transition, which is less complex than the spectra which fall at longer wavelengths.

V. Discussion

The deuterium quadrupole interaction in the water molecule may be employed to investigate the electric field gradient tensor at the deuterium site. Specifically,

$$[3] \qquad q_J = \frac{2J}{2J+3} \sum_g \frac{\langle P_g^2 \rangle}{J(J+1)} V_{gg}$$

where q_J is the spectral quadrupole constant, g

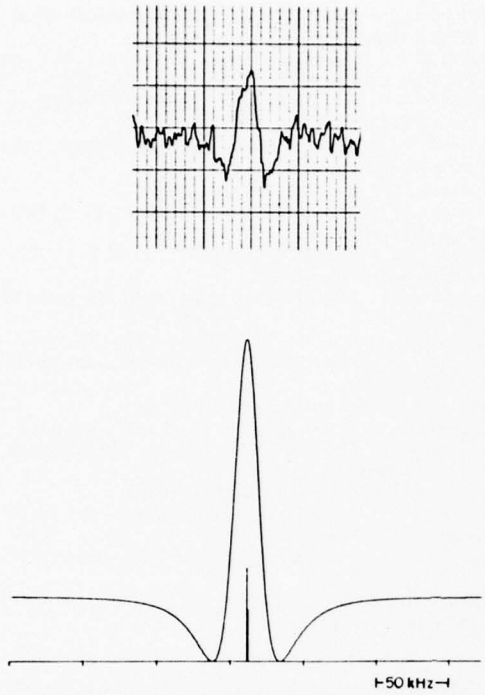

FIG. 7. Experimental and theoretical spectra of the $J = 1 \rightarrow 0$, $F_N = 0$ transition in ND_3.

TABLE 3. Hyperfine constants of $J = 1 \rightarrow 0$ of ND_3

Constant	Value (kHz)
$(eQq_J)_N$	816.2 ± 1.1[a]
C_N	2.0 ± 1.5
$(eQq_J)_D$	19.9 ± 0.8
C_D	-2.2 ± 0.8
$\langle 11\|D_{zz}(DD)\|11\rangle$	-0.13[b]
$\langle 11\|D_{zz}(ND)\|11\rangle$	-0.15[b]

[a]Uncertainties represent one standard deviation of the experimental data.
[b]Calculated from molecular geometry.

TABLE 4. Hyperfine spectrum of ND_3 for $J = 1 \rightarrow 0$

Upper state	Observed[a] (kHz)	Calculated (kHz)	Difference (kHz)
$F_N = 0$	2037.7 ± 0.8	2037.7	0.0
	235.3 ± 2.9	235.4	−0.1
$F_N = 2$	214.3 ± 1.9	213.2	1.1
	181.7 ± 3.0	182.2	−0.5
	-1002.9 ± 1.3	−1002.9	0.0
$F_N = 1$	-1032.4 ± 1.4	−1032.5	−0.1
	-1060.8 ± 1.4	−1060.7	0.1

[a]Measured relative to 309 909 388 kHz. Uncertainties represent one standard deviation of the experimental data.

refers to the molecular principal inertial axes, P_g is the rotational angular momentum along g, and V_{gg} are components of the electric field gradient tensor. Combination of spectroscopic data from HDO and D_2O allow complete solution of V due to the rotation of the molecular inertial axes from one isotopic form of water to the other. As a result of Laplace's equation and molecular symmetry, the tensor may be described by values of two of its components and by the location of its principal axes in the molecular plane. Posener (1960) first performed such an evaluation of the electric field gradient tensor in water. Using beam maser techniques, Bluyssen *et al.* (1967*a*,*b*) were able to significantly improve this analysis. As was pointed out by Bluyssen *et al.* (1967*a*,*b*), Posener erroneously attributed the wrong direction to the angle of rotation from the O—D bond to the principal axis system of the tensor V. The direction of the angle of rotation has more recently been incorrectly reported in the literature (De Lucia *et al.* 1974) because of an erroneous communication to the authors. Posener's data, as well as that of Bluyssen *et al.* and the present experiment, indicate that the principal axes of the quadrupole tensor are rotated from the O—D bond direction by approximately 1° clockwise about Posener's positive ζ axis.

Figure 8 shows the correct geometry for the location of the quadrupole tensor relative to the direction of the molecular bond, and Table 5 gives the components of V in its own principal axis system. These results are calculated from all available data except that from the 7_{44} and 7_{34} states which Verhoeven *et al.* (1968) have shown to be contaminated by centrifugal distortion effects. The uncertainties shown in Table 5 include contributions from both experimental uncertainties and model errors. The model errors

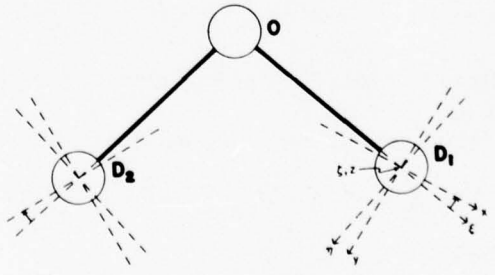

FIG. 8. Rotation of the quadrupole tensor from the OD bond direction. The positive ζ, z axes point *into* the paper for D_1. Different sign conventions and (or) axis assignments would be required for D_2.

TABLE 5. Components of the quadrupole coupling tensor in its principal axis system

	D_2O	D_2S
V_{xx}	307.5 ± 0.6	149.0
V_{yy}	-132.6 ± 0.6	−59.8
V_{zz}	-174.9 ± 0.6	−89.2
a	$-1^\circ 16' \pm 3'$	$-1^\circ 35'$

arise principally from neglect of centrifugal distortion and isotope effects. These errors were not included in the earlier calculation of Bluyssen *et al.* (1967*a*,*b*) because their smaller data set did not provide adequate redundancy for their evaluation.

Also included in Table 5 are similar results for D_2S (De Lucia and Cederberg (1971). It is interesting and reassuring to note the similarity both in the rotation of the principal axis of the V tensor from the bond direction and the deviation from cylindrical symmetry for both molecules.

Acknowledgements

We would like to thank Professor J. W. Cederberg for many useful suggestions and Professor Walter Gordy for his support and encouragement of this work.

BECKER, G. and ANGEW, Z. 1963. Phys. **15**, 281.

BLUYSSEN, H., VERHOEVEN, J., and DYMANUS, A. 1967*a*. Phys. Lett. A, **25**, 214.

BLUYSSEN, H., DYMANUS, A., REUSS, J., and VERHOEVEN, J. 1967*b*. Phys. Lett. A, **25**, 584.

CEDERBERG, J. W. 1972. Am. J. Phys. **40**, 159.

COOK, R. L. and DE LUCIA, F. C. 1971. Am. J. Phys. **39**, 1433.

DE LUCIA, F. C. and CEDERBERG, J. W. 1971. J. Mol. Spectrosc. **40**, 52.

DE LUCIA, F. C. and GORDY, W. 1969. Phys. Rev. **187**, 58.

DE LUCIA, F. C., HELMINGER, P., and KIRCHHOFF, W. H. 1974. J. Phys. Chem. Ref. Data, **3**, 211.

DYKE, T. R., TOMASEVICH, G. R., KLEMPERER, W., and FALCONER, W. E. 1972. J. Chem. Phys. **57**, 2277.

GARVEY, R. M. and DE LUCIA, F. C. 1974. J. Mol. Spectrosc. **50**, 38.

GARVEY, R. M., DE LUCIA, F. C., and CEDERBERG, J. W. 1976. Mol. Phys. **31**, 265.

GORDON, J. P. 1955. Phys. Rev. **99**, 1253.

GORDON, J. P., ZEIGER, H. J., and TOWNES, C. H. 1955. Phys. Rev. **99**, 1264.

HELMINGER, P., COOK, R. L., and DE LUCIA, F. C. 1971. J. Mol. Spectrosc. **40**, 125.

KANTROWITZ, A. and GREY, J. 1951. Rev. Sci. Instrum. **22**, 328.

KING, W. C. and GORDY, W. 1953. Phys. Rev. **90**, 319.

KRUPNOV, A. F. and SKVORTSOV, V. A. 1964. Sov. Phys. JETP, **18**, 74.

MARCUSE, D. 1961. J. Appl. Phys. **32**, 743.

MEDNIKOV, O. I. and PARYGIN, V. H. 1963. Radiotekh. Elektron. **8**, 653; *Engl. transl.* Radio Eng. Electron. Phys. USSR, **8**, 685.

POSENER, D. W. 1960. Aust. J. Phys. **13**, 168.

THADDEUS, P., KRISHER, L. C., and LOUBSER, J. H. N. 1964. J. Chem. Phys. **40**, 257.

VAN DIJK, F. A. and DYMANUS, A. 1970. Chem. Phys. Lett. **5**, 387.

VERHOEVEN, J., BLUYSSEN, H., and DYMANUS, A. 1968. Phys. Lett. A, **26**, 424.

Appendix

The matrix elements of the various Hamiltonian terms for the nuclear hyperfine interactions in ND_3 may be conveniently evaluated in the coupling scheme:

$$\begin{aligned} \boldsymbol{J} + \boldsymbol{I}_N &= \boldsymbol{F}_N \\ \boldsymbol{I}(D_1) + \boldsymbol{I}(D_2) + \boldsymbol{I}(D_3) &= \boldsymbol{I}_D \\ \boldsymbol{F}_N + \boldsymbol{I}_D &= \boldsymbol{F} \end{aligned} \qquad [A.1]$$

In the equations to follow the states are designated by specific cases of the general form $\langle KJI_NF_NI_DFM|$. For brevity, the Hamiltonian is retained in Cartesian form.

$$[A.2]\quad \left\langle 011\ F_N I_D FM \left| \frac{1}{6}\boldsymbol{V}(N)\cdot\boldsymbol{Q}(N) \right| 011\ F_N I_D FM \right\rangle = (-1)^{F_N} \begin{Bmatrix} 1 & 1 & 2 \\ 1 & 1 & F_N \end{Bmatrix} (15/2)(eQq_J)_N$$

$$[A.3]\quad \langle 011\ F_N I_D FM|\boldsymbol{I}(N)\cdot\boldsymbol{C}(N)\cdot\boldsymbol{J}|011\ F_N I_D FM\rangle = (-1)^{F_N} \begin{Bmatrix} 1 & 1 & 1 \\ 1 & 1 & F_N \end{Bmatrix} (6)(C_J)_N$$

The relationship between C_J and C is considered by Cook and De Lucia (1971)

$$[A.4]\quad \left\langle 011\ F_N' I_D' FM \left| \frac{1}{6}\sum_{i=1}^{3} \boldsymbol{Q}(D_i)\cdot\boldsymbol{V}(D_i) \right| 011\ F_N I_D FM \right\rangle =$$

for $I_D' = I_D = 3$:

$$(-1)^{2F_N+1+F}[(2F_N'+1)(2F_N+1)]^{1/2} \begin{Bmatrix} F_N' & F_N & 2 \\ 3 & 3 & F \end{Bmatrix} \begin{Bmatrix} 1 & F_N' & 1 \\ F_N & 1 & 2 \end{Bmatrix} \left(9\sqrt{\frac{7}{2}}\right) (eQq_J)_D$$

for $I_D' = I_D = 1$:

$$(-1)^{2F_N+1+F}[(2F_N'+1)(2F_N+1)]^{1/2}\begin{Bmatrix}F_N' & F_N & 2\\ 1 & 1 & F\end{Bmatrix}\begin{Bmatrix}1 & F_N' & 1\\ F_N & 1 & F\end{Bmatrix}\frac{27}{2}(eQq_J)_D$$

for $I_D' = 1$, $I_D = 3$:

$$(-1)^{2F_N+1+F}[(2F_N'+1)(2F_N+1)]^{1/2}\begin{Bmatrix}F_N' & F_N & 2\\ 3 & 1 & F\end{Bmatrix}\begin{Bmatrix}1 & F_N' & 1\\ F_N & 1 & 2\end{Bmatrix}(3\sqrt{21})(eQq_J)_D$$

[A.5] $$\left\langle 011\ F_N'I_DFM\left|\sum_{i=1}^{3}\boldsymbol{I}(D_i)\cdot\boldsymbol{C}(D_i)\cdot\boldsymbol{J}\right|011\ F_NI_DFM\right\rangle = (-1)^{2F_N+I_D+F+1}$$

$$\times[(2F_N'+1)(2F_N+1)(2I_D+1)(I_D+1)I_D]^{1/2}\begin{Bmatrix}F_N' & F_N & 1\\ I_D & I_D & F\end{Bmatrix}\begin{Bmatrix}1 & F_N' & 1\\ F_N & 1 & 1\end{Bmatrix}(\sqrt{6})(C_J)_D$$

[A.6] $$\left\langle 011\ F_N'I_DFM\left|\sum_{i=1}^{3}\boldsymbol{I}(N)\cdot\boldsymbol{D}(ND_i)\cdot\boldsymbol{I}(D_i)\right|011\ F_NI_DFM\right\rangle = (-1)^{F_N+I_D'+F+1}$$

$$\times[3(2F_N'+1)(2F_N+1)(2I_D+1)(I_D+1)I_D]^{1/2}\begin{Bmatrix}F_N' & F_N & 1\\ I_D & I_D & F\end{Bmatrix}\begin{Bmatrix}1 & 1 & 2\\ 1 & 1 & 1\\ F_N' & F_N & 1\end{Bmatrix}$$

$$\times 15\sqrt{2}\langle 11|D_{zz}(\mathrm{ND})|11\rangle$$

$\langle 11|D_{zz}|11\rangle$ is the specialized form of $\langle J\,J|D_{zz}|J\,J\rangle$, the spin–spin interaction term, discussed by De Lucia and Cederberg (1971).

[A.7] $$\left\langle 011\ F_N'I_D'FM\left|\frac{1}{2}\sum_{\substack{i,j=1\\ i\neq j}}\boldsymbol{I}(D_i)\cdot\boldsymbol{D}(D_iD_j)\cdot\boldsymbol{I}(D_j)\right|011\ F_NI_DFM\right\rangle =$$

for $I_D' = I_D = 3$:

$$(-1)^{2F_N+F+1}[(2F_N'+1)(2F_N+1)]^{1/2}\begin{Bmatrix}F_N' & F_N & 2\\ 3 & 3 & F\end{Bmatrix}\begin{Bmatrix}1 & F_N' & 1\\ F_N & 1 & 2\end{Bmatrix}(18\sqrt{14})\langle 11|D_{zz}(\mathrm{DD})|11\rangle$$

for $I_D' = I_D = 1$:

$$(-1)^{2F_N+F+1}[(2F_N'+1)(2F_N+1)]^{1/2}\begin{Bmatrix}F_N' & F_N & 2\\ 1 & 1 & F\end{Bmatrix}\begin{Bmatrix}1 & F_N' & 1\\ F_N & 1 & 2\end{Bmatrix}(-6)\langle 11|D_{zz}(\mathrm{DD})|11\rangle$$

for $I_D' = 1$, $I_D = 3$:

$$(-1)^{2F_N+F+1}[(2F_N'+1)(2F_N+1)]^{1/2}\begin{Bmatrix}F_N' & F_N & 2\\ 3 & 1 & F\end{Bmatrix}\begin{Bmatrix}1 & F_N' & 1\\ F_N & 1 & 2\end{Bmatrix}(-3\sqrt{21})\langle 11|D_{zz}(\mathrm{DD})|11\rangle$$

J. Quant. Spectrosc. Radiat. Transfer, Vol. 17, pp. 751–754. Pergamon Press 1977. Printed in Great Britain

PRESSURE BROADENING OF HYDROGEN SULFIDE†

PAUL HELMINGER‡

Department of Physics, University of South Alabama, Mobile, AL 36688, U.S.A.

and

FRANK C. DE LUCIA

Department of Physics, Duke University, Durham, NC 27706, U.S.A.

(*Received* 12 *October* 1976)

Abstract—Microwave measurements of the self-broadening parameters of four pure rotational transitions of H_2S have been carried out in the millimeter and submillimeter wavelength region. The resulting parameters are (in MHz torr $^{-1}$): $1_{1,0} - 1_{0,1}$, 7.18 ± 0.5; $2_{2,0} - 2_{1,1}$, 6.78 ± 0.5; $2_{1,1} - 2_{0,2}$, 9.10 ± 0.5; $3_{3,0} - 3_{2,1}$, 7.76 ± 0.5. In addition, Anderson theory calculations have been carried out for these transitions and are found to be in good agreement.

INTRODUCTION

BECAUSE H_2S is a light asymmetric rotor without transitions in the conventional microwave region, we have used high resolution millimeter and submillimeter microwave techniques[1] to measure the self-broadening parameters of four pure-rotational transitions of H_2S in the region between 150 and 400 GHz. To the best of our knowledge, these results are the first experimental measurements of the pressure broadening parameters of H_2S. We have also carried out Anderson theory[2] calculations and find them to be in good agreement with our experimental values.

These results are of both theoretical and practical importance. H_2O is the only other light asymmetric species for which experimental line-broadening data have been reported and some of these data are in substantial conflict with theoretical predictions.[3] H_2S is both a minor constituent of the atmosphere and one of the principal molecular components of the interstellar medium.

EXPERIMENTAL TECHNIQUE AND RESULTS

We have discussed in previous publications the techniques for producing and detecting millimeter and submillimeter microwave energy.[1] Our pressure-broadening measurement technique follows closely the double modulation scheme of RUSK.[4] Figure 1 shows an outline of our apparatus. Millimeter wave energy in the 50–60 GHz region was produced by an OKI 55V11 klystron. A small amount of this energy was compared with an accurate local frequency standard and the rest coupled onto a crystal harmonic generator. The resultant harmonic energy in the 150–400 GHz region was transmitted by quasi-optical techniques through the sample cell and detected by a 1.6°K InSb photodetector. The pressure-broadened line acted as a discriminator for the small 10 kHz FM modulation that was applied to the tube. The resulting 10 kHz signal was amplified by the tuned amplifiers of a PAR HR-8 lock-in and displayed on an oscilloscope. A cathetometer and oil manometer were used to monitor pressure. Although H_2S is well behaved and reaches equilibrium pressure rapidly, measurements were made both in series of increasing and decreasing pressure and on different days to avoid possible systematic effects. Because rotational transitions of light asymmetric rotors are such strong absorbers in the millimeter and submillimeter spectral region, we used absorption cell lengths as short as 10 cm. Even so, it was necessary to include a correction for the large absorption by[5]

$$\Delta\nu = \sqrt{(3)}\delta\nu\left(1 - \frac{1}{4}a_0 l + \frac{5}{32}(a_0 l)^2 - \cdots\right), \tag{1}$$

†This work was supported by the Army Research Office, Grant Number DAHCO4 74 G 0034.
‡Travel to Duke University provided by a grant from the Southern Regional Education Board.

Table 1. Hydrogen sulfide line broadening parameters

Transition	Line Frequency (GHz)	Experimental[a] Broadening Data (MHz/Torr)	Corrected Self Broadening Parameter (MHz/Torr)	Anderson Theory Value (MHz/Torr)
$^{1}_{1,0} - {}^{1}_{0,1}$	168	7.80	7.18 ± 0.5	6.58
$^{2}_{0,2} - {}^{2}_{1,1}$	216	8.69	8.10 ± 0.5	7.21
$^{2}_{2,0} - {}^{2}_{1,1}$	393	7.14	6.78 ± 0.5	6.99
$^{3}_{3,0} - {}^{3}_{2,1}$	300	8.52	7.76 ± 0.5	7.14

[a] Line widths measured at 300° K.

DISCUSSIONS

Until this work, H_2O was the only light asymmetric rotor for which comparison could be made of experimental and theoretical pressure-broadening parameters. Unfortunately, only the microwave measurements of the $3_{1,3} - 2_{2,0}$[4] and $6_{1,6} - 5_{2,3}$[11] transitions are in good agreement with the theoretical predictions. Several i.r. measurements all gave results that are about 50% higher than the values of BENEDICT and KAPLAN.[3] The good agreement between our microwave results and theory, coupled with the fact that the apparent discrepancies in H_2O are all based on lower resolution i.r. measurements, would indicate that Anderson's theory is capable of giving good results for pure rotational transitions of light asymmetric species. Recent microwave work by NERF[12] on the somewhat heavier H_2CO leads to the same conclusion.

TEJWANI and YENUNG[13] have recently carried out Anderson's theory calculations on H_2S with and without the inclusion of higher order interactions. Their results are in general agreement with ours (~10%) although the differences are substantially greater than the differences between our H_2O calculations and those of Benedict and Kaplan.

REFERENCES

1. P. HELMINGER, F. C. DE LUCIA and W. GORDY, *Phys. Rev. Lett.* **25**, 1397 (1970).
2. P. W. ANDERSON, *Phys. Rev.* **76**, 647 (1949).
3. G. BIRNBAUM, *Advan. Chem. Phys.* **12**, 487 (1967).
4. J. R. RUSK, *J. Chem. Phys.* **42**, 493 (1965).
5. H. J. BABROV, Private communication.
6. P. A. HELMINGER and F. C. DE LUCIA, *Bull. Am. Phys. Soc.* **21**, 380 (1976).
7. W. S. BENEDICT and L. D. KAPLAN, *JQSRT* **4**, 453 (1964).
8. C. J. TSAO and B. CURNUTTE, *JQSRT* **2**, 41 (1962).
9. P. HELMINGER, R. L. COOK and F. C. DE LUCIA, *J. Chem. Phys.* **56**, 4581 (1972).
10. C. HUISZOON and A. DYMANUS, *Physica* **31**, 1049 (1965).
11. H. J. LIEBE, M. C. THOMPSON, JR. and T. A. DILLON, *JQSRT* **9**, 1 (1969).
12. R. B. NERF, *J. Molec. Spectrosc.* **58**, 451 (1975).
13. G. D. T. TEJWANI and E. S. YEUNG, *JQSRT* to be published.

JOURNAL OF MOLECULAR SPECTROSCOPY 66, 206–218 (1977)

"Forbidden" Rotational Spectra of Symmetric-Top Molecules: PH_3 and PD_3[1]

DAVID A. HELMS AND WALTER GORDY

Department of Physics, Duke University, Durham, North Carolina 27706

A millimeter-wave spectrometer having a sensitivity of 4×10^{-10} cm^{-1} in the 2-mm region has been constructed for observation of extremely weak millimeter-wave spectra of gases. It has been used to measure $J \rightarrow J$, $K = 0 \leftarrow 3$ transitions in PH_3 and $J \rightarrow J$, $K = 0 \leftarrow 3$ as well as $K = \pm 1 \leftarrow \pm 4$ transitions in PD_3. The B_0 and C_0 spectral constants (in MHz) are: for PH_3, $B_0 = 133\,480.15 \pm 0.12$ and $C_0 = 117\,488.85 \pm 0.16$; for PD_3, $B_0 = 69\,471.10 \pm 0.03$ and $C_0 = 58\,974.37 \pm 0.05$. The effective ground-state values obtained for the bond angle and bond length are: for PH_3, r_0 (Å) $= 1.420_0$ and $\alpha_0(^\circ) = 93.34_5$; for PD_3, r_0 (Å) $= 1.417_6$ and $\alpha_0(^\circ) = 93.35_9$. The corresponding zero-point-average values were calculated to be: for PH_3, r_z (Å) $= 1.4269_9 \pm 0.0002$ and $\alpha_z(^\circ) = 93.228_7$; for PD_3, r_z (Å) $= 1.4226_5 \pm 0.0001$ and $\alpha_z(^\circ) = 93.256_7 \pm 0.004$. For both species, the equilibrium values are r_e (Å) $= 1.4115_9 \pm 0.0006$ and $\alpha_e(^\circ) = 93.32_8 \pm 0.02$.

1. INTRODUCTION

The pure rotational transitions normally observed for symmetric-top molecules conform to the selection rules $\Delta J = \pm 1$, $\Delta K = 0$. As a result of their axial symmetry, there is no off-axis component of the permanent dipole moment to couple a radiation field with the rotation about the symmetry axis. Hence, resonance radiation does not normally induce changes in the K quantum number which measures the angular momentum about this axis. Consequently, the moment of inertia for rotation about the symmetry axis, and the associated centrifugal distortion constants, cannot be obtained from the normal rotational spectra.

As a result of theoretical developments and notable advancements in the experimental techniques for spectral detection, it has become possible to detect rotational transitions in the ground vibrational state corresponding to changes in the energy of rotation about the symmetry axis of symmetric-top molecules, i.e., changes in the K quantum number. For molecules with C_{3v} symmetry, such as PH_3 and PD_3 which are reported here, the observable transitions—forbidden in the normal theory—correspond to K changes of ± 3.

The possibility of $\Delta K = \pm 3$ changes in molecules of C_{3v} symmetry was apparently first recognized in 1967 by Hanson (*1*). The basic theory for such transitions was later contributed by Watson (*2*). These transitions were first detected as pure rotational spectra in 1973 by Chu and Oka (*3*), who observed $\Delta J = 0$, $K = \pm 1 \leftarrow \mp 2$ transitions in PH_3 occurring in the 43.7 to 47.4 GHz region. In 1974 they reported (*4*) similar

[1] This work was supported by the Army Research Office, Grant DAAG29-77-G-0007.

ISSN 0022-2852

measurements of $\Delta J = 0$, $K = \pm 1 \leftarrow \mp 2$ transitions for PD_3 in the 29.9 to 30.8 GHz region, and for AsH_3 in the 21.2 to 21.8 GHz region. Chu and Oka were helped in their measurements by the line frequency predictions based on the previous observation of $\Delta(K - l) = \pm 3$ vibration–rotation transitions of PH_3 and AsH_3 by Maki, Sams, and Olson (*5*). Likewise, our detection (*6*) of the higher-frequency $K = 0 \leftarrow 3$ forbidden transition of PH_3 and PD_3 was assisted by a preliminary prediction of their frequencies from the results of Maki *et al.* as well as those of Chu and Oka.

The need for observation of these higher K transitions described in this paper was indicated by Chu and Oka (*4*), who reported that their spectrometer was not sufficiently sensitive at the higher frequencies to detect them. Measurements of these transitions confirm the assignments of the frequencies measured by Chu and Oka and provide increased accuracy in the values of the spectral constants, particularly those influenced by the distortion caused by rotation about the symmetry axis. For observation of weak transitions such as these in the shorter millimeter-wave region, we designed the exceptionally sensitive millimeter-wave spectrometer described below.

The Q-branch $\Delta K = \pm 3$ transitions represent only one class of forbidden transitions in symmetric molecules included in the general theory of Watson *et al.* (*2, 7*) and others (*8, 9*). Oka (*10*) has recently written an excellent review of the experimental and theoretical developments of this relatively new type of spectra. It should be mentioned that forbidden transitions of symmetric-top molecules in vibrationally excited states were theoretically predicted many years earlier by Mizushima and Venkateswarlu (*11*), before sufficiently sensitive spectrometers were available for their detection. In the ground vibrational state the off-axis dipole moment which couples the radiation field to the rotation is induced by centrifugal distortion. The selection rules are determined by the molecular symmetry. In the molecules studied here, the rotation about the b axis of inertia induces a small dipole moment perpendicular to the symmetry axis which leads to a slight admixture of the K levels and a breakdown of the $\Delta K = 0$ selection rule. The threefold symmetry about the c axis limits this admixture to K levels differing by 3. It is of interest that centrifugal distortion due to rotation about the symmetry axis can likewise generate a small dipole component along the symmetry axis. This component is of no particular consequence in molecules such as PH_3, which already has a permanent dipole moment along the symmetry axis, but it can give rise to forbidden $\Delta J = \pm 1$ transitions in molecules such as CH_4, which has no permanent dipole moment. In fact, $\Delta J = 1$ rotational transitions of CH_4, SiH_4, and GeH_4 have been observed by Rosenberg *et al.* (*12–15*) in the far-infrared region. Forbidden transitions of CH_4 in the ground vibrational state have also been detected in the microwave region by Holt, Gerry, and Ozier (*16*). These and other forbidden spectra of symmetric-top molecules are treated in Oka's review (*10*). He also reports that he and his associates have recently detected $\Delta K = \pm 3$ transitions of NH_3 with an infrared laser (*17*).

2. EXPERIMENTAL DETAILS

The microwave spectrometer used in these measurements has: for the millimeter-wave source, a klystron-driven harmonic generator; for the absorption cell, a high-Q Fabry–Perot transmission cavity (semiconfocal arrangement); and for millimeter-wave

detection, an indium–antimonide detector operated at 1.6 K. The power from the harmonic generator is injected into the cavity by way of a small, rectangular aperture (0.075×0.034 in.) in the center of the flat, circular mirror. The power level in the cavity is monitored by radiation from another small, rectangular aperture in the same plate, the output from which is channeled to the indium–antimonide detector. The Q of the resonant cavity mode as indicated by the $\nu_0/\Delta\nu$, the resonant frequency divided by the half-width of the Lorentzian mode shape, is approximately 600 000 at 140 GHz.

In operation, the resonant cavity is filled with the absorbing sample of gas to a pressure of about 15 to 25 μm. The klystron is tuned so that the proper harmonic coincides with the predicted absorption frequency, and the cavity is adjusted to resonate at that frequency. The klystron harmonic is then locked to the peak of the cavity resonance, and the cavity is tuned through the molecular absorption line. The drop in the monitored power resulting from the change in the loaded Q of the cavity corresponds to the detected spectral line.

To achieve control of the klystron frequency by the cavity, a 2.6 kHz sine wave is superimposed on the klystron reflector to sweep the harmonic back and forth across the center of the cavity resonance. The signal produced at the detector (with the loop opened) changes phase by 180° as the klystron is tuned through the cavity resonance. This detector signal is processed by a phase-lock-in amplifier which generates a correction voltage with the proper phase-and-time response to lock the klystron harmonic to the peak of the cavity resonance. Thus, as the cavity is tuned by movement of the curved mirror in and out, the klystron harmonic and the cavity resonance track together. In practice, the amplitude of the 2.6 kHz stabilizing signal is reduced to about 40 mV, or less, to keep most of the harmonic power within the envelope of the cavity-response curve.

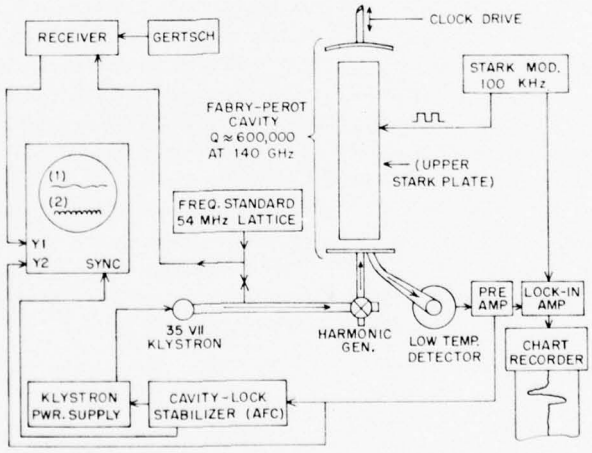

FIG. 1. Diagram of spectrometer.

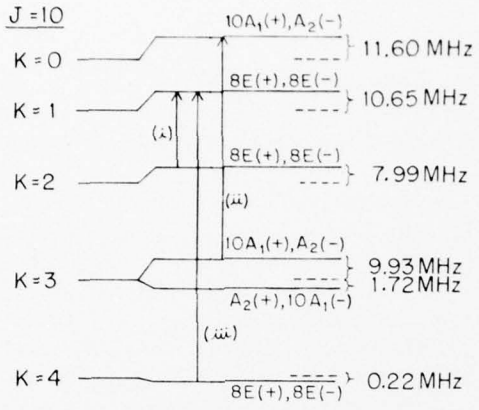

FIG. 2. Energy level diagram of the first five K states for $J = 10$ of PD_3 showing the energy shifts caused by the $\mathcal{H}'$ perturbation, the $K = 3$ splitting, the level symmetry (under particle exchange), and the nuclear spin degeneracy. The transition indicated by (i) is that measured by Chu and Oka (*4*). Those indicated by (ii) and (iii) were measured in this work.

The inside of the cavity is fitted with Stark-modulation plates which are positioned well out of the microwave field to avoid lowering the Q. A square-wave generator is used to produce Stark modulation of the absorption line at 100 kHz. As the clock-driven cavity tunes through the absorption, the detector signal is processed by a phase-lock-in amplifier referenced to the 100-kHz signal. The first-derivative line-shape signal from the amplifier is displayed on the chart recorder (see Fig. 1). After exploratory scans to establish the shape of the line, the peak of the cavity response is tuned to the center of the absorption-line contour, and the corresponding klystron frequency is measured with a frequency standard monitored by station WWVB. Repeated measurements are made for each direction of approach to the line center. The accuracy achieved for the line-frequency measurements is estimated to be 1 part in 10^8. The sensitivity of our spectrometer ($\approx 4 \times 10^{-10}$ cm^{-1} at 144 GHz for a time constant of 1 sec) enables us to measure the weak $\Delta K = \pm 3$ transitions with this high precision. The factors limiting the sensitivity appear to be the degree of klystron stability, the power available from the harmonic generator, and the extraneous vibrations of the cavity end plates.

3. THEORETICAL BACKGROUND

As a result of centrifugal distortion, the rotational wavefunction $\psi_{J,K}$ of a molecule having C_{3v} symmetry mixes slightly with the wavefunction $\psi_{J,K\pm 3}$ in the ground vibrational state. The term in the Hamiltonian responsible for the interaction may be ex-

pressed (*18*) as

$$\mathcal{H}' = (\hbar^4\tau_{zzzz}/4)[(J^3_+ + J^3_-)J_z + J_z(J^3_+ + J^3_-)], \tag{1}$$

where τ_{zzzz} is a centrifugal distortion constant and J_z, J_+, and J_- are rotational operators.

In the absence of the perturbing $\mathcal{H}'$ term, the rotational levels are all doubly degenerate for each value of K ($K \neq 0$). Figure 2 illustrates the effect of the perturbation on the $J = 10$ energy levels in PD_3. The energy levels corresponding to $K \neq 3$ are raised or lowered, but they remain degenerate with symmetry E. The $K = 3$ level is, however, split into A_1 and A_2 components. The + and − signs indicate the parity of the total wavefunction. The symmetry assignments A_1, A_2, and E indicate the symmetry of the rovibrational wavefunction (excluding spin) for an interchange of two hydrogens. The integer preceding the symmetry assignment (A_1, A_2, or E) indicates the nuclear statistical weight of the state. The symmetry selection rules for Q-type $\Delta K = \pm 3$ transitions (19) are $\pm \leftrightarrow \pm$, along with $A_1 \leftrightarrow A_1$, $A_2 \leftrightarrow A_2$, or $E \leftrightarrow E$.

Each unperturbed energy level of a symmetric-top molecule is normally doubly degenerate for each nonzero value of K. It is necessary to form linear combinations of $\psi_{J,+K}$ and $\psi_{J,-K}$ in order to obtain wavefunctions which have the proper symmetry for an exchange of two of the hydrogens. The new wavefunctions for PH_3, $\psi^+_{J,K}$ and $\psi^-_{J,K}$, are defined in terms of the wavefunctions $\psi_{J,+K}$ and $\psi_{J,-K}$ and the nuclear wavefunctions $\alpha\beta\beta$, $\alpha\beta\alpha$, etc. (where α and β stand for spin up and spin down, respectively) as follows (*20*): for $K \neq 0$ or a multiple of 3,

$$\psi^{\pm}_{J,K} = (1/6^{\frac{1}{2}})[\psi_{J,+K}(\beta\alpha\alpha + \alpha\beta\alpha e^{2\pi iK/3} + \alpha\alpha\beta e^{4\pi iK/3}) \pm \psi_{J,-K}(\beta\alpha\alpha + \alpha\beta\alpha e^{-2\pi iK/3} + \alpha\alpha\beta e^{-4\pi iK/3})] \tag{2}$$

and

$$\psi^{\pm}_{J,K} = (1/6^{\frac{1}{2}})[\psi_{J,+K}(\alpha\beta\beta + \beta\alpha\beta e^{2\pi iK/3} + \beta\beta\alpha e^{4\pi iK/3}) \pm \psi_{J,-K}(\alpha\beta\beta + \beta\alpha\beta e^{-2\pi iK/3} + \beta\beta\alpha e^{-4\pi iK/3})]; \tag{3}$$

for $K = 0$,

$$\psi^{+}_{J,0} = (1/3^{\frac{1}{2}})\psi_{J,0}\begin{Bmatrix}\beta\alpha\alpha + \alpha\beta\alpha + \alpha\alpha\beta \\ \alpha\beta\beta + \beta\alpha\beta + \beta\beta\alpha\end{Bmatrix}, \tag{4a}$$

and for $K = 3$

$$\psi^{\pm}_{J,K} = (1/6^{\frac{1}{2}})(\psi_{J,+K} \pm \psi_{J,-K})\begin{Bmatrix}\alpha\alpha\alpha \\ \beta\beta\beta \\ \beta\alpha\alpha + \alpha\beta\alpha + \alpha\alpha\beta \\ \alpha\beta\beta + \beta\alpha\beta + \beta\beta\alpha\end{Bmatrix}. \tag{4b}$$

The similar wavefunctions for PD_3 are more complicated because of the spin value $I = 1$ for D.

The formulas giving the energy levels may be expressed (*21*, *22*) for $K \neq 3$ as:

$$\frac{E(J,K)}{h} = F(J,K) + \left(\frac{h^4\tau_{zzzz}}{4h}\right)^2 \left\{ \frac{(2K-3)^2[J(J+1)-K(K-1)][J(J+1)-(K-1)(K-2)][J(J+1)-(K-2)(K-3)]}{F(J,K)-F(J,K-3)} + \frac{(2K+3)^2[J(J+1)-K(K+1)][J(J+1)-(K+1)(K+2)][J(J+1)-(K+2)(K+3)]}{F(J,K)-F(J,K+3)} \right\}; \quad (5)$$

and for $K = 3$ as

$$\frac{E^-(J,3)}{h} = F(J,3) + \left(\frac{h^4\tau_{zzzz}}{4h}\right)^2 \left\{ \frac{81[J(J+1)-12][J(J+1)-20][J(J+1)-30]}{F(J,3)-F(J,6)} \right\} + \left[h_0 - \frac{18(h^4\tau_{zzzz}/4h)^2}{F(J,0)-F(J,3)} \right] J(J+1)[J(J+1)-2][J(J+1)-6], \quad (6)$$

and

$$\frac{E^+(J,3)}{h} = F(J,3) + \left(\frac{h^4\tau_{zzzz}}{4h}\right)^2 \left\{ \frac{81[J(J+1)-12][J(J+1)-20][J(J+1)-30]}{F(J,3)-F(J,6)} \right\} - h_0 J(J+1)[J(J+1)-2][J(J+1)-6], \quad (7)$$

where

$$F(J,K) = B[J(J+1)-K^2] + CK^2 - D_J J^2(J+1)^2 - D_{JK} J(J+1)K^2 - D_K K^4 + H_{JJK} J^2(J+1)^2 K^2 + H_{JKK} J(J+1)K^4 + L_{JJKK} J^2(J+1)^2 K^4 + L_{JJJK} J^3(J+1)^3 K^2. \quad (8)$$

These $K = 3$ levels contain the term $\pm h_0 J(J+1)[J(J+1)-2][J(J+1)-6]$, first derived by Nielsen and Dennison (*23*) in their explanation of the anomalous effects in $K = 3$ lines observed by early microwave spectroscopists. The total splitting of the $K = 3$ levels is

$$\Delta\nu = [E^-(J,3) - E^+(J,3)]/h$$
$$= \left[2h_0 - \frac{18(h^4\tau_{xxxz}/4h)^2}{F(J,0) - F(J,3)}\right] J(J+1)[J(J+1)-2][J(J+1)-6]. \quad (9)$$

The part of Eq. (9) that is enclosed in brackets is not a constant because of the presence of the $F(J,0) - F(J,3)$ expression in the denominator. The denominator $F(J,0) - F(J,3)$ is a power series in $J(J+1)$:

$$F(J,0) - F(J,3) = 9(B-C)\left[1 + \frac{9D_K}{B-C} + \frac{D_{JK} - 9H_{JKK}}{B-C} J(J+1) - \frac{H_{JJK} + 9L_{JJKK}}{B-C} J^2(J+1)^2 - \frac{L_{JJJK}}{B-C} J^3(J+1)^3\right]. \quad (10)$$

It is not sufficient to retain only the first term, $9(B-C)$. We found that a simultaneous, least-squares fit of the available data for normal transitions and forbidden transitions for the molecular constants did not converge properly unless the full expression was used.

The line strengths of the forbidden $\Delta K = \pm 3$ transitions (1, 2) are given by

$$S = \tfrac{1}{4}(\theta^{xx}{}_x)^2_{\text{eff}}(J \mp K)(J \mp K - 1)(J \mp K - 2) \times (J \pm K + 1)(J \pm K + 2)(J \pm K + 3)(2J+1)/J(J+1) \quad (11)$$

where

$$(\theta^{xx}{}_x)_{\text{eff}} = \theta^{xx}{}_x + h^4\tau_{xxxz}\mu_z/[2h(B-C)] \quad (12)$$

is the effective dipole moment inducing the transition. The term,

$$\theta^{xx}{}_x = 2(B)^2\left[\frac{a^{xx}{}_3}{\nu^2_3}\left(\frac{\partial\mu_x}{\partial Q_3}\right) + \frac{a^{xx}{}_4}{\nu^2_4}\left(\frac{\partial\mu_x}{\partial Q_4}\right)\right], \quad (13)$$

is an induced dipole component which results from admixture of the ground vibrational state with excited vibrational modes. This contribution, first recognized by Watson (*2*), is called vibrational intensity borrowing by Oka (*10*). The last term results from centrifugally induced mixing of rotational levels of the ground vibrational state. This contribution to the forbidden transitions, first derived by Hansen (*1*), is called rotational intensity borrowing by Oka (*10*). In this expression τ_{xxxz} is the centrifugal distortion constant in $\mathcal{H}'$ of Eq. (1), μ_z is the permanent dipole moment, and C and B are the spectral constants with reference to the symmetry axis and the perpendicular axis, respectively.

For the present molecules, the contribution of the vibrational intensity borrowing is small in comparison with that of the rotational intensity borrowing. For PH_3, Chu and Oka (*4*) calculated that $\theta^{xx}{}_x = 1.6 \times 10^{-5}$ D and that the centrifugally induced moment, the second term of Eq. (12), is 8.3×10^{-5} D. The relative contributions of these mo-

ments to the forbidden line strengths, Eq. (12), is $(1.6/8.3)^2 = 0.037$. Thus, for PH_3 in the ground vibrational state, the contribution of the vibrational mixing to the intensities of the $\Delta K = \pm 3$ transitions is negligible in comparison with that from rotational mixing. Chu and Oka also estimate that the centrifugal rotational intensity borrowing is the dominant term for PD_3.

4. RESULTS

Twelve $K = 0 \leftarrow 3$ transitions of PH_3 as well as ten $K = \pm 1 \leftarrow \pm 4$ and five $K = 0 \leftarrow 3$ transitions in PD_3 were measured. The observed frequencies are given in Tables I and II. Displacement in positions of lines of PH_3 caused by the Nielsen–Dennison splitting (*23*) of the $K = 3$ levels (105 MHz for $J = 10$ in PH_3) increased the difficulty of their detection. This splitting does not occur in the transitions observed by Chu and Oka (*4*), but it has been directly observed for PH_3 by Davis *et al.* (*24*) in a molecular beam resonance experiment. Location of the $K = 0 \leftarrow 3$ transitions would have been even more difficult were it not for our access to their molecular beam measurements.

The $\Delta K = \pm 3$ transitions exhibit a rapid change in the observed intensity with increasing value of J. Figure 3 illustrates the calculated intensity profile (see Eq. (14)). This variation is due partly to the increase in the rotationally induced coupling moment with J and partly to the variation in the population of J states. At the temperature of the observation, 300 K, the intensity reaches a maximum for $J = 10$. The solid vertical bars in Fig. 3 correspond to transitions that we have measured. The dashed vertical bars representing calculated lines have been included for better indication of the trend. Figure 4 shows actual recordings of two lines.

The peak absorption coefficients listed in Tables I and II were calculated from the formula,

$$\alpha(\mathrm{cm}^{-1}) = \frac{1.147 \times 10^{-13}}{\Delta\nu T^{\frac{3}{2}}} \nu_0^2 \left(1 - \frac{h\nu_0}{2kT}\right) \times \exp(-E_{J,K}/kT)[(B^2C)^{\frac{1}{2}} g_K g_I S[(J, K \pm 3) \leftarrow (J, K)]], \quad (14)$$

where the line-strength factor S is given by Eq. (11), $T = 300$ K, g_I is the reduced nuclear statistical weight factor (*25*), g_K is the statistical weight factor for each K level, and $\Delta\nu = 20$ MHz is the line breadth at a pressure of 1 Torr. This value for the $\Delta\nu$ is the same as that used by Chu and Oka (*4*) for PH_3. Other factors included in the numerical constant are described in Ref. (*25*).

We had little difficulty in detecting the $J = 3$, $\Delta J = 0$, $K = 0 \leftarrow 3$ transition which has a predicted intensity of only 7×10^{-10} cm^{-1}. From comparisons of the signal-to-noise ratios for the four weaker lines of PH_3 and PD_3 with the calculated line intensities given in Tables I and II, we estimate the sensitivity of our spectrometer to be approximately 4×10^{-10} cm^{-1}.

A combined computer analysis was made of the available frequencies for different types of transitions measured by us and by others as listed in Tables I and II. The analysis consisted of a least-squares fitting of 10 molecular constants to the observed frequencies of PH_3 and 9 to those of PD_3. The program calculates the difference in the energy levels by use of Eqs. (5)–(8) with assumed values of the molecular constants.

TABLE I

Observed Frequencies and Calculated Intensities for the PH_3 Transitions

Transition	Observed Frequency ν (MHz)	ν Obs - ν Calc	a_{max} (Calc) (10^{-9} cm^{-1})
Normal Rotational Transitions			
$J+1 \leftarrow J$ $K \leftarrow K$ (a)			
J = 0 K = 0	266 944.82	0.00	
1 0	533 794.32	0.00	
1 1	533 816.01	0.00	
Forbidden Rotational Transitions			
$J \leftarrow J$ $K = 1 \leftarrow \pm 2$ (b)			
J = 6	47 341.16	0.41	2.2
7	47 178.66	-0.27	3.4
8	46 983.04	0.09	4.6
9	46 871.48	-0.14	5.3
10	46 377.80	-0.03	5.7
11	46 058.52	-0.05	5.5
12	45 714.84	-0.06	5.0
13	45 347.84	-0.07	4.2
14	44 958.68	-0.14	3.3
15	44 548.88	0.04	2.4
16	44 119.80	0.53	1.6
17	43 671.08	-0.32	1.1
$J \leftarrow J$ $K = 0 \leftarrow 3$ (c)			
J = 3	143 701.63	-0.09	0.7
4	143 331.01	-0.13	3.4

TABLE I (continued)

Transition	Observed Frequency ν (MHz)	ν Obs - ν Calc	a_{max} (Calc) (10^{-9} cm^{-1})
5	142 859.93	0.05	8.8
6	142 319.00	0.12	17.1
7	141 679.05	0.13	27.2
8	140 950.44	0.02	37.1
9	140 133.10	-0.14	44.8
10	139 226.81	0.07	48.5
11	138 228.01	-0.03	47.9
12	137 134.66	-0.02	43.5
13	135 941.42	0.00	36.6
14	134 641.42	0.02	28.6
Molecular Beam Resonance Transitions			
K = 3 Splittings (d)			
J = 3	0.062	0.000	
4	0.434	-0.001	
5	1.734	-0.007	
6	5.196	-0.016	
7	12.969	-0.027	
8	28.483	-0.025	
9	56.855	0.031	

(a) P. Helminger and W. Gordy, Phys. Rev. 188, 100 (1969).

(b) Chu and Oka, Ref. 4.

(c) Present work.

(d) Davies, et al., Ref. 24.

TABLE II
Observed Frequencies and Calculated Intensities for the PH_3 Transitions

Transition	Observed Frequency ν(MHz)	ν Obs - ν Calc	σ_{max} (Calc) (10^{-26} cm.$^{-1}$)
Normal Rotational Transitions			
$J+1 \leftarrow J$ $K \leftarrow K$ (a)			
J = 0 K = 0	138 938.17	0.06	
1 0	277 861.71	-0.01	
1 1	277 866.93	-0.04	
2 0	416 716.39	0.03	
2 1	416 724.18	-0.03	
2 2	416 747.81	0.01	
Forbidden Rotational Transitions			
$J \leftarrow J$ $K \pm 1 \leftarrow \pm 2$ (b)			
J = 13	30 805.64	0.18	0.79
14	30 700.67	-0.04	0.82
15	30 587.40	0.06	0.82
16	30 471.60	-0.02	0.78
17	30 347.32	-0.11	0.71
18	30 217.40	0.16	0.62
19	30 081.32	0.15	0.53
20	29 939.20	0.22	0.43

TABLE II (continued)

Transition	Observed Frequency ν(MHz)	ν Obs - ν Calc	σ_{max} (Calc) (10^{-26} cm^{-1})
$J \leftarrow J$ $K = 0 \leftarrow 3$ (c)			
J = 9	93 448.65	-0.04	2.2
10	93 285.70	0.02	3.0
11	93 099.29	-0.09	3.7
12	92 729.42	-0.02	4.3
13	92 425.42	0.05	4.7
$J \leftarrow J$ $K = \pm 1 \leftarrow \pm 4$ (c)			
J = 9	186 857.87	-0.02	7.8
10	186 873.65	0.00	10.7
11	186 153.32	0.01	13.6
12	184 827.62	0.15	16.1
13	184 207.02	0.00	18.0
14	183 852.42	-0.08	19.0
15	183 124.72	-0.07	19.1
16	182 534.73	-0.02	18.4
17	181 913.22	-0.04	16.9
18	181 281.35	0.09	14.8

(a) P. Helminger and W. Gordy, Phys. Rev. 188, 100 (1969).

(b) Chu and Oka, Ref. 4.

(c) Present work.

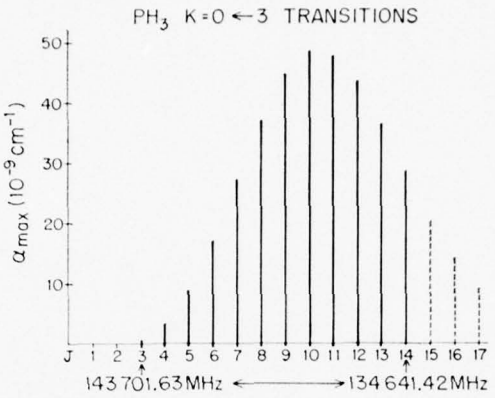

FIG. 3. Calculated intensities for the $K = 0 \leftarrow 3$ lines observed in the present work (solid lines) and for some not observed (dotted lines).

Transition frequencies are calculated and compared to the measured transition frequencies to generate new estimates of the molecular constants. This iterative process is repeated many times by the computer until convergence is attained. The degree of fitting of the complete frequency set is shown by column 3 of Tables I and II. The molecular constants for PH_3 and PD_3 obtained from the combined analyses are listed in Table III. The constants h_0 and τ_{zzzz} for PD_3 are rather well determined since we were able to measure both the $K = \pm 1 \leftarrow \pm 4$ and $0 \leftarrow 3$ transitions. These same two constants for PH_3 are not nearly so well determined, because of their high statistical correlation and the lack of data from the $K = \pm 1 \leftarrow \pm 4$ transitions. The large uncertainties in the relative values of h_0 and the τ_{zzzz} do not appreciably limit the accuracy of the values of the other constants for PH_3.

There are only two independent structural parameters in PH_3 or PD_3, the bond angle and bond length. With the two measured moments, $I_b = h/8\pi^2 B_0$ and $I_c = h/8\pi^2 C_0$, an effective zero-point vibrational structure can be calculated for both species. The effective structural parameters thus derived are listed in Table IV. They are limited in

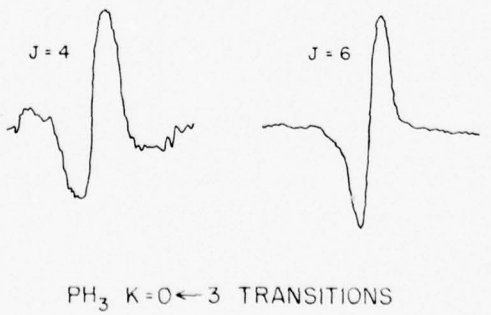

FIG. 4. Recordings of the $J = 4$ and $J = 6$, $K = 0 \leftarrow 3$, lines for PH_3 at 300 K.

TABLE III
Molecular Constants

Molecular Constant	PH_3	PD_3
B_0	133 480.15 ± 0.12 MHz	69 471.10 ± 0.03 MHz
C_0	117 489.85 ± 0.10 MHz	58 974.37 ± 0.05 MHz
D_J	3.947 ± 0.016 MHz	1.021 ± 0.002 MHz
D_{JK}	-6.132 ± 0.001 MHz	-1.312 ± 0.001 MHz
D_K	4.177 ± 0.011 MHz	1.023 ± 0.002 MHz
$\pi^4\tau_{xxxx}/4h$	0.62 ± 0.03 MHz	0.221 ± 0.005 MHz
H_{JJK}	-1.09 ± 0.04 kHz	-0.091 ± 0.004 kHz
h_0	67.6 ± 2.2 Hz	9.41 ± 0.22 Hz
L_{JJKK}	4.7 ± 0.7 Hz	
L_{JJJK}	0.52 ± 0.03 Hz	0.044 ± 0.005 Hz

accuracy by the uncorrected inertial defect. A second structure, the zero-point average structure (*4*) can also be calculated for each species from the observed B_0 and C_0 values. This structure was calculated by Chu and Oka for PH_3. We have recalculated the zero-point average values for the structural parameters with the B_0 and C_0 values derived from a computer analysis of the measured ground-state rotational transitions, as described above. The resulting parameters, listed in Table IV, are essentially the same as those obtained by Chu and Oka; the method used for calculation of the average

TABLE IV
Comparison of Different Structures for Phosphine

	Zero-point Effective[a]	Zero-point Average[b]	Equilibrium[b]
		PH_3	
r_{PH} (Å)	1.420_0	$1.4203_9 \pm 0.0002$	$1.4116_9 \pm 0.0006$
∠HPH (°)	93.34_5	$93.328_7 \pm 0.005$	$93.32_8 \pm 0.02$
		PD_3	
r_{PD} (Å)	1.417_6	$1.4226_5 \pm 0.0001$	$1.4116_9 \pm 0.0006$
∠DPD (°)	93.35_9	$93.296_7 \pm 0.004$	$93.32_8 \pm 0.02$

a. Uncorrected for inertial defects.

b. Calculated as described by Chu and Oka, Ref. 4.

structural values is the one they describe. Discussion of the significance or meaning of the various types of structures and methods for calculations of each type is given by Gordy and Cook (*25*).

ACKNOWLEDGMENTS

We wish to thank T. Oka, W. B. Olson, and A. G. Maki for helpful communications.

RECEIVED: February 28, 1977

REFERENCES

1. H. M. HANSON, *J. Mol. Spectrosc.* **23**, 287 (1967).
2. J. K. G. WATSON, *J. Mol. Spectrosc.* **40**, 536 (1971).
3. F. Y. CHU AND T. OKA, *J. Mol. Spectrosc.* **48**, 612 (1973).
4. F. Y. CHU AND T. OKA, *J. Chem. Phys.* **60**, 4612 (1974).
5. A. G. MAKI, R. L. SAMS, AND W. B. OLSON, *J. Chem. Phys.* **58**, 4502 (1973).
6. D. HELMS AND W. GORDY, *Bull. Am. Phys. Soc.* **21**, 380 (1976).
7. J. K. G. WATSON, *J. Mol. Spectrosc.* **55**, 498 (1975).
8. F. MICHELOT, J. MORET-BAILLY, AND K. FOX, *J. Chem. Phys.* **60**, 2606, 2610 (1974).
9. I. OZIER, *J. Mol. Spectrosc.* **56**, 124 (1975).
10. T. OKA, Forbidden rotational transitions, *in* "Molecular Spectroscopy: Modern Research" (K. Narahari Rao and C. W. Mathews, Eds.), Vol. II, p. 229, Academic Press, New York, 1976.
11. M. MIZUSHIMA AND P. VENKATESWARLU, *J. Chem. Phys.* **21**, 705 (1953).
12. A. ROSENBERG, I. OZIER, AND A. K. KUDIAN, *J. Chem. Phys.* **57**, 568 (1972).
13. A. ROSENBERG AND I. OZIER, *Chem. Phys. Lett.* **13**, 400 (1973).
14. A. ROSENBERG AND I. OZIER, *Can. J. Phys.* **52**, 575 (1974).
15. A. ROSENBERG AND I. OZIER, *J. Chem. Phys.* **58**, 5168 (1973).
16. C. W. HOLT, M. C. L. GERRY, AND I. OZIER, *Phys. Rev. Lett.* **31**, 1033 (1973).
17. D. LAUGHTON, S. M. FREUND, AND T. OKA, *J. Mol. Spectrosc.* **62**, 263 (1976).
18. T. OKA, *J. Chem. Phys.* **47**, 5410 (1967).
19. G. HERZBERG, "Infrared and Raman Spectra of Polyatomic Molecules," Van Nostrand–Reinhold, Princeton, N. J., 1945. See also JON T. HOUGEN, *J. Chem. Phys.* **37**, 1433 (1962).
20. T. M. SUGDEN AND C. N. KENNEY, "Microwave Spectroscopy of Gases," Van Nostrand, New York, 1965.
21. G. AMAT, H. H. NIELSEN, AND G. TARRAGO, "Rotation–Vibration of Polyatomic Molecules," Marcel Dekker, New York, 1971.
22. W. B. OLSON, private communication.
23. H. H. NIELSEN AND D. DENNISON, *Phys. Rev.* **72**, 1011 (1947).
24. P. DAVIES, R. NEUMANN, S. WOFSY, AND W. KLEMPERER, *J. Chem. Phys.* **55**, 3564 (1971).
25. W. GORDY AND R. COOK, "Microwave Molecular Spectra," Wiley–Interscience, New York, 1970.

(4)

The study of laser processes by millimeter and submillimeter microwave spectroscopy[a)]

Frank C. De Lucia

Department of Physics, Duke University, Durham, North Carolina 27706
(Received 5 July 1977; accepted for publication 31 August 1977)

Millimeter and submillimeter microwave spectroscopy is shown to be a powerful technique for the study of the fundamental processes of molecular lasers. The calculation of absolute chemical compositions, excitation parameters, and the observation of collisional deexcitation are demonstrated for the HCN FIR laser.

PACS numbers: 42.55.Hq, 33.20.Ea, 52.70.Gw

Although a number of techniques have been described for the study of the fundamental processes of molecular lasers,[1-5] much remains to be understood about their chemistry, excitation mechanisms, and decay pathways. This letter reports the results of experiments that demonstrate the unique capabilities of millimeter and submillimeter microwave spectroscopy in this field.

In this spectral region, molecular laser plasmas are transparent except at molecular resonances and emit insignificant noise. This latter property is directly related to the well-known difficulty of producing radiation in the submillimeter/far-infrared region of the spectrum. Equally important, the noise modulation of the probing signal due to plasma fluctuations decreases rapidly as the signal frequency is increased from the centimeter-wave region into the millimeter and submillimeter region. Rotational line strengths also increase as approximately $1/\lambda^3$ and their transition moments are orders of magnitude stronger than those of the vibrational transitions studied in the infrared. Because of the widely tunable spectral coverage of our technique, studies of both nonradiative states and species as well as those that participate directly in the lasing process are possible. The sharpness of the resonances ($\Delta\nu \leq 1$ MHz) is such that the different states and species are well resolved and can be studied independently. Of equal importance is the direct relation between the experimental observables (frequencies, absorption coefficients, linewidths, and lifetimes) and the dynamics of the molecular laser systems.

Our experiment is shown in Fig. 1.[6] Microwave energy in the 30–60-GHz range is produced by a reflex klystron. A small portion of this signal is compared with a frequency standard and the rest matched onto a crystal harmonic generator. The harmonic output of this generator (typically 3rd → 12th harmonic) is trans-

[a)]Work supported by the U.S. Army Research Office, Grant No. DAAG29-77-G-0007.

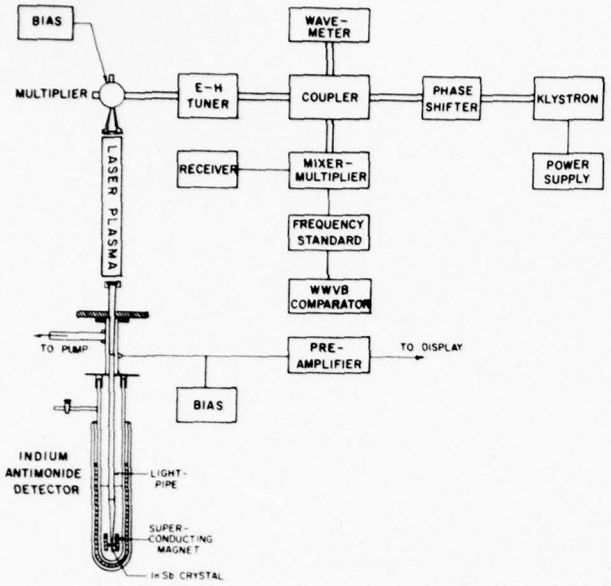

FIG. 1. Spectrometer for the study of laser plasmas.

mitted through the laser tube by quasioptical techniques and detected by a 1.4 K InSb photodetector. The sensitivity of this technique is such that states whose populations are $\sim 10^9/\mathrm{cm}^3$ can be seen in real time on an oscilloscope screen with large signal to noise.

It can be shown that to a good approximation the absorption coefficient α for a linear molecule can be written

$$\alpha\,(\mathrm{cm}^{-1}) = (4.94\times10^{-3})F_v\mu^2\nu_0^3/\Delta\nu T^2, \tag{1}$$

where ν_0 (GHz) is the transition frequency, $\Delta\nu$ (MHz/Torr) is the linewidth, μ (D) is the dipole moment, T (K) is the temperature, and F_v is the fraction of molecules in the vibrational state.[7] This relation assumes that the rotational states and molecular velocities are in equilibrium and can be described by a temperature T. For pure rotational spectra μ and ν_0 are known to high accuracy and $\Delta\nu$ can be accurately measured from the high-resolution microwave data. The

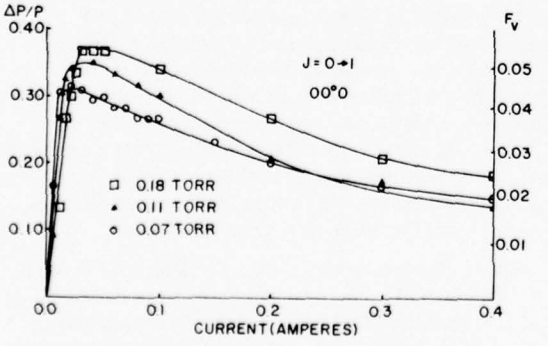

FIG. 2. Total HCN concentration derived from the $J=0\rightarrow1$ rotational absorption in the ground vibrational state.

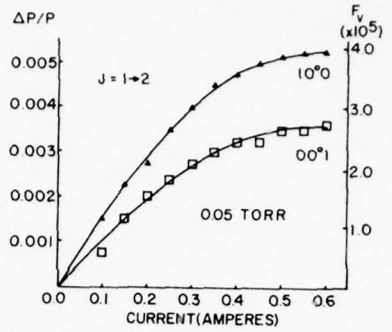

FIG. 3. Excitation of the 10^00 and 00^01 vibrational states of HCN.

relation

$$\Delta P/P = 1 - \exp(-\alpha l) \tag{2}$$

relates the experimental data $\Delta P/P$ with α and ultimately with F_v.

Three studies of the HCN FIR molecular laser which illustrate the kinds of information that can be acquired are described below. CH_3CN was used as the fuel.

The total HCN concentration is an important, but unknown, parameter of the laser. Chantry[8] estimates it as 1 μm partial pressure for typical operating conditions, and Schötzan and Kneubühl[4] have measured with a mass spectrometer the *relative* concentration as a function of discharge current. Figure 2 shows results calculated from measurements on the $J=0\rightarrow1$ transition of the 00^00 vibrational state. In our experiment, the HCN concentration is maximum at a remarkably low current (typically 0.01 A) and decreases substantially at higher currents.

The well-known HCN laser mechanism of Lide and Maki[3] depends upon the near degeneracy of $J=10$ in the 11^10 and 04^00 vibrational states and a population inversion between them in the laser plasma. This inversion has often been attributed[8,9] to the metastable nature of the 10^00 state and the bending stack built upon it. Figure 3 shows the absolute populations of the 10^00 and 00^01 states as a function of the discharge current. It should be noted that these states are essentially equally populated and that the "metastable" nature of 10^00 is thus shown not to be a requirement for a population excess.

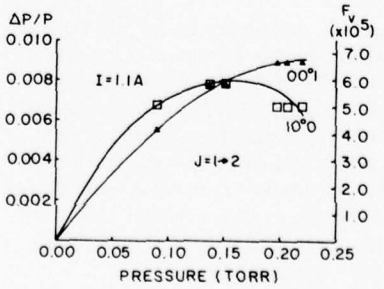

FIG. 4. Pressure dependence of the excitation of the 10^00 and 00^01 vibrational states of HCN.

Figure 4 shows the population of $10^{0}0$ and $00^{0}1$ as a function of pressure. These results are consistent with a model in which resonant deexcitation between the $(0,n,0)$ and $(1,n-3,0)$ bending stacks is an important limiting factor on the operating pressure of the HCN laser. On the other hand, the $(0,n,1)$ stack is not in close resonance with another family of states and maintains its excitation at substantially higher pressures.

In conclusion, we have demonstrated the kinds of information that can be obtained in a very direct manner from our experiments. It is clear that they have applicability both to other states and species found in the HCN laser and to molecular lasers in general. These data provide both constraints and tests for models of the complex dynamics of these systems as well as suggestions for new models.

The author would like to thank the Research Corporation for its support of this work.

[1]H.J. Schötzau and F. Kneubühl, IEEE J. Quantum Electron. QE-11, 817 (1975).
[2]L.E. Sharp and A.T. Wetherell, Appl. Opt. 11, 1737 (1972).
[3]D.R. Lide and A.G. Maki, Appl. Phys. Lett. 11, 52 (1967).
[4]H.J. Schötzau and F. Kneubühl, Appl. Phys. 6, 25 (1975).
[5]M. Yamanaka, T. Yamauchi, and H. Yoshimaga, Jpn. J. Appl. Phys. 10, 1601 (1971).
[6]P. Helminger, F.C. De Lucia, and W. Gordy, Phys. Rev. Lett. 25, 1397 (1970).
[7]W. Gordy and R.L. Cook, *Microwave Molecular Spectra* (Wiley-Interscience, New York, 1970).
[8]G.W. Chantry, *Submillimetre Spectroscopy* (Academic, New York, 1971).
[9]J.P. Pichamuthu, J. Phys. D 7, 1096 (1974).

JOURNAL OF MOLECULAR SPECTROSCOPY 65, 330 331 (1977)

NOTES

Centrifugal Distortion in Water and Hydrogen Sulfide[1]

It is the intent of this note to present specific results pertaining to the changes in molecular geometry of water and hydrogen sulfide which are induced by centrifugal effects in rotational states of the molecules. Hydrogen, deuterium, and tritium substitutions are considered. A general expression for centrifugally induced geometry changes has been presented by Toyama *et al.* (*1*) but specific results included only the symmetric forms of water, H_2O and D_2O. A sign error is present in that work but appears to be only typographical, as the numerical results given are correct. The term $\mu \sin \alpha$ in Eq. (53) should be negative. Considerable simplification occurs in the symmetric cases and a calculation of centrifugal distortion in HDO, DTS, etc., must proceed from the most general approach.

TABLE I. Coefficients of Eq. (3) for Water and Hydrogen Sulfide[a]

	ρ	$\Delta r/r$	$\Delta\alpha$		$\Delta r/r$	$\Delta\alpha$
H_2O	a	1.016	-10.742	H_2S	0.300	-2.878
	b	0.293	3.041		0.212	2.238
	c	0.247	0.000		0.126	0.012
D_2O	a	0.565	-5.976	D_2S	0.159	-1.525
	b	0.147	1.521		0.106	1.120
	c	0.126	0.070		0.064	0.025
T_2O	a	0.415	-4.390	T_2S	0.112	-1.075
	b	0.098	1.016		0.071	0.748
	c	0.086	0.090		0.044	0.029

	ρ	$\Delta r_1/r_1$	$\Delta r_2/r_2$	$\Delta\alpha$		$\Delta r_1/r_1$	$\Delta r_2/r_2$	$\Delta\alpha$
HDO	a	0.969	0.673	-9.192	HDS	0.372	0.083	-2.639
	b	0.065	0.293	1.488		0.008	0.179	0.705
	c	0.111	0.204	0.030		0.046	0.088	0.013
HTO	a	0.955	0.606	-9.160	HTS	0.374	0.075	-2.855
	b	0.028	0.232	0.857		0.002	0.125	0.370
	c	0.066	0.170	0.034		0.026	0.074	0.012
DTO	a	0.541	0.449	-5.334	DTS	0.189	0.071	-1.359
	b	0.072	0.157	1.117		0.021	0.116	0.632
	c	0.084	0.117	0.076		0.037	0.054	0.022

[a] All coefficients have been multiplied by 10^4; angles are in radians; r_1 is associated with the lighter atom in the asymmetric species.

[1] This work supported by the U.S. Army Research Office, Grant DAHCO4 74 G 0034.

ISSN 0022-2852

The general expression for the distortion effects are given in Ref. (*1*) in matrix form

$$\langle \mathbf{R} \rangle_{\text{cent}} = \mathbf{F}_R^{-1}\mathbf{G}_R^{-1}\mathbf{B}\Phi\mathbf{X}, \tag{1}$$

where

$$\langle \mathbf{R} \rangle_{\text{cent}} = \begin{pmatrix} \Delta r_1 \\ \Delta r_2 \\ (r_1 r_2)^{\frac{1}{2}}\Delta\alpha \end{pmatrix} \tag{2}$$

and **X** is, in the case of the bent triatomic molecule, a nine component vector describing the position of the three nuclei in a body fixed Cartesian coordinate system which is parallel to the molecular inertial axes. $\mathbf{F}_R$, $\mathbf{G}_R$, **B**, and Φ are defined in Ref. (*1*). As was shown by the authors of Ref. (*1*), it is convenient to rewrite Eq. (1) as

$$\langle R \rangle_{\text{cent}} = \rho_a\langle P_a^2 \rangle + \rho_b\langle P_b^2 \rangle + \rho_c\langle P_c^2 \rangle, \tag{3}$$

where *a*, *b*, and *c* designate the molecular inertial axes and $\langle P_a^2 \rangle$, etc., are the expectation values of the angular momentum component operators along the molecular equilibrium axes. These values may be easily calculated for any specific rotational level of a given molecule (*2*). The vector coefficients ρ_a, ρ_b, and ρ_c of Eq. (3), which are defined in Ref. (*1*), have been evaluated and are presented in Table I for water and hydrogen sulfide. Coefficients for H_2O and D_2O have been recalculated for completeness.

The force constants used are those of Cook, De Lucia, and Helminger (*3*, *4*). As noted by the authors of Refs. (*3*) and (*4*), model errors produce significant uncertainties in the values of the force constants. The constants used are those obtained from infrared data with equal weighting. These uncertainties are the primary limitation to the accuracy of the coefficients of this work and those of Ref. (*1*). Symmetric forms of water and hydrogen sulfide distort symmetrically and only one coefficient is necessary to describe the change in bond length. In the case of the asymmetric forms, changes in both bonds must be specified. In Table I, r_1 refers to the bond extending from the apex atom to the atom of least mass.

REFERENCES

1. M. Toyama, T. Oka, and Y. Morino, *J. Mol. Spectrosc.* **13**, 193 (1964).
2. W. Gordy and R. L. Cook, "Microwave Molecular Spectra," Wiley–Interscience, New York, 1970.
3. R. L. Cook, F. C. De Lucia, and P. Helminger, *J. Mol. Spectrosc.* **53**, 62 (1974).
4. R. L. Cook, F. C. De Lucia, and P. Helminger, *J. Mol. Struct.* **28**, 237 (1975).

R. Michael Garvey[2]

Department of Physics
Duke University
Durham, North Carolina 27706

Received: August 18, 1976

[2] Present address: National Bureau of Standards, Boulder, Colorado 80302.

Millimeter spectrum and molecular constants of silicon monoxide*

E. Lowry Manson, Jr., William W. Clark, Frank C. De Lucia, and Walter Gordy
Department of Physics, Duke University, Durham, North Carolina 27706
(Received 4 August 1976)

A new high-temperature millimeter-wave microwave spectrometer has been constructed and used to measure a wide range of vibrational and rotational states of silicon monoxide. This work results in accurate rest frequencies for all of the intersteller SiO maser transitions that have been observed as well as accurate measurements or predictions of all transitions that are likely to be of astrophysical interest. In addition, the Dunham spectral and potential constants are calculated for the three major isotopic species. For $^{28}Si^{16}O$: $Y_{01} = 21787.453(11)$ MHz, $Y_{11} = -151.026(11)$ MHz, $Y_{21} = 70.5(24)$ kHz, $Y_{02} = -29.38(13)$ kHz, $a_0 = 5.390(22) \times 10^5$ cm^{-1}, $a_1 = -2.9899(41)$, $a_2 = 5.7(7)$, $a_3 = -9.0(5)$. The calculated equilibrium parameters for $^{28}Si^{16}O$ are $B_e = 21787.5(10)$ MHz, $\omega_e = 1252.(3)$ cm^{-1}, $\omega_e x_e = 5.96(71)$ cm^{-1}, and $r_e = 1.50973(4)$ A.

INTRODUCTION

In 1968, Törring[1] reported the laboratory measurement of the $J = 0 \rightarrow 1$ rotational transitions of $^{28}Si^{16}O$ in the 43-GHz region for four vibrational states, $v = 0, 1, 2, 3$. Meanwhile, a maser signal at 86 243 MHz, observed by radioastronomers[2] in the nebular source Orion A, has been assigned to the $J = 2 \rightarrow 1$, $v = 1$ transition of $^{28}Si^{16}O$ by Lovas and Johnson[3] from a theoretical prediction of the frequency based on Törring's measurement of the $J = 0 \rightarrow 1$ transition. Since that time, SiO maser emission lines corresponding to the transitions $v = 1$, $J = 1 \rightarrow 0$; $v = 1$, $J = 2 \rightarrow 1$; $v = 1$, $J = 3 \rightarrow 2$; and $v = 2$, $J = 1 \rightarrow 0$ have been observed in 20 astronomical sources.[4]

With the present work, direct laboratory measurements have been made of the frequencies of all of the transitions which give rise to the important maser signals from outer space, and measurements of the rotational spectrum of $^{28}Si^{16}O$ are extended to 303 926.96 GHz. These measurements, shown in Table I, include seven rotational transitions of $^{28}Si^{16}O$ in five vibrational states. They allow precise evaluation of the centrifugal distortion effects which influence all rotational and vibrational constants of the molecule and which cannot be evaluated from the $J = 0 \rightarrow 1$ transition alone. These constants make possible the accurate prediction of all transitions that are likely to be of astrophysical interest. Figure 1 shows the laboratory, real-time oscilloscope display of the most commonly observed astrophysical maser, the $J = 2 \rightarrow 1$, $v = 1$ transition.

EXPERIMENT

A sufficient concentration of silicon monoxide vapor for microwave absorption measurements was produced by the heating of a homogeneous mixture of silicon and silicon dioxide to 1350 °C in a high-temperature reaction chamber which also served as the microwave absorption cell. This combination of reaction chamber and absorption cell consisted of a Mullite MV30 ceramic tube (9 × 45 cm) concentrically positioned inside a cold-rolled steel pipe (25 × 105 cm) which was connected to a pumping line. For the purpose of mechanical support and thermal insulation, the volume between the ceramic tube and the outer steel jacket was filled with A.P. Green G-26 insulating firebricks. The heating element was constructed from ten graphite welding rods which were electrically connected in series and equally spaced around the inside of the Mullite tube.

A tapered horn combined with a Teflon lens focused the microwave radiation into the reaction chamber and through the vapor above the reactants. The radiation emerging from the reaction zone was then focused onto a sensitive InSb radiation detector operated at 1.6 °K. The detected absorption-line signals, after amplification, were displayed on an oscilloscope for the frequency measurements. Description of the millimeter-wave spectrometer and measuring techniques are given in an earlier publication.[5]

DATA AND ANALYSIS

The most accurate formulas for analysis of the rotational spectra of diatomic molecules are provided by Dunham theory.[6] Dunham solved the Schrödinger wave equation for the diatomic vibrating rotor with a potential function of the form

$$V(\xi) = ch a_0 \xi^2 (1 + a_1 \xi + a_2 \xi^2 + \cdots) , \quad (1)$$

where $\xi = (r - r_e)/r_e$, $a_0 = \omega_e^2/4B_e$, and $a_1, a_2, \ldots$ are the potential constants. His solution for the rotation-vibration energies is expressed by the

TABLE I. Observed transitions of silicon monoxide.

$J \rightarrow J+1$	v	Measured frequencies (MHz)	Difference from calculated frequencies (MHz)
		$^{28}Si^{16}O$	
0→1	0	43 423.76[a]	−0.04
	1	43 122.03[a]	0.00
	2	42 820.48[a]	−0.06
	3	42 519.34[a]	0.01
1→2	0	86 846.96	0.07
	1	86 243.37	0.02
	2	85 640.46	0.09
2→3	0	130 268.61	0.04
	1	129 363.24	−0.02
3→4	0	173 688.31	0.16
	1	172 481.15	0.09
	2	171 275.28	0.18
	3	170 070.35	0.07
4→5	0	217 104.98	0.09
	1	215 595.95	−0.09
	2	214 088.54	−0.06
	3	212 582.60	0.04
	4	211 077.87	−0.07
5→6	0	260 518.02	−0.09
	1	258 707.45	−0.04
6→7	0	303 926.96	−0.15
		$^{29}Si^{16}O$	
0→1	0	42 879.82[a]	0.00
		$^{30}Si^{16}O$	
0→1	0	42 373.34[a]	0.00

[a] Reference 1.

series

$$E_{v,J} = h \sum_{l,m} Y_{l,m} (v+\tfrac{1}{2})^l [J(J+1)]^m , \qquad (2)$$

in which the coefficients $Y_{l,m}$ are now known as

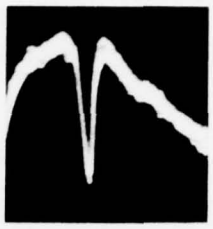

FIG. 1. Video display of the $J=1\rightarrow 2$, $v=1$ transition of $^{28}Si^{16}O$.

Dunham's constants. Each $Y_{l,m}$ is a function of the molecular parameters $r_e, a_0, a_1, a_2, \ldots$ which appear in Eq. (1). In terms of the familiar spectroscopic constants,

$$Y_{10} \approx \omega_e , \quad Y_{01} \approx B_e , \quad Y_{11} \approx -\alpha_e , \quad Y_{21} \approx \gamma_e , \qquad (3)$$
$$Y_{20} \approx -\omega_e x_e , \quad Y_{02} \approx -D_e , \quad Y_{12} \approx -\beta_e , \quad Y_{03} \approx H_e .$$

With the selection rules $J \rightarrow J+1$ and $v \rightarrow v$ for pure rotational transitions, Eq. (2) predicts the rotational frequencies to be

$$\nu_{v,J\rightarrow v,J+1} = 2[Y_{01} + Y_{11}(v+\tfrac{1}{2}) + Y_{21}(v+\tfrac{1}{2})^2 + \cdots](J+1) + 4Y_{02}(J+1)^3 + \cdots , \qquad (4)$$

where only terms which give a detectable contribution to the spectra reported in this paper are retained. For the less abundant isotopic species the Dunham isotope relation,

$$Y'_{l,m} = (\mu/\mu')^{(l+2m)/2} Y_{l,m} , \qquad (5)$$

is accurate to within experimental error for all $Y_{l,m}$ except $Y_{0,1}$. In Eq. (5) μ' denotes the reduced mass of the less abundant species, and the unprimed parameters, $Y_{l,m}$ and μ, refer to the parent species ($^{28}Si^{16}O$).

The silicon monoxide microwave spectrum was analyzed by substitution of each measured absorption frequency and the appropriate J and v quantum numbers into Eq. (4). In this manner a

TABLE II. Comparison of molecular constants measured in this work with previous values.

Constants	$^{28}Si^{16}O$ This work[a]	$^{28}Si^{16}O$ Others	$^{29}Si^{16}O$ This work	$^{29}Si^{16}O$ Others	$^{30}Si^{16}O$ This work	$^{30}Si^{16}O$ Others
Y_{01} (MHz)	21 787.453(11)	21 787.462(25)[b]	21 514.046(13)	21 514.074(25)[b]	21 259.494(13)	21 259.425(25)[b]
Y_{11} (MHz)	−151.026(11)	−151.05(4)[b]	−148.193(11)	−148.22(4)[b]	−145.570(11)	−145.59(4)[b]
Y_{21} (kHz)	70.5(24)	76.(1)[b]	68.7(24)	74.(1)[b]	67.1(24)	72.(1)[b]
Y_{02} (kHz)	−29.38(13)	−29.9(1)[b,c]	−28.64(13)	−29.2(1)[b,c]	−27.97(13)	−28.5(1)[b,c]
B_e (MHz)	21 787.5(10)		21 514.1(10)		21 259.5(10)	
ω_e (cm^{-1})	1 252.(3)	1 241.4(1)	1 244.(3)		1 237.(3)	
$\omega_e x_e$ (cm^{-1})	5.96(71)	5.9(1)	5.89(71)		5.82(71)	

[a] Numbers in parentheses represent one standard deviation.
[b] Reference 1.
[c] Reference 7.

TABLE III. Potential constants and equilibrium bond length for silicon monoxide.

	This work[a]	Ref. 1
a_0	$5.390(22)\times10^5$ cm^{-1}	$5.298(1)\times10^5$ cm^{-1}
a_1	−2.9899(41)	−2.973(2)
a_2	5.7(7)	5.58(10)
a_3	−9.0(5)	−8.32(75)
r_e	1.509 733(40) Å	1.509 732(40) Å

[a] Errors are in standard deviation.

set of N simultaneous equations in six unknowns was constructed, where N is the number of experimentally measured frequencies and where the six unknown constants are Y_{01}, Y_{11}, Y_{21}, and Y_{02} for $^{28}Si^{16}O$, plus the Y_{01} values for $^{29}Si^{16}O$ and $^{30}Si^{16}O$. By the method of least squares, this set of equations was solved for these constants. The vibrational constants Y_{10} and Y_{20} were calculated for each isotopic species by use of the following relations:

$$Y_{10} = (4Y_{01}^3/ - Y_{02})^{1/2} \tag{6}$$

and

$$Y_{20} = \tfrac{3}{2}Y_{01}(a_2 - \tfrac{5}{4}a_1^2)\,, \tag{7}$$

where a_1 and a_2 are the Dunham potential constants which appear in Eq. (1).

RESULTS AND COMMENTS

Table II summarizes the results of this analysis and gives a comparison of the rotational, vibrational, and potential constants derived from our measurements with those obtained by others.

TABLE IV. Predicted rotational spectrum of silicon monoxide.

Transition		$^{28}Si^{16}O$		$^{29}Si^{16}O$		$^{30}Si^{16}O$	
v	$J\rightarrow J'$	Predicted frequency	Uncertainty	Predicted frequency	Uncertainty	Predicted frequency	Uncertainty
0	0→1	43 423.798	0.015	42 879.820	0.025	42 373.340	0.025
1	0→1	43 122.027	0.015	42 583.710	0.028	42 082.469	0.028
2	0→1	42 820.539	0.015	42 287.874	0.030	41 791.866	0.030
3	0→1	42 519.332	0.015	41 992.314	0.030	41 501.531	0.030
4	0→1	42 218.407	0.026	41 697.028	0.035	41 211.465	0.034
5	0→1	41 917.764	0.052	41 402.018	0.053	40 921.667	0.052
0	1→2	86 846.891	0.028	85 758.953	0.050	84 746.009	0.050
1	1→2	86 243.350	0.020	85 166.732	0.056	84 164.266	0.056
2	1→2	85 640.373	0.022	84 575.061	0.060	83 583.060	0.060
3	1→2	85 037.959	0.025	83 983.940	0.060	83 002.391	0.060
4	1→2	84 436.110	0.052	83 393.369	0.070	82 422.259	0.069
5	1→2	83 834.824	0.103	82 803.348	0.106	81 842.663	0.103
0	2→3	130 268.574	0.037	128 636.710	0.076	127 117.335	0.076
1	2→3	129 363.262	0.027	127 748.379	0.085	126 244.721	0.085
2	2→3	128 458.796	0.030	126 860.873	0.092	125 372.912	0.092
3	2→3	127 555.176	0.034	125 974.192	0.092	124 501.908	0.092
4	2→3	126 652.402	0.075	125 088.335	0.105	123 631.710	0.104
5	2→3	125 750.473	0.153	124 203.303	0.158	122 762.317	0.154
0	3→4	173 688.142	0.046	171 512.406	0.104	169 486.647	0.104
1	3→4	172 481.060	0.035	170 327.964	0.118	168 323.162	0.117
2	3→4	171 275.105	0.041	169 144.623	0.127	167 160.750	0.127
3	3→4	170 070.278	0.045	167 962.381	0.126	165 999.411	0.126
4	3→4	168 866.579	0.098	166 781.239	0.142	164 839.147	0.140
5	3→4	167 664.008	0.202	165 601.196	0.210	163 679.957	0.205
0	4→5	217 104.891	0.058	214 385.351	0.138	211 853.275	0.137
1	4→5	215 596.037	0.052	212 904.800	0.157	210 398.918	0.156
2	4→5	214 088.594	0.061	211 425.623	0.168	208 945.902	0.167
3	4→5	212 582.560	0.062	209 947.820	0.166	207 494.230	0.165
4	4→5	211 077.936	0.122	208 471.392	0.183	206 043.899	0.181
5	4→5	209 574.722	0.249	206 996.339	0.264	204 594.912	0.258
0	5→6	260 518.114	0.084	257 254.860	0.181	254 216.546	0.180
1	5→6	258 707.489	0.086	255 478.198	0.206	252 471.317	0.204
2	5→6	256 898.557	0.095	253 703.185	0.219	250 727.699	0.217
3	5→6	255 091.317	0.094	251 929.823	0.216	248 985.692	0.214
4	5→6	253 285.768	0.152	250 158.109	0.232	247 245.296	0.228
5	5→6	251 481.912	0.298	248 388.046	0.322	245 506.510	0.315

Törring[1] could not determine the effects of centrifugal distortion from his microwave measurements alone; but, by combining his accurate measurements of the $J = 0 \rightarrow 1$ transition with the earlier measurements of the vibrational spectra of SiO by Lagerqvist and Uhler,[7] he was able to make corrections for these effects in his derived constants. We believe that the vibrational constant ω_e, which we have derived entirely from microwave measurements (see Table II), is more accurate than the values obtained more directly from vibrational spectra. The inclusion of Törring's frequencies for the $J = 0 \rightarrow 1$ transitions with our results did not alter the constants derived from our results alone. We conclude that his measurements are at least as accurate as ours.

Table III gives the Dunham potential constants a_0, a_1, a_2, a_3 which were calculated from the $Y_{l,m}$'s of Table II. The Y_{12} constant, which is necessary for the computation of the constants a_2 and a_3 but not recorded in Table II, was found to be zero within the limits of experimental error. A contribution to the uncertainty in the a_i from a calculated upper limit for Y_{12} is included in our estimates of the uncertainty in the a_i. This contribution, as well as other contributions, was neglected in Törring's uncertainties. Although our listed uncertainties are somewhat larger than those quoted for previous work, our a_i values are, in fact, substantially more accurate. The values for B_e which appear in Table II were obtained from Y_{01} by application of the Dunham correction. The wobble-stretch correction is zero to within experimental error, but a calculated upper limit on it is included in the uncertainty.[5]

Table IV shows a set of predictions of all transitions that appear to be of possible astrophysical interest as well as the uncertainties in these predictions. For the higher v, J states, these predictions are comparable in accuracy with the experimental observations, but at low v, J they are substantially better.

---

*Supported by U. S. Army Research Office, Grant DAHCO4 74 G0034.

[1]T. Törring, Z. Naturforsch. 23a, 777 (1968).
[2]L. E. Snyder and D. Buhl, Astrophys. J. 189, L31 (1974).
[3]F. J. Lovas and D. R. Johnson (unpublished).
[4]L. E. Snyder and D. Buhl, Astrophys. J. 197, 329 (1975).
[5]E. L. Manson, F. C. De Lucia, and W. Gordy, J. Chem. Phys. 62, 1040 (1975).
[6]J. L. Dunham, Phys. Rev. 41, 721 (1932).
[7]A. Lagerqvist and U. Uhler, Ark. Fys. 6, 95 (1953).

(8)

Millimeterwave spectroscopy of active laser plasmas; the excited vibrational states of HCN[a)]

Franck C. De Lucia

Department of Physics, Duke University, Durham, North Carolina 27706

Paul A. Helminger[b)]

Department of Physics, University of South Alabama, Mobile, Alabama 36688
(Received 30 June 1977)

Millimeter and submillimeter microwave techniques have been used for the spectroscopic study of an HCN laser plasma. Forty-seven rotational transitions in 12 excited vibrational states have been observed. Numerous rotational, vibrational, and perturbation parameters have been calculated from these data. A discussion of experimental techniques is included.

I. INTRODUCTION

The selective excitation of vibrational states in discharges or in the products of discharges is the basis for a number of important molecular lasers. Calculations based on oscillation threshold conditions show that these highly excited states are sufficiently populated in active laser plasmas for study by the techniques of quasioptical millimeter and submillimeter microwave spectroscopy. Most molecular lasers are active on small molecular species with large rotational constants and favorable partition functions. As a result, spectral coverage throughout the millimeter region and into the submillimeter region is required if for no other reason than to reach the transitions of interest. Microwave studies of these highly excited vibrational states are uncommon due to their vanishingly small populations at room temperature.

Many interesting and complex vibration–rotation interactions become important at microwave resolution and can be studied by these techniques. In addition, they are a powerful means for the study of the physics of the complex molecular laser systems. We have given a preliminary report on a study of the HCN laser[1] and a full discussion will be published elsewhere.

HCN has been extensively studied in the infrared and has been the prototype molecule for investigations of vibration–rotation interactions in linear molecules.[2–6] Rotational transitions in the ground vibrational state were among the first to be observed by millimeter microwave spectroscopy[7] and transitions in low lying, thermally populated vibrational states have also been investigated.[5,6,8] In this paper are reported spectroscopic studies in the millimeter and submillimeter microwave region of 12 excited vibrational states of HCN. Included are the 11^10 and 04^00 states which are the basis of the well known laser emission in the far infrared.

II. EXPERIMENTAL

The millimeter and submillimeter wave region of the spectrum is in many ways ideal for the study of the molecular species contained in laser plasmas. A corollary of the well-known difficulty of producing radiation in this spectral region is that laser plasmas emit almost no interfering radiation. It can also be shown that the noise modulation of the microwave signal due to fluctuations in the index of refraction which result from plasma instabilities decreases systematically with increases in frequency. In addition, at lower microwave frequencies, the quasioptical techniques that allow the remote sampling of the plasma are difficult and rotational line strengths decrease as approximately ν^3. At infrared wavelengths the vibrational transitions are orders of magnitude weaker than the strong pure-rotational transitions studied in this work, and the emission of noise increases sharply. It is interesting to note that other spectroscopic techniques have been unable to establish the existence of HCN in *any* vibrational state in the laser plasma.[9]

Figure 1 shows the details of the system used for this study.[10] Energy in the millimeter and submillimeter region is produced by klystron driven crystal harmonic generation. The output of this generator is focused by quasioptical techniques through the laser plasma and detected by an InSb photodetector which operates at 1.4 °K. Because only the stretching modes are preferentially excited in a laser discharge,[1] the lower energy bending modes were thermally populated in a cell at 600 °K. The sensitivity of this technique is such that all studies reported in this paper are either the result of real time measurements on an oscilloscope screen or lock-in techniques with $\tau \leq 1$ sec.

III. THEORY

In principle, the energy levels and rotational transition frequencies of HCN can be calculated by construction and diagonalization of the vibration–rotation Hamiltonian. Although this procedure leads directly to the unperturbed spectral constants, it requires iterative nonlinear fitting and makes prediction of unobserved spectral lines cumbersome. As a result, the emphasis in this section will be placed upon the relation between effective constants defined by

$$E_r = B_{\rm eff} J(J+1) - D_{\rm eff} J^2(J+1)^2 + H_{\rm eff} J^3(J+1)^3 , \quad (1)$$

and the unperturbed spectral constants of the several vibrational states, B_v, D_v, q_v, q'_v, etc.

[a)] This work was supported by the U. S. Army Research Office, Grant No. DAAG29-77-G-0007.

[b)] Travel to Duke University supported by the Southern Regional Education Board of Atlanta.

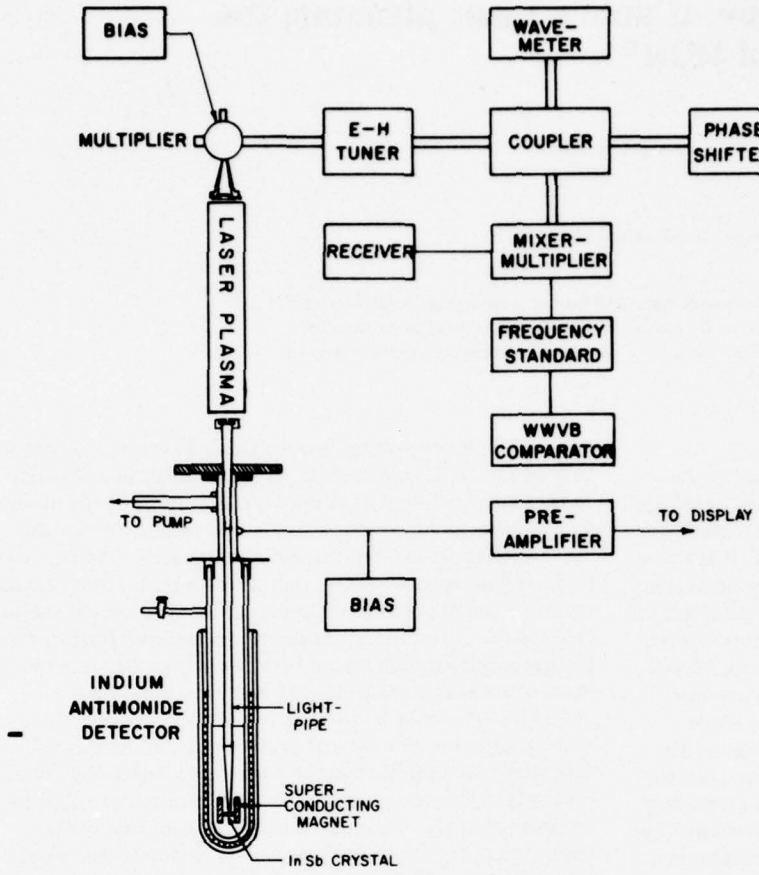

FIG. 1. Spectrometer for the study of laser plasmas.

A. Effects of *l*-type doubling

The basic theory of l-type doubling has been developed by Amat and Nielsen[11,12] and extended and applied by Maki and Lide.[5] The notation used here is consistent with that of Ref. 5.

For linear triatomic molecules vibrational states are specified as v_1, v_2^l, v_3, and states with $l = 0, 1, 2, 3\ldots$ are referred to as Σ, π, Δ, Φ, ... For all states with $v_2 \geq 1$, there exists a multiplet of vibrational states that is degenerate in the harmonic approximation. The contributions of l-type resonances to the lifting of these degeneracies can be calculated by the solution of a secular determinant of dimension (v_2+1).

For $v_2 = 1$, the secular determinant is of the form

$$\begin{vmatrix} E_v^0 - \epsilon & \frac{1}{2}W_{11} \\ \frac{1}{2}W_{11} & E_v^0 - \epsilon \end{vmatrix} = 0 , \tag{2}$$

with $W_{11} = q_v J(J+1)$. E_v^0 is the unperturbed energy of the 01^10 state. The rotational contribution to this energy is

$$E_v = B_v[J(J+1) - l^2] - D_v[J(J+1) - l^2]^2 . \tag{3}$$

When centrifugal distortion in the l-type doubling constant is included, Eq. (2) gives for its solutions

$$E_v^{\pm} = B_v[J(J+1) - l^2] \pm \tfrac{1}{2}q_v J(J+1) \mp \tfrac{1}{2}q_v' J^2(J+1)^2 - D_v[J(J+1) - l^2]^2 . \tag{4}$$

It should be recognized that this equation contains terms of the form $B_v l^2$ and $D_v l^4$ that are not functions of J and do not contribute to the rotational frequencies. In this paper these will be considered to be part of the vibrational energy, thereby making Eqs. (1) and (3) compatible. Equation (4) can be factored into coefficients of $J(J+1)$ and $J^2(J+1)^2$ to give

$$B_{eff}^{\pm} = B_v \pm \tfrac{1}{2}q_v + 2D_v \tag{5}$$

$$D_{eff}^{\pm} = D_v \pm \tfrac{1}{2}q_v' . \tag{6}$$

For $v_2 = 2$ the secular determinant is of the form[5]

$$\begin{vmatrix} E_\Delta^0 - \epsilon & W_{20} & 0 \\ W_{20} & E_\Sigma^0 - \epsilon & W_{20} \\ 0 & W_{20} & E_\Delta^0 - \epsilon \end{vmatrix} = 0 \tag{7}$$

with

$$W_{20} = (q_v/\sqrt{2})[J^2(J+1)^2 - 2J(J+1)]^{1/2} .$$

Solution of this equation gives

$$E_\Sigma = E_\Sigma^0 + \tfrac{1}{2}\delta - \tfrac{1}{2}\{\delta^2 + 4q_v^2[J^2(J+1)^2 - 2J(J+1)]\}^{1/2} \tag{8}$$

$$E_{\Delta d} = E_\Delta^0 \tag{9}$$

$$E_{\Delta_c} = E^0_\Delta - \tfrac{1}{2}\delta + \tfrac{1}{2}\{\delta^2 + 4q_v^2[J^2(J+1)^2 - 2J(J+1)]\}^{1/2}, \tag{10}$$

where $\delta = E^0_\Delta - E^0_\Sigma$. The rotational contribution to E^0_Σ and E^0_Δ is given by Eq. (3).

For transitions in the millimeter and submillimeter microwave region, these expressions can be expanded and compared with Eq. (1) to give

$$E_\Sigma = E^0_\Sigma - (q_v^2/\delta)[J^2(J+1)^2 - 2J(J+1)] \tag{11}$$

$$B_v = B_{eff} - 2(q_v^2/\delta) \tag{12}$$

$$D_v = D_{eff} - (q_v^2/\delta) \tag{13}$$

$$E_{\Delta c} = E^0_\Delta + (q_v^2/\delta)[J^2(J+1)^2 - 2J(J+1)] \tag{14}$$

$$B_v = B_{eff} + 2q_v^2/\delta - 8D_v \tag{15}$$

$$D_v = D_{eff} + (q_v^2/\delta) \tag{16}$$

$$E_{\Delta d} = E^0_\Delta \tag{17}$$

$$B_v = B_{eff} - 8D_v \tag{18}$$

$$D_v = D_{eff}\ . \tag{19}$$

For $v_2 = 3$, the secular determinant is of the form

$$\begin{vmatrix} E^0_\phi - \epsilon & W_{31} & 0 & 0 \\ W_{31} & E^0_\pi - \epsilon & W_{11} & 0 \\ 0 & W_{11} & E^0_\pi - \epsilon & W_{31} \\ 0 & 0 & W_{31} & E^0_\phi - \epsilon \end{vmatrix} = 0\ , \tag{20}$$

with $W_{31} = [\sqrt{3}\,q_v/2][J^2(J+1)^2 - 8J(J+1) + 12]^{1/2}$. Solution of this equation gives

$$E_{\pi_d} = E^0_\pi + \tfrac{1}{2}\delta + \tfrac{1}{2}W_{11} - \tfrac{1}{2}\{[\delta - W_{11}]^2 + 4W_{31}^2\}^{1/2} \tag{21}$$

$$E_{\phi_d} = E^0_\phi - \tfrac{1}{2}\delta + \tfrac{1}{2}W_{11} + \tfrac{1}{2}\{[\delta - W_{11}]^2 + 4W_{31}^2\}^{1/2} \tag{22}$$

$$E_{\pi_c} = E^0_\pi + \tfrac{1}{2}\delta - \tfrac{1}{2}W_{11} - \tfrac{1}{2}\{[\delta + W_{11}]^2 + 4W_{31}^2\}^{1/2} \tag{23}$$

$$E_{\phi_c} = E^0_\phi - \tfrac{1}{2}\delta - \tfrac{1}{2}W_{11} + \tfrac{1}{2}\{[\delta + W_{11}]^2 + 4W_{31}^2\}^{1/2}, \tag{24}$$

where $\delta = E^0_\phi - E^0_\pi$. When centrifugal distortion is included, for π_d states

$$B_v = B_{eff} - q_v - 6q_v^2/\delta - 2D_v \tag{25}$$

$$D_v = D_{eff} - q'_v - \tfrac{3}{4}(q_v^2/\delta) \tag{26}$$

$$H_v = H_{eff} + q_v^3/\delta^2 \tag{27}$$

For π_c states:

$$B_v = B_{eff} + q_v - 6q_v^2/\delta - 2D_v \tag{28}$$

$$D_v = D_{eff} + q'_v - \tfrac{3}{4}(q_v^2/\delta) \tag{29}$$

$$H_v = H_{eff} - q_v^3/\delta^2\ . \tag{30}$$

Only the $l = 0$ state of $v_2 = 4$ was studied and since there is no l degeneracy for this state, perturbation theory may be used to calculate the effects of l doubling.

$$E_\Sigma = E^0_\Sigma + \frac{2[W_{02}]^2}{E_\Sigma - E_\Delta} = E^0_\Sigma - \frac{3q_v^2}{\delta}[J^2(J+1)^2 - 2J(J+1)] + \frac{12\gamma_{11}q_v^2}{\delta^2}[J^3(J+1)^3 - 2J^2(J+1)^2], \tag{31}$$

and

$$B_v = B_{eff} - 6q_v^2/\delta \tag{32}$$

$$D_v = D_{eff} - \frac{3q_v^2}{\delta} - \frac{24\gamma_{11}q_v^2}{\delta^2} \tag{33}$$

$$H_v = H_{eff} - 12\gamma_{11}q_v^2/\delta^2\ . \tag{34}$$

The term which contains γ_{11} results from the expansion of $E_\Sigma - E_\Delta$ and accounts for the difference between the rotational constants of the 04^00 and 04^20 states.

B. Effects due to Coriolis coupling between 11^10 and 04^00

Because a near degeneracy exists between the rotational levels of the 11^10 and 04^00 vibrational states at $J = 10$, it is not possible to fit either the 11^10 or 04^00 data on the basis of the effective constants of Eq. (1). The perturbation between the states can be given by[4]

$$\Delta^2 = \delta^2 + 4J(J+1)W_{\alpha i}^2\ , \tag{35}$$

where δ is the separation of the unperturbed states, Δ the separation of the perturbed states, and $W_{\alpha i}$ the Coriolis constants. δ is a function of J and can be expressed as

$$\delta = \Delta E_0 - \Delta BJ(J+1) + \Delta DJ^2(J+1)^2\ , \tag{36}$$

where ΔE_0 represents vibrational energy difference between the two states.

III. RESULTS

A. Observed frequencies and effective rotational constants

Table I displays the forty-seven rotational transitions in 12 different excited vibrational states that have been observed. With the exception of the rotational transitions in the 04^00 and 11^10 states, all may be represented by the effective rotational constants of Eq. (1). These effective constants are shown in Table II. Also included are precise ground-state constants which were calculated from the results of a beam maser experiment of De Lucia and Gordy.[13]

B. Unperturbed rotational constants

Since the rotational levels of the 10^00, 20^00, 00^01, 00^02, and 10^01 are essentially unperturbed, the effective constants of Table II are also the unperturbed spectral constants for these states.

Table III shows the unperturbed rotational constants for all states for which corrections between the effective and unperturbed constants are necessary. Equations (5) and (6) show that the constants for 01^10 can be obtained by the averaging of the effective constants for the two components and subtracting $2D_v$. A similar procedure was used for the 01^11 state. Equations (11)–(13) were used to calculate the constants of the 02^00 and the results of Eqs. (14)–(19) were used for the 02^20 state. Because the $J = 0 \rightarrow 1$ and $1 \rightarrow 2$ transitions do not exist for states with $l = 2$, there is no experimental redundancy within the 02^20 state and the listed standard deviations reflect estimated experimental uncertainty. Equations (25)–(30) were used to calculate the constants for the 03^10 state.

TABLE I. Observed transition frequencies in vibrationally excited HCN (MHz).[a]

	$J=0\rightarrow1$		$J=1\rightarrow2$		$J=2\rightarrow3$		$J=3\rightarrow4$	
State	Observed	Obs.-calc.	Observed	Obs.-calc.	Observed	Obs.-calc.	Observed	Obs.-calc.
$01^{1c}0$	...		177 238.73[b]	0.04	265 852.68	−0.02	354 460.33	0.01
$01^{1d}0$	...		178 136.50[b]	−0.02	267 199.37	0.01	356 255.71	0.00
$02^{0}0$	89 087.69[b]	0.04	178 170.38	0.01	267 243.15	−0.07	356 301.33	0.04
$02^{2d}0$	...		...		267 109.37		356 135.46	
$02^{2c}0$	...		...		267 120.02		356 162.77	
$03^{1c}0$	...		177 698.78	0.02	266 540.00	−0.04	355 371.69	0.02
$03^{1d}0$	...		179 547.32	−0.10	269 312.89	0.16	359 067.86	−0.07
$04^{0}0$			179 127.26[c]		268 663.29[c]			
$10^{0}0$	88 027.28[d]	0.03	176 052.38	−0.01	264 073.30	−0.01	352 087.89	0.01
$20^{0}0$	87 419.40[d]	0.06	174 836.53	−0.04	262 249.60	0.01	349 656.27	−0.00
$00^{0}1$	88 006.69[d]	0.03	176 011.26	0.03	264 011.53	−0.08	352 005.76	0.04
$00^{0}2$			174 725.29		262 082.87			
$10^{0}1$	87 415.29	0.07			262 237.31	−0.07	349 640.22	0.04
$01^{1c}1$	...				264 005.10		351 996.75	
$01^{1d}1$	...		176 919.08		265 373.12			
$11^{1c}0$	...				264 019.77[c]	−0.09	352 016.88[c]	0.07
$11^{1d}0$	...		176 913.10		265 364.36			

[a]Corrected for quadrupole splittings.
[b]From Ref. 6.
[c]See footnote b, Table II.
[d]These lines have also been observed by R. C. Woods (private communication).

C. The $11^{1}0/04^{0}0$ system

The $11^{1}0$ and $04^{0}0$ states must be considered together because of the Coriolis coupling between them. This is an exceedingly important and interesting system. It is the basis of the well known far-infrared laser.[14] The absolute frequency measurement of the laser emissions[15] coupled with the pure rotational transition measured in this study make possible the calculation of a number of parameters to high accuracy, including the centrifugal distortion parameters for both states, the Coriolis interaction constant W_{a1}, and the energy difference between the two vibrational states ΔE_0. These constants are shown in Table IV and the transition frequencies calculated from them are compared with the observed frequencies shown in Table V. It is interesting to note that vibrational energy difference between the $04^{0}0$ and $11^{1}0$ states has been calculated to ± 0.0001 cm^{-1}.

In addition to the Coriolis perturbation, both the $11^{1}0$ and $04^{0}0$ states are affected by l-type doubling. Equations (32) and (33) provide the corrections for the $04^{0}0$ state, but values of q_v and δ are required. The value of q_v can be extrapolated from the values for the $01^{1}0$, $02^{2}0$, and $03^{1}0$ states and Maki gives $E^{0}_{\Delta} - E^{0}_{\Sigma}$ to be 15.225 cm^{-1}. The unperturbed values of both $B_{04^{0}0}$ and $D_{04^{0}0}$ are shown in Table III. $D_{04^{0}0}$ is a very sensitive test of q_v and δ. Its value is in good agreement with its expected value and this serves as a confirmation of the values of q_v and δ used in Eq. (33).

TABLE II. Effective rotational constants for excited vibrational states of HCN (MHz).

	B_{eff}		D_{eff}	
State	Constant	σ	Constant	σ
$00^{0}0$	44 315.9757	0.0004	0.08724	0.00006
$01^{1c}0$	44 310.381	0.013	0.0888	0.0005
$01^{1d}0$	44 534.851	0.004	0.0902	0.0002
$02^{0}0$	44 544.233	0.014	0.2054	0.0006
$02^{2d}0$	44 519.895		0.0926	
$02^{2c}0$	44 519.563		−0.0245	
$03^{1c}0$	44 425.766[a]	0.013	0.1350[a]	0.0005
$03^{1d}0$	44 887.974[a]	0.050	0.1397[a]	0.0021
$04^{0}0$	44 785.584[b]	0.051	0.45297[b]	0.00034
$10^{0}0$	44 013.803	0.006	0.0881	0.0003
$20^{0}0$	43 709.846	0.014	0.0879	0.0006
$00^{0}1$	44 003.505	0.015	0.08716	0.0006
$00^{0}2$	43 681.998		0.0844	
$10^{0}1$	43 707.783	0.036	0.0863	0.0014
$01^{1c}1$	44 002.465		0.0898	
$01^{1d}1$	44 230.503		0.0917	
$11^{1c}0$	44 004.714[b]	0.037	0.08873[b]	0.00016
$11^{1d}0$	44 229.006		0.0912	

[a]Interactions with $03^{3}0$ produce an H_{eff} that makes a significant contribution at low J. To reproduce the calculated frequencies of Table I; for $03^{1c}0$, $H_{eff} = -1.52\times10^{-5}$ MHz, and for $03^{1d}0$, $H_{eff} = +1.52\times10^{-5}$ MHz.
[b]Because of the Coriolis perturbation between the rotational levels of the $04^{0}0$ and $11^{1c}0$ states, these constants will not reproduce the rotational levels without the use of Eqs. (35) and (36) and the constants in Table IV.

TABLE III. Unperturbed rotational constants of the perturbed excited vibrational states of HCN (MHz).

	B_v		D_v	
State	Constants	σ	Constant	σ
$01^{1}0$	44 422.438	0.007	0.0895	0.0003
$02^{0}0$	44 544.004	0.014	0.0908	0.0006
$02^{2}0$	44 519.112	0.050	0.0914	0.0015
$03^{1}0$	44 656.332	0.026	0.0933	0.0010
$04^{0}0$	44 784.866	0.05	0.0937	0.0005
$01^{1}1$	44 116.303	0.05	0.0908	0.0010
$11^{1}0$	44 116.680	0.05	0.0900	0.0010

TABLE IV. Spectral constants calculated from the $04^00/11^1c_0$ system (MHz).

Constant	Value	σ
W_{ai}	112.27	0.06
ΔE_0	78663.1	4.0
$(B_{04}0_0)_{eff}$	44785.58	0.05
$(D_{04}0_0)_{eff}$	0.45297	0.00034
$(B_{11}1c_0)_{eff}$	44004.71	0.04
$(D_{11}1c_0)_{eff}$	0.08873	0.00016

D. Vibrational effects of moments of inertia

The relation between the effective and equilibrium constants can be expressed as

$$B_v = B_e - \sum_i \alpha_i(v_i + \tfrac{1}{2}d_i) + \sum_{ij} \gamma_{ij}(v_i + \tfrac{1}{2}d_i)(v_j + \tfrac{1}{2}d_j) + \sum_{ijk} \epsilon_{ijk}(v_i + \tfrac{1}{2}d_i)(v_j + \tfrac{1}{2}d_j)(v_k + \tfrac{1}{2}d_k) + \gamma_{11} l^2 . \quad (37)$$

Table VI shows a comparison between the constants calculated from extensive infrared data and the previously existing microwave data[6] and an analysis of our microwave data alone. It is necessary to include the ϵ_{222} term in our expansion because of the significantly larger amount of microwave data now available. Previously, microwave data for only two excited bending modes were available and they essentially determined α_2 and γ_{22}. It is interesting to note that ϵ_{222} makes a significant contribution to the B_v of the lower bending modes as evidenced by the differences between the B_e, α_2, and γ_{22} of the two analyses.

TABLE V. Analysis of the $04^00/11^1c_0$ system (MHz).

Transition $v'-v''$ $J'-J''$	Observed	Obs.-calc.	Coriolis Perturbation
04^00-04^00 2–1	179127.26	0.12	−0.69
04^00-04^00 3–2	268663.29	−0.08	−1.15
04^00-04^00 9–8	804750.9[a]	0.00	−61.35
04^00-04^00 10–9	894414.2[a]	0.28	524.42
11^10-04^00 10–9	890760.7[a]	−0.27	−327.87
11^10-04^00 11–10	964313.4[a]	0.28	−517.22
11^10-11^10 2–1	176016.82	0.08	0.69
11^10-11^10 3–2	264019.77	−0.09	1.15
11^10-11^10 4–3	352016.88	0.07	1.79
11^10-11^10 11–10	967965.8[a]	−0.28	335.07

[a]Measured frequencies of HCN laser emission lines from Ref. 14.

TABLE VI. Equilibrium rotational constant expansion (MHz).

Constant	This work Value	σ	Reference 6 Value	σ
B_e	44511.62	0.03	44512.36	0.23
α_1	300.028	0.03	299.043	0.57
α_2	−108.369	0.05	−106.774	0.075
α_3	312.983	0.03	313.163	0.270
γ_{11}	−0.893	0.009	−1.049	0.300
γ_{12}	−3.583	0.033	−4.116	0.075
γ_{13}	6.448	0.027	6.625	0.210
γ_{22}	0.762	0.027	1.532	0.015
γ_{23}	6.332	0.033	6.434	0.075
γ_{33}	−4.521	0.018	−4.527	0.008
ϵ_{222}	0.094	0.003	...	...
γ_{11}	−6.224	0.006	−6.056	0.010

Although our constants result from a fit of 12 constants to only 13 microwave data points, the constants which result accurately predict, with the several exceptions, the infrared ΔB which were used in the previous analysis and the weighted addition of this infrared data to our analysis makes no significant change in our calculated constants.

The ΔB's which are not well predicted are interesting. The value of ΔB for 02^20-02^00 is $-80.72\pm0.30\times10^{-5}$ cm^{-1}.[5] The microwave value for this ΔB is $-83.02\pm0.17\times10^{-5}$ cm^{-1}, an analysis of all microwave data predicts $-83.05\pm0.03\times10^{-5}$ cm^{-1}, and an analysis of all microwave data except B_{02^20} predicts -83.09×10^{-5} cm^{-1}. Since the calculation of the previous value requires a complicated and indirect calculation, assumptions about other spectroscopic constants, and since a more recent version of this calculation now gives $-82.23\pm0.24\times10^{-5}$ cm^{-1},[16] it would seem reasonable to conclude that this does not represent any real inconsistency with our analysis.

Our predictions of the ΔB for the 12^00-01^10 band differs by about three times the stated uncertainty of $\pm0.7\times10^{-5}$ cm^{-1}. But the difference between this ΔB and the ΔB for the 12^20-01^10 is $-80.80\pm1.1\times10^{-5}$ cm^{-1}. This value is in excellent agreement with the 02^20-02^00 ΔB of Ref. 6, but differs from both the newer $\Delta B_{02^20-02^00}$ of Ref. 16 and our microwave data.

The value of ΔB for 05^10-01^10 of 1590 ± 15 cm^{-1} differs from our predicted value by 20 cm^{-1}. It is interesting to note that the 12^00, 12^20 and 05^10 are involved in a Coriolis interaction and were analyzed together.

Recently, Maki[16] has made some highly precise measurements on hot bands of HCN and has results which question the completeness of Eq. (37). For example, he finds $\Delta B(12^00-02^00) = -999.26(31)\times10^{-5}$ cm and $\Delta B(12^20-02^20) = -999.95(29)\times10^{-5}$ cm. In the context of Eq. (37) these two values should be the same. At face value these results require terms to be added to Eq. (37) which mix v_i and l. However, it is also possible that since the analyses used to produce these re-

sults require the fixing of energy levels and spectroscopic constants derived from microwave and other infrared experiments and since the uncertainties quoted do not include systematic errors in the experiments, errors in the fixed energy levels and constants, or model errors, the actual uncertainties are somewhat larger and no inconsistency exists. It should be pointed out that the ΔB predicted from the microwave numbers and Eq. (37) generally fall within the range of values for the infrared multiplet. In addition to providing improved spectral parameters, this calculation is necessary for the assignment of the rotational transitions in several of the vibrational states studied. This is because of the near degeneracy caused by the similar values of B_{eff} for $11^{1d}0$ and $01^{1d}1$ and for 001, $11^{1c}0$, and $01^{1c}1$.

IV. CONCLUSIONS

It has been demonstrated that millimeter and submillimeter microwave spectroscopy is an effective and sensitive probe of active laser plasmas. Since these plasmas contain large, nonequilibrium populations in excited vibrational states, these studies also yield substantial amounts of new, high precision microwave data. These results make possible the calculation of the rotational spectrum of HCN over a wide range of vibrational and rotational states. For most states these calculations are especially convenient because of the relations provided between the effective and unperturbed constants.

It should also be noted that this is a technique that can be used for the study of the otherwise inaccessible excited vibrational states of many molecules. Because the kinetic and rotational temperatures remain approximately ambient, this technique is substantially more sensitive than the hot cell method, especially for highly excited states.

ACKNOWLEDGMENTS

We would like to thank Dr. Arthur G. Maki for illumination about certain aspects of the infrared data analysis and Mr. Arthur Charo for useful suggestions about the manuscript.

The Research Corporation provided support in part for this work.

[1]F. C. De Lucia, Ohio State Molecular Spectroscopy Symposium, RE2 (1976).
[2]D. H. Rank, G. Shorinko, D. P. Eastman, and T. A. Wiggins, J. Opt. Soc. Am. **50**, 421 (1960).
[3]W. W. Brim, J. M. Hoffman, H. H. Nielsen, and K. Narahari Rao, J. Opt. Soc. Am. **50**, 1208 (1960).
[4]A. G. Maki and L. R. Blaine, J. Mol. Spectrosc. **12**, 45 (1964).
[5]A. G. Maki and D. R. Lide, Jr., J. Chem. Phys. **47**, 3206 (1967).
[6]G. Winnewisser, A. G. Maki, and D. R. Johnson, J. Mol. Spectrosc. **31**, 149 (1971).
[7]A. G. Smith, W. Gordy, J. W. Simmons, and W. V. Smith, Phys. Rev. **75**, 260 (1949).
[8]T. Torring, Z. Physik **161**, 179 (1961).
[9]G. W. Chantry, *Submillimeter Spectroscopy*, (Academic, London and New York, 1971).
[10]P. Helminger, F. C. De Lucia, and W. Gordy, Phys. Rev. Lett. **25**, 1397 (1970).
[11]G. Amat and H. W. Nielsen, J. Mol. Spectrosc. **2**, 152 (1958).
[12]G. Amat and H. H. Nielsen, J. Mol. Spectrosc. **2**, 163 (1958).
[13]F. C. De Lucia and W. Gordy, Phys. Rev. **187**, 58 (1969).
[14]D. R. Lide, Jr. and A. G. Maki, Appl Phys. Lett. **11**, 62 (1967).
[15]L. O. Hocker and A. Javan, Phys. Lett. **25A**, 489 (1967).
[16]A. G. Maki, J. Mol. Spectrosc. **58**, 308 (1975).

JOURNAL OF MOLECULAR SPECTROSCOPY 69, 473–481 (1978)

"Forbidden" Millimeter-Wave Transitions in Arsine [1]

DAVID A. HELMS AND WALTER GORDY

Department of Physics, Duke University, Durham, North Carolina 27706

A millimeter-wave spectrometer having a sensitivity of 4×10^{-10} cm^{-1} in the 2-mm region has been used for observation of the "forbidden" transitions $J \rightarrow J$, $K = \pm 4 \rightarrow \pm 1$ and $J \rightarrow J$, $K = \pm 5 \rightarrow \pm 2$ in AsH_3. A comprehensive computer analysis was made of the frequencies measured in this work together with available microwave frequencies of other transitions. This analysis provides accurate values of the rotational constants, nuclear quadrupole couplings, and effective structural parameters of the molecule. The spectral constants B_0 and C_0 (in MHz) are 112 470.597 and 104 884.665, respectively.

I. INTRODUCTION

In a previous paper (*1*) we reported observations of forbidden $\Delta K = \pm 3$ microwave transitions in PH_3 and PD_3. Our measurements of $K = 3 \rightarrow 0$ transitions in PH_3 and $K = 3 \rightarrow 0$ and $K = \pm 4 \rightarrow \pm 1$ transitions in PD_3 confirmed the assignments of the lower-frequency $K = \pm 2 \rightarrow \mp 1$ transitions of PH_3 and of PD_3 reported by Chu and Oka (*2*), and improved significantly the molecular constants, especially C_0. A similar investigation is here described for arsine.

Transitions in AsH_3 obeying the $\Delta J = 0$, $\Delta K = \pm 3$ selection rules were first observed by Chu and Oka (*2*). They reported eight transitions obeying the selection rules $\Delta J = 0$, $K = \pm 2 \rightarrow \mp 1$, $\Delta F = 0$ in the frequency range of 21.16 to 21.84 GHz. The large As quadrupole coupling splits the $K = \pm 2 \rightarrow \mp 1$ line into two doublets, each component of which is an unresolved doublet. Chu and Oka combined their value of C_0 with the known value of B_0 (*3*) and with other information to obtain the zero-point effective, the zero-point average, and the equilibrium structures. Recently, Olson *et al.* (*4*) reported their observation of "perturbation-allowed" transitions of the type $\Delta|K - l| = \pm 3$ in the ν_1 and ν_3 infrared bands of AsH_3. They combined their $\Delta|K - l| = \pm 3$ infrared measurements with the $K = \pm 2 \rightarrow \mp 1$ microwave measurements of Chu and Oka and with the normally allowed $\Delta K = 0$ microwave measurements of Helminger *et al.* (*3*) to obtain both a set of ground state molecular constants and an associated zero-point-effective structure. Olson *et al.* then used the constants for the ν_2 and ν_4 bands given by Sarka, *et al.* (*5*) with their constants for the ν_1 and ν_3 bands to determine the equilibrium structure. Our detection of the $K = \pm 4 \rightarrow \pm 1$ and the $K = \pm 5 \rightarrow \pm 2$ forbidden transitions was assisted by a preliminary prediction of their frequencies from the results of Helminger *et al.*, of Olson *et al.*, and of Chu and Oka.

[1] This work was supported by the U. S. Army Research Office, Grant No. DAAG29-77-G-0007.

0022-2852/78/0693-0473$02.00/0

The need for observation of the higher $K = \pm 4 \rightarrow \pm 1$ and $K = \pm 5 \rightarrow \pm 2$ millimeter-wave transitions described in this paper was indicated by Chu and Oka (*2*), who reported that their spectrometer was not sufficiently sensitive at the higher frequencies to detect them. Measurements of these transitions confirm the assignments of the frequencies measured by Chu and Oka and provide increased accuracy in the values of the spectral constants, particularly those influenced by the distortion caused by rotation about the symmetry axis. For observation of very weak transitions such as these in the shorter millimeter-wave region, we designed an exceptionally sensitive millimeter-wave spectrometer, which is described in the earlier paper (*1*).

The Q-branch $\Delta K = \pm 3$ transitions represent only one class of forbidden transitions in symmetric top molecules included in the general theory of Watson (*6*, *7*) and others (*8*, *9*). Oka (*10*) has recently written an excellent review of the experimental and theoretical developments of this relatively new type of spectra. In the ground vibrational state, the off-axis dipole moment which couples the radiation field to the rotation is induced by centrifugal distortion. The selection rules are determined by the molecular symmetry. In AsH_3, the rotation about the b-axis of inertia induces a small dipole moment ($\approx 3.938 \times 10^{-5}$ D) perpendicular to the symmetry axis which leads to a slight admixture of the K levels and a breakdown of the familiar $\Delta K = 0$ selection rule. The threefold symmetry about the c-axis limits this admixture to K levels differing by three units. It is of interest that centrifugal distortion due to rotation about the symmetry axis can likewise generate a small dipole component along the symmetry axis. This component is of no particular consequence in molecules such as PH_3, PD_3, and AsH_3 which already have permanent dipole moments along the symmetry axis, but it can give rise to forbidden $\Delta J = \pm 1$ transitions in molecules such as CH_4 which has no permanent dipole moment. In fact, $\Delta J = 1$ rotational transitions in CH_4, SiH_4, and GeH_4 have been observed by Rosenberg *et al.* (*11–14*) in the far-infrared region. Kreiner *et al.* (*15*) have used Laser–Stark spectroscopy to measure the distortion-induced dipole moment of GeH_4. Forbidden transitions of CH_4 in the ground vibrational state have also been detected in the microwave region by Holt *et al.* (*16*). At a recent symposium, Kagann *et al.* (*17*) reported their observations of over 140 Q-type $\Delta K = \pm 3$ microwave transitions in OPF_3.

II. EXPERIMENTAL DETAILS

The millimeter-wave spectrometer and the experimental procedure used in these measurements are described in the earlier paper (*1*). The high sensitivity of this spectrometer ($\approx 4 \times 10^{-10}$ cm^{-1} at 144 GHz for a time constant of 1 sec) made possible the measurement of these weak $\Delta K = \pm 3$ transitions with an estimated accuracy of three parts in 10^7.

III. THEORETICAL BACKGROUND

As a result of centrifugal distortion, the rotational wavefunction $\psi_{J,K}$ of a molecule having C_{3v} symmetry mixes slightly with the wavefunction $\psi_{J,K\pm 3}$ in the ground vibrational state. The term in the Hamiltonian responsible for the interaction may be ex-

pressed (*18*) as

$$H' = \frac{h^4\tau_{zzzz}}{4}[(J_+^3 + J_-^3)J_z + J_z(J_+^3 + J_-^3)], \tag{1}$$

where τ_{zzzz} is a centrifugal distortion constant and J_z, J_+, and J_- are rotational operators.

In the absence of the perturbing H' term, the rotational levels are all doubly degenerate for each value of K, ($K \neq 0$). The energy levels corresponding to $K \neq 3$ are raised or lowered, but they remain degenerate with symmetry E. The $K = 3$ level, however, is split into A_1 and A_2 components. The designations A_1, A_2, and E indicate the symmetry of the rovibrational wavefunction (excluding spin). In the case of AsH_3, each of the energy levels is split further into $(2I + 1)$ components by the quadrupole interaction of the $As(I = \frac{3}{2})$ nucleus. The symmetry selection rules for Q-type $\Delta K = \pm 3$ transitions (*19*) are $+ \leftrightarrow -$, along with $A_1 \leftrightarrow A_2$, or $E \leftrightarrow E$.

The formulas giving the energy levels may be expressed (*20*, *21*) for $K \neq 3$ as:

$$\begin{aligned}\frac{E(F,J,K)}{h} &= G(J,K) + \tfrac{1}{2}[C_N + (C_K - C_N)K^2/J(J+1)] \\ &\times [F(F+1) - I(I+1) - J(J+1)] - eQq\left(3\frac{K^2}{J(J+1)} - 1\right) Y(J, \tfrac{3}{2}, F) + \left(\frac{h^4\tau_{zzzz}}{4h}\right)^2 \\ &\times \left\{\frac{(2K-3)^2[J(J+1) - K(K-1)][J(J+1) - (K-1)(K-2)][J(J+1) - (K-2)(K-3)]}{G(J,K) - G(J,K-3)}\right. \\ &\left. + \frac{(2K+3)^2[J(J+1) - K(K+1)][J(J+1) - (K+1)(K+2)][J(J+1) - (K+2)(K+3)]}{G(J,K) - G(J,K+3)}\right\}; \end{aligned} \tag{2}$$

and for $K = 3$ as

$$\begin{aligned}\frac{E^-(F,J,3)}{h} &= G(J,3) + \tfrac{1}{2}[C_N + (C_K - C_N)K^2/J(J+1)] \\ &\times [F(F+1) - I(I+1) - J(J+1)] - eQq\left(3\frac{K^2}{J(J+1)} - 1\right) Y(J, \tfrac{3}{2}, F) \\ &+ \left(\frac{h^4\tau_{zzzz}}{4h}\right)^2 \frac{81[J(J+1) - 12][J(J+1) - 20][J(J+1) - 30]}{G(J,3) - G(J,6)} \\ &+ \left\{h_0 - 18\left(\frac{h^4\tau_{zzzz}}{4h}\right)^2 \Big/ [G(J,0) - G(J,3)]\right\} \\ &\times J(J+1)[J(J+1) - 2][J(J+1) - 6], \end{aligned} \tag{3}$$

TABLE I

Observed Frequencies and Calculated Intensities for the AsH_3 Transitions

Transition			Observed Frequency ν (MHz)	ν Obs-ν Calc	a_{max} (calc) (10^{-10} cm^{-1})
Normal Rotational Transitions					
$J \rightarrow J+1$	$K \rightarrow K$	$F \rightarrow F'$ (a)			
J = 0	K = 0	F = 3/2 → 5/2	224 937.78	-0.01	
0	0	3/2 → 3/2	224 896.85	-0.02	
0	0	3/2 → 1/2	224 909.86	0.02	
1	0	5/2 → 7/2	449 792.43	0.02	
1	0	5/2 → 5/2	449 751.38	0.00	
1	0	3/2 → 3/2	449 821.08	0.02	
1	0	1/2 → 3/2	449 748.06	-0.01	
1	1	5/2 → 7/2	449 813.69	0.03	
1	1	3/2 → 5/2	449 772.90	-0.01	
1	1	1/2 → 3/2	449 823.85	-0.06	
Forbidden Rotational Transitions					
$J \rightarrow J$	$K = \pm 2 \rightarrow \mp 1$	$F \rightarrow F$ (b)			
J = 9		F = 15/2	21 835.96	0.01	1.7
10		17/2	21 627.60	-0.10	1.9
10		19/2	21 624.66	0.29	
11		19/2	21 402.76	0.08	2.0
11		21/2	21 399.84	-0.07	
12		21/2	21 161.96	-0.14	1.9
12		23/2	21 159.68	-0.07	
$J \rightarrow J$	$K = \pm 4 \rightarrow \pm 1$	$F \rightarrow F$ (c)			
J = 8		F = 15/2	110 694.86	0.03	18.7
9		19/2	109 737.88	-0.11	17.9
9		21/2	109 758.26	-0.04	17.9
9		15/2	109 761.53	-0.03	17.9
10		21/2	108 694.21	0.00	20.8
10		19/2	108 696.65	0.04	20.8
10		23/2	108 710.90	0.06	20.8
10		17/2	108 713.34	0.09	20.8

(*continued*)

and

$$\frac{E^+(F,J,3)}{h} = G(J,3) + \tfrac{1}{2}[C_N + (C_K - C_N)K^2/J(J+1)]$$
$$\times [F(F+1) - I(I+1) - J(J+1)] - eQq\left(3\frac{K^2}{J(J+1)} - 1\right)Y(J, \tfrac{3}{2}, F)$$
$$+ \left(\frac{h^4\tau_{zzzz}}{4h}\right)^2 \frac{81[J(J+1)-12][J(J+1)-20][J(J+1)-30]}{G(J,3) - G(J,6)}$$
$$- h_0(J(J+1)[J(J+1)-2][J(J+1)-6], \quad (4)$$

where

$$G(J,K) = B[J(J+1) - K^2] + CK^2 - D_J J^2(J+1)^2 - D_{JK}J(J+1)K^2$$
$$- D_K K^4 + H_{JJK}J^2(J+1)^2K^2 + H_{JKK}J(J+1)K^4$$
$$+ L_{JJKK}J^2(J+1)^2K^4 + H_K K^6 + L_{JJJK}J^3(J+1)^3K^2. \quad (5)$$

TABLE I—*Continued*

Transition		Observed Frequency ν (MHz)	ν Obs-ν Calc	a_{max} (calc) (10^{-10} cm^{-1})
$J \rightarrow J$ $K = \pm 4 \rightarrow \pm 1$ $F \rightarrow F$ (c) (continued)				
11	23/2	107 564.50	0.02	22.1
11	21/2	107 566.25	-0.05	22.1
11	25/2	107 578.28	-0.05	22.1
11	19/2	107 580.14	-0.02	22.1
12	25/2	106 364.89	-0.02	21.5
12	23/2	106 356.38	0.04	21.5
12	27/2	106 366.72	0.09	21.5
12	21/2	106 368.17	0.11	21.5
13	27/2	105 072.41	-0.06	19.4
13	25/2	105 073.65	0.06	19.4
13	29/2	105 082.50	-0.02	19.4
13	23.2	105 083.61	-0.03	19.4
14	29/2	103 725.04	-0.06	16.3
14	27/2	103 725.85	-0.16	16.3
14	31/2	103 733.80	0.00	16.3
14	25/2	103 734.66	-0.06	16.3
15	31/2	102 322.08	0.00	12.9
15	29/2	102 322.95	0.13	12.9
15	33/2	102 329.74	0.05	12.9
$J \rightarrow J$ $K = \pm 5 \rightarrow \pm 2$ $F \rightarrow F$ (c)				
$J =$ 8	$F =$ 17/2	155 785.04	0.07	20.3
8	15/2	155 791.36	0.02	20.3
8	19/2	155 820.52	-0.02	20.3
8	13/2	155 826.92	0.01	20.3
9	19/2	154 443.53	0.10	28.4
9	17/2	154 448.00	0.02	28.4
9	21/2	154 471.86	-0.03	28.4
9	15/2	154 476.40	-0.04	28.4
10	21/2	152 972.59	-0.07	34.7
10	19/2	152 975.92	-0.10	34.7
10	23/2	152 995.93	0.01	34.7
10	17/2	152 999.27	-0.03	34.7

(*continued*)

The $Y(J, I, F)$ which appears in the contribution from the quadrupole interaction may be expressed as:

$$Y(J, I, F) = \frac{\frac{3}{4}C(C+1) - I(I+1)J(J+1)}{2I(2I-1)(2J-1)(2J+3)}, \tag{6}$$

where

$$C = F(F+1) - I(I+1) - J(J+1), \qquad \text{and where } \mathbf{F} = \mathbf{J} + \mathbf{I}. \tag{7}$$

($I = \frac{3}{2}$ in the case of AsH_3 considered here.) The $K = 3$ levels contain the term $\pm h_0 J(J+1)[J(J+1) - 2][J(J+1) - 6]$, first derived by Nielsen and Dennison (*22*) in their explanation of the anomalous effects in $K = 3$ lines observed by early microwave spectroscopists. Unfortunately, we were unable to evaluate the splitting constant h_0 for AsH_3 because the frequencies of the Q-type $K = 3 \rightarrow 0$ series occur below the operating range of our spectrometer.

The line strengths of the forbidden $\Delta K = \pm 3$ transitions (*6*, *23*) are given by

$$S = \tfrac{1}{4}(\theta_z^{xx})_{\text{eff}}^2 (J \mp K)(J \mp K - 1)(J \mp K - 2)(J \pm K + 1)(J \pm K + 2) \times (J \pm K + 3)(2J+1)/J(J+1), \tag{8}$$

TABLE I—*Continued*

Transition		Observed Frequency ν (MHz)	ν Obs-ν Calc	a_{max} (calc) (10^{-10} cm^{-1})
J → J	K = ±5 → ±2 F → F (c) (continued)			
11	23/2	151 380.19	-0.02	38.0
11	21/2	151 382.73	-0.03	38.0
11	25/2	151 398.62	0.02	38.0
11	19/2	151 402.07	-0.10	38.0
12	25/2	149 674.47	-0.02	37.9
12	23/2	149 676.46	-0.02	37.9
12	27/2	149 690.90	-0.01	37.9
12	21/2	149 692.95	0.06	37.9
13	27/2	147 868.05	0.06	34.8
13	25/2	147 866.70	0.14	34.8
13	29/2	147 879.07	0.02	34.8
13	23/2	147 880.72	0.09	34.8
14	29/2	145 962.56	0.07	29.7
14	27/2	145 963.82	0.05	29.7
14	31/2	145 974.66	-0.02	29.7
14	25/2	145 975.96	-0.01	29.7
15	31/2	143 979.43	-0.10	23.7
15	29/2	143 980.44	-0.14	23.7
15	33/2	143 990.14	-0.07	23.7
15	27/2	143 991.25	-0.00	23.7
16	33/2	141 930.83	0.02	17.8
16	31/2	141 931.74	0.07	17.8
16	35/2	141 940.26	0.04	17.8
16	29/2	141 941.05	-0.03	17.8

(a) P. Helminger, E. Beeson, Jr., and W. Gordy, Ref. 3.

(b) Cha and Oka, Ref. 2. One frequency from this reference was omitted.

(c) Present work.

where

$$(\theta_x^{xz})_{\text{eff}} = \theta_x^{xz} + h^4 \tau_{xxxz} \mu_z / [2h(B - C)] \tag{9}$$

is the effective dipole moment inducing the transition. The term,

$$\theta_x^{xz} = 2(B)^2 \left[\frac{a_3^{xz}}{\nu_3^2} \left(\frac{\partial \mu_x}{\partial Q_3} \right) + \frac{a_4^{xz}}{\nu_4^2} \left(\frac{\partial \mu_x}{\partial Q_4} \right) \right], \tag{10}$$

is an induced dipole component which results from admixture of the ground vibrational state with excited vibrational modes. The last term of Eq. (9) results from centrifugally induced mixing of rotational levels of the ground vibrational state. In this expression, τ_{xxxz} is the centrifugal distortion constant in H' of Eq. (1), μ_z is the permanent dipole moment, and C and B are the spectral constants with respect to the symmetry axis and the perpendicular axis, respectively.

The contribution of the "vibrational intensity borrowing" [first term in Eq. (9)] is small in comparison with that of the "rotational intensity borrowing" [second term in Eq. (9)] (2). For PH_3, the relative contribution of these two terms to the forbidden line strengths, Eq. (8), is $(1.6/8.3)^2 = 0.037$, and it is estimated that the relative contribution is even smaller in AsH_3. Thus, for AsH_3 in the ground vibrational state the contribution of the vibrational mixing to the intensities of the $\Delta K = \pm 3$ transitions

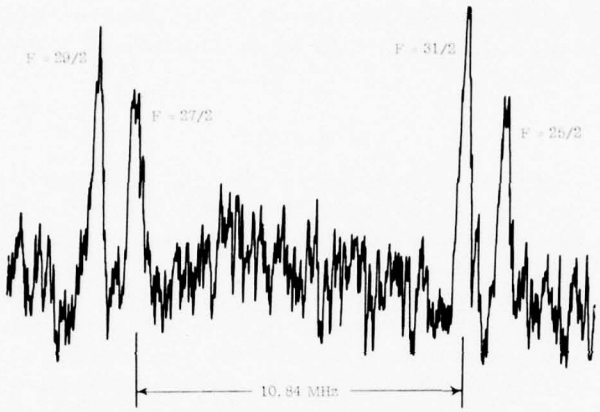

FIG. 1. Single scan of Q-type $K = \pm 5 \rightarrow \pm 2$ multiplet for $J = 14$.

is negligible in comparison with that from rotational mixing. We used the value of τ_{zzzz} from the analysis of the transition data to calculate the value of $(\theta_x{}^{xx})_{\text{eff}}$ used in the calculation of the intensities. The peak absorption coefficients, $\alpha_{\max}$, listed in Table I were calculated from the formula,

$$\alpha_{\max}(\text{cm}^{-1}) = \frac{1.147 \times 10^{-13}}{\Delta\nu T^{\frac{1}{2}}} \nu_0{}^2 \left(1 - \frac{h\nu_0}{2kT}\right)$$

$$\times \exp[-E(F, J, K)/kT](B^2C)^{\frac{1}{2}} g_K g_n S[(F, J, K \pm 3) \leftarrow (F, J, K)], \quad (11)$$

where S is given by Eq. (8), $T = 300$ K, g_n is the reduced nuclear statistical weight

TABLE II

Molecular Constants

Molecular Constant	Value	Standard Deviation σ*	
B_0	112 470.597	0.030	MHz
C_0	104 884.665	0.043	MHz
D_0^J	2.9257	0.0039	MHz
D_J^{JK}	-3.7164	0.0004	MHz
D_K^{JK}	3.4126	0.0021	MHz
$(h^3\tau_{xxxz}/4h)$	0.679	0.003	MHz
H_J^{JJK}	-0.239	0.009	kHz
H_K^{JJK}	1.990	0.047	kHz
L_{JJJK}	0.701	0.011	Hz
L_{JJKK}	-1.729	0.067	Hz
C_K^N	0.111	0.016	MHz
C_K^K	0.113	0.017	MHz
(eQq)	-102.58	0.11	MHz
$[h^3\tau_{xxxz}\mu_z/2h(B-C)]$	3.938	0.017	10^{-5}D
r_0	1.5201381	0.0000002	Å
α_0	91.975798	0.000006	(°)

* One standard deviation.

factor, g_K is the statistical weight factor for each K level, and $\Delta\nu = 20$ MHz is the line breadth at a pressure of 1 Torr. This value for the $\Delta\nu$ is the same as that used by Chu and Oka (*2*) for AsH_3.

IV. RESULTS

Twenty-seven $K = \pm 4 \rightarrow \pm 1$ and thirty-six $K = \pm 5 \rightarrow \pm 2$ transitions were measured in this work. The observed frequencies are given in Table I. Figure 1 shows a chart recording of a single scan of the Q-type $K = \pm 5 \rightarrow \pm 2$ multiplet for $J = 14$. The quadrupole doublet is well resolved.

A combined computer analysis was made of the available frequencies for different types of transitions measured by us and by others as listed in Table I. The analysis consisted of a least-squares fitting of thirteen molecular constants to the observed frequencies of AsH_3. The program calculates the difference in the energy levels by use of Eqs. (2)–(7) with assumed values of the molecular constants. Transition frequencies are calculated and compared to the measured transition frequencies to generate new estimates of the molecular constants. This iterative procedure is repeated by the computer until convergence is attained. The degree of fitting of the complete frequency set is shown by column 3 of Table I. The molecular constants for AsH_3 obtained from the combined analysis are listed in Table II.

The two independent zero-point-effective structural parameters for AsH_3, r_0 and α_0, were calculated from the B_0 and C_0; the resulting values are listed at the bottom of Table II. The standard deviations recorded for these values reflect only those uncertainties in the measurement of B_0 and C_0 and do not indicate the possible errors in the absolute values which depend on Planck's constant.

RECEIVED: August 19, 1977

REFERENCES

1. D. HELMS AND W. GORDY, *J. Mol. Spectrosc.* **66**, 206 (1977).
2. F. Y. CHU AND T. OKA, *J. Chem. Phys.* **60**, 4612 (1974).
3. P. HELMINGER, E. L. BEESON, JR., AND W. GORDY, *Phys. Rev. A* **3**, 122 (1971).
4. W. B. OLSON, A. G. MAKI, AND R. L. SAMS, *J. Mol. Spectrosc.* **55**, 252 (1975).
5. K. SARKA, D. PAPOUSEK, AND K. NARAHARI RAO, *J. Mol. Spectrosc.* **37**, 1 (1971).
6. J. K. G. WATSON, *J. Mol. Spectrosc.* **40**, 536 (1971).
7. J. K. G. WATSON, *J. Mol. Spectrosc.* **55**, 498 (1975).
8. F. MICHELOT, J. MORET-BAILLY, AND K. FOX, *J. Chem. Phys.* **60**, 2606, 2610 (1974).
9. I. OZIER, *J. Mol. Spectrosc.* **56**, 124 (1975).
10. T. OKA, *in* "Molecular Spectroscopy: Modern Research," (K. N. Rao and C. W. Matthews, Eds.), Vol. II, p. 229, Academic Press, New York (1976).
11. A. ROSENBERG, I. OZIER, AND A. K. KUDIAN, *J. Chem. Phys.* **57**, 568 (1972).
12. A. ROSENBERG AND I. OZIER, *Chem. Phys. Lett.* **13**, 400 (1933).
13. A. ROSENBERG AND I. OZIER, *Canad. J. Phys.* **52**, 575 (1974).
14. A. ROSENBERG AND I. OZIER, *J. Chem. Phys.* **58**, 5168 (1973).
15. W. A. KREINER, U. ANDRESEN, AND T. OKA, *J. Chem. Phys.* **66**, 4662 (1977).
16. C. W. HOLT, M. C. L. GERRY, AND I. OZIER, *Phys. Rev. Lett.* **31**, 1033 (1973).
17. R. H. KAGANN, I. OZIER, AND M. C. L. GERRY, TG12, "Thirty-Second Symposium on Molecular Spectroscopy, Ohio State University, 13–17 June 1977."
18. T. OKA, *J. Chem. Phys.* **47**, 5410 (1967).

19. G. HERZBERG, "Infrared and Raman Spectra of Polyatomic Molecules," Van Nostrand-Reinhold, Princeton, N. J., 1945; see also J. T. HOUGEN, *J. Chem. Phys.* **37**, 1433 (1962).
20. G. AMAT, H. H. NIELSEN, AND G. TARRAGO, "Rotation-Vibration of Polyatomic Molecules," Dekker, New York, 1971.
21. W. B. OLSON, private communication.
22. H. H. NIELSEN AND D. DENNISON, *Phys. Rev.* **72**, 1011 (1947).
23. H. M. HANSON, *J. Mol. Spectrosc.* **23**, 287 (1967).

JOURNAL OF MOLECULAR SPECTROSCOPY 70, 263–269 (1978)

Centrifugal Distortion Analysis of the Ground Vibrational States of $H_2{}^{17}O$ and $H_2{}^{18}O$[1]

PAUL HELMINGER[2]

Department of Physics, University of South Alabama, Mobile, Alabama 36688

AND

FRANK C. DE LUCIA

Department of Physics, Duke University, Durham, North Carolina 27706

Centrifugal distortion analyses of combined infrared-microwave data sets for $H_2{}^{17}O$ and $H_2{}^{18}O$ have been performed. These analyses make possible critical evaluation of data points and results in substantially improved energy levels. The Fraley-Rao interpolation rule for the prediction of $H_2{}^{17}O$ energy levels is examined and extended.

INTRODUCTION

Several years ago we published centrifugal distortion analyses for a number of isotopic species of water. Except for the $H_2{}^{16}O$ (*1*), $H_2{}^{17}O$ (*2*), and $H_2{}^{18}O$ (*3*) species these were based entirely upon microwave data. Because for these species it was not possible to measure enough microwave lines, it was necessary to include infrared data in our calculations. Although at the time of our analyses extensive $H_2{}^{16}O$ infrared data was available, only a modest amount of $H_2{}^{18}O$ data (*4*, *5*) and virtually no $H_2{}^{17}O$ data had been published. In this paper we report new analyses of $H_2{}^{17}O$ and $H_2{}^{18}O$ that include substantial amounts of new infrared data in addition to our earlier microwave data.

Because a centrifugal distortion analysis has substantially fewer degrees of freedom than a purely algebraic combination difference analysis and because the former are more sensitive to "bad" data points which can be eliminated,[3] more accurate and reliable energy levels can be obtained. In addition, the independent analyses of the three isotopic species make possible a critical evaluation and refinement of the Fraley-Rao interpolation rule for the prediction of $H_2{}^{17}O$ energy levels.

[1] This work is supported by the U.S. Army Research Office, Grant DAAG29-77-G-0007.

[2] Travel to Duke University supported by Southern Regional Educational Board.

[3] For an enlightening discussion of a mathematician's view on the rejection of data, see F. J. Anscombe and J. W. Tukey, Technometrics **5**, 141 (1963).

0022-2852/78/0702-0263$02.00/0

$H_2{}^{17}O$ ANALYSIS

We have combined 46 of the far-infrared lines reported by Winther (*6*), 31 combination differences calculated from the data of Toth *et al.* (*8*), 20 combination differences calculated from the data of Camy-Peyret *et al.* (*9*), and our seven microwave lines (*2*) in a weighted Watson analysis.[4] The assigned weights were inversely proportional to the square of the expected uncertainty and ranged from 10^7 for the microwave lines to one for Winther's weakest lines. In order to carefully screen the data, each of the 104 data points was removed (in groups) from the analysis and predicted on the basis of the remaining data. With the exception of a few lines at high J_τ, the uncertainty in each of the predictions was $< \pm 0.01$ cm^{-1} and most were much better. For all the lines contained in the data set, the agreement between the calculated uncertainty in the prediction and the expected experimental uncertainty was satisfactory except for the data points listed in Table I. While only one of these data points is dramatically bad (the rest are off by about 0.05 cm^{-1}), they are all substantially worse than the data retained in the analysis. The spectral constants which result from our analysis are shown in Table II and the energy levels calculated from them in Table III. Four places are retained in the energy levels because it has been found that the analyses successfully predict unanalyzed microwave lines to this accuracy.

$H_2{}^{16}O$ AND $H_2{}^{18}O$ ANALYSES

The $H_2{}^{18}O$ energy levels shown in Table III result from an analysis very similar to the $H_2{}^{17}O$ analysis discussed above except that each of the data subsets is larger and a total of 240 data points were analyzed. At the highest J_τ it was not possible to establish with certainty the reliability of the infrared data points because of the scattered nature of the data. However, at lower J_τ the deviations of several points from the fit were inconsistent with their assigned weights and they were eliminated from the fit. These are shown in Table IV.

The $H_2{}^{16}O$ energy levels listed in Table III are those which result from the original analysis (*1*) of 15 microwave lines and the infrared data available to us at that time.

TABLE I

Data Points Removed from $H_2{}^{17}O$ Analysis

Levels	Obs-Calc (cm^{-1})	Ref.
$5_{32} - 5_{23}$	0.084	6
$4_{23} - 4_{14}$	0.049	6
$5_{41} - 6_{43}$	-0.567	9[a]

[a] The reassignment by Winther (Ref. 6) of one of the transitions of Ref. 9 which leads to the $6_{16} - 8_{18}$ combination difference seems to be correct and is included in our analysis.

[4] For a detailed discussion of our analysis technique, see Ref. (*1*)

TABLE II

Rotation and Distortion Constants of the Ground Vibrational State of Water (MHz)

Constant	$H_2{}^{16}O$		$H_2{}^{17}O$		$H_2{}^{18}O$	
	Value[a]	σ	Value[a]	σ	Value[a]	σ
a	835 840.288	0.50	830 282.791	1.6	825 366.844	1.0
b	435 351.717	0.45	435 357.289	2.6	435 356.685	0.8
c	278 138.700	0.45	277 505.735	2.6	276 948.998	0.8
Δ_J	37.59422	0.02	37.59414	0.09	37.54579	0.017
Δ_{JK}	-172.9128	0.17	-171.8532	0.3	-171.1683	0.13
Δ_K	973.29052	0.10	960.46634	0.5	949.88229	0.2
δ_J	15.21040	0.010	15.34663	0.04	15.23181	0.011
δ_K	41.0502	0.15	41.4538	1.2	38.8850	0.2
$H_J\cdot(10^2)$	1.56556	0.020	1.82110	0.12	1.53906	0.019
$H_{JK}\cdot(10^2)$	-4.2081	0.6			-3.1738	0.4
$H_{KJ}\cdot(10^1)$	-5.09508	0.10	-6.42468	2.6	-5.21898	0.12
$H_K\cdot(10^0)$	3.733028	0.008	3.745123	0.06	3.624767	0.017
$h_J\cdot(10^3)$	7.79579	0.09	10.18803	0.6	8.04641	0.14
$h_{JK}\cdot(10^2)$	-2.5165	0.11	3.7859	2.4	-2.4187	0.25
$h_K\cdot(10^0)$	1.0971	0.03	1.1495	0.13	1.0488	0.04
$L_{JK}\cdot(10^3)$	-3.0647	0.46			-4.6449	0.6
$L_{KKJ}\cdot(10^2)$	1.02952	0.12			1.46700	0.16
$L_K\cdot(10^2)$	-2.340138	0.08	-1.517327	0.17	-2.617359	0.11
$\ell_J\cdot(10^6)$					-2.59	0.8
$\ell_{JK}\cdot(10^4)$			-4.257	2.6		
$\ell_K\cdot(10^2)$	-1.3546	0.10	-0.326	0.2	-1.32008	0.13
$P_K\cdot(10^5)$	5.19841	0.07	4.71660	1.5	5.72244	0.4
$p_K\cdot(10^5)$	3.7603	1.0				

[a] The large number of digits retained in the higher order constants is required in order to reproduce the energy levels to experimental uncertainty.

More recent energy levels (*10*), based upon the high resolution experimental data of Guelachvili (and apparently upon our microwave data, too), result in essentially the same energy levels over the J_τ range of the original analysis.

FRALEY-RAO INTERPOLATION RULE

The Fraley-Rao (*4*) interpolation rule can be stated as

$$\frac{\nu_{17} - \nu_{16}}{\nu_{18} - \nu_{16}} = k \tag{1}$$

Table V shows the result of the application of this rule to the observed microwave transitions of $H_2{}^{17}O$. It is obvious that large deviations exist. A similar effect has been observed for microwave transitions of D_2O (*11*). However, critical inspection of the

TABLE III

Energy Levels of the Ground Vibrational States of Water (cm^{-1})

	$H_2{}^{16}O$	$H_2{}^{17}O$	$H_2{}^{18}O$
1_{01}	23.7945	23.7735	23.7550
1_{11}	37.1372	36.9311	36.7457
1_{10}	42.3718	42.1870	42.0235
2_{02}	70.0911	70.0647	69.9276
2_{12}	79.4965	79.2273	78.9887
2_{11}	95.1762	94.9706	94.7858
2_{21}	134.8019	134.1453	133.4759
2_{20}	136.1642	135.4312	134.7833
3_{03}	136.7622	136.5378	136.3369
3_{13}	142.2788	141.9024	141.5682
3_{12}	173.3665	173.1102	172.8832
3_{22}	206.3019	205.4820	204.7561
3_{21}	212.1568	211.4369	210.7985
3_{31}	285.2199	283.5615	282.0950
3_{30}	285.4191	283.7077	282.2075
4_{04}	222.0536	221.6212	221.2344
4_{14}	224.8388	224.3043	223.8288
4_{13}	275.4881	275.1305	274.8037
4_{23}	300.3628	299.4389	298.6206
4_{22}	315.7801	315.0786	314.4599
4_{32}	382.5177	380.8048	379.2924
4_{31}	383.8433	382.1772	380.7033
4_{41}	488.1083	485.2082	482.6445
4_{40}	488.1348	485.2361	482.6736
5_{05}	325.3489	324.6613	324.0472
5_{15}	326.6221	325.8803	325.2161
5_{14}	389.4591	388.8787	388.3612
5_{24}	416.2094	415.1269	414.1689
5_{23}	446.5114	445.7931	445.1591
5_{33}	503.9687	502.1802	500.5973
5_{32}	508.8127	507.1764	505.7298
5_{42}	610.1160	607.1629	604.5461
5_{41}	610.3428	607.4014	604.7945
5_{51}	742.0744	737.6190	733.6817
5_{50}	742.0777	737.6225	733.6854
6_{06}	446.6976	445.7193	444.8467
6_{16}	447.2631	446.2446	445.3467
6_{15}	542.9078	541.9646	541.1810
6_{25}	552.9121	551.6058	550.4519
6_{24}	602.7743	601.9598	601.2382
6_{34}	648.9786	647.0694	645.3837
6_{33}	661.5489	659.3894	658.0111
6_{43}	756.7262	753.7094	751.0354
6_{42}	757.7816	754.8182	752.1899
6_{52}	888.6029	884.0865	880.0806
6_{51}	888.6368	884.1228	880.1189
6_{61}	1045.0623	1038.7644	1033.1986
6_{60}	1045.0627	1038.7648	1033.1991
7_{07}	586.2446	584.9403	583.7782
7_{17}	586.4800	585.1610	583.9969
7_{16}	704.2166	702.8811	701.6952
7_{26}	709.6092	708.0092	706.5992
7_{25}	782.4110	781.3750	780.4830
7_{35}	816.6931	814.6007	812.7628
7_{34}	842.3560	840.8091	839.5505
7_{44}	927.7438	924.6402	921.8983
7_{43}	931.2371	928.3024	925.7023
7_{53}	1056.6510	1055.0641	1050.9958
7_{52}	1059.8398	1055.2667	1051.2086
7_{62}	1216.1966	1209.82[illegible]	1204.1766
7_{61}	1216.2043	1209.82[illegible]	1204.1821
7_{71}	1394.8190	1386.41[illegible]	1378.9899
7_{70}	1394.8191	1386.41[illegible]	1378.9899

TABLE III—*Continued*

	$H_2{}^{16}O$	$H_2{}^{17}O$	$H_2{}^{18}O$
8_{08}	744.0648	742.3976	740.9125
8_{18}	744.1636	742.4825	740.9889
8_{17}	882.8934	881.0929	879.4956
8_{27}	885.6017	883.6428	881.9156
8_{26}	982.9139	981.4921	980.2218
8_{36}	1006.1139	1003.7614	1001.7065
8_{35}	1050.1580	1048.6671	1047.3304
8_{45}	1122.7063	1119.4733	1116.6358
8_{44}	1131.7742	1128.9465	1126.4425
8_{54}	1255.1689	1250.4961	1246.3755
8_{53}	1255.9137	1251.2843	1247.2128
8_{63}	1411.6216	1405.1541	1399.4402
8_{62}	1411.6520	1405.1877	1399.4754
8_{72}	1580.7053	1582.1979	1574.6833
8_{71}	1580.7058	1582.1986	1574.6840
8_{81}	1789.0395	1778.2960	1768.8142
8_{80}	1789.0395	1778.2960	1768.8142

energy levels of Table III show that they obey the rule

$$\frac{E_{17} - E_{16}}{E_{18} - E_{16}} = k \tag{2}$$

where $k = 0.5307 \rightarrow 0.5275$. This results directly from

$$\frac{A_{17} - A_{16}}{A_{18} - A_{16}} = 0.5307 \qquad \text{and} \qquad \frac{C_{17} - C_{16}}{C_{18} - C_{16}} = 0.5275$$

with the change in rotational energy due to isotopic substitution given by

$$\Delta E = \frac{\partial E}{\partial A}\Delta A + \frac{\partial E}{\partial B}\Delta B + \frac{\partial E}{\partial C}\Delta C \tag{3}$$

and $\Delta B \approx 0$ for an on axis isotopic substitution. As a result at high K_{-1} where

TABLE IV

Data Points Removed from $H_2{}^{18}O$ Analysis

Levels	Obs-Calc (cm^{-1})	Ref.
$2_{20} - 1_{11}$	0.029	6
$5_{24} - 4_{13}$	0.040	6
$6_{33} - 5_{24}$	-0.049	6
$7_{44} - 7_{35}$	0.040	6
$8_{54} - 7_{25}$	-0.041	6
$8_{27} - 8_{18}$	0.042	6
$7_{25} - 6_{25}$	0.047	8
$6_{52} - 5_{50}$	-0.021	9
$7_{25} - 6_{25}$	-0.884	9
$8_{27} - 7_{25}$	0.883	9

TABLE V

Values of the Fraley Rao Constant for Observed Microwave Transitions

Transition	k
$1_{10} - 1_{01}$	0.530807
$2_{11} - 2_{02}$	0.532543
$3_{13} - 2_{20}$	0.532021
$4_{14} - 3_{21}$	0.536887
$4_{23} - 3_{30}$	0.531228
$5_{15} - 4_{22}$	0.493528
$6_{16} - 5_{23}$	0.523757

$\partial E/\partial A = \langle P_a^2 \rangle$ is large and $\partial E/\partial C \approx \langle P_c^2 \rangle$ is small, $k \approx 0.5307$. Conversely at low K_{-1}, $k \approx 0.5275$.

Equation (2) can be rewritten for transitions as

$$\frac{\nu_{17} - \nu_{16}}{\nu_{18} - \nu_{16}} = k^l + (k^u - k^l)\frac{E_{18}{}^u - E_{16}{}^u}{\nu_{18} - \nu_{16}} \tag{4}$$

where the superscripts refer to the upper and lower energy levels of the transition. The correction term is large in regions where the dominant terms of Eq. (3) are changing, especially for transitions whose frequency changes little upon isotopic substitution. The lines of Table V which show the greatest deviations from Eq. (1) are the same lines that Eq. (4) predicts to have these variations.

COMPARISON WITH *OTHER* ENERGY LEVELS AND CONCLUSIONS

Our original $H_2{}^{17}O$ analysis was based upon our measured microwave data and distortion constants calculated from the $H_2{}^{16}O$ and $H_2{}^{18}O$ analyses. A comparison between the energy levels which resulted from this and those of Table III show exceedingly close agreement (typically 0.002 cm^{-1}) up to the 5_{41} level. At higher J_τ the agreement is still good (typically 0.002 cm^{-1} at low K_{-1} up to 0.02 cm^{-1} at high K_{-1}) except for the 6_{61} and 6_{60} levels. These are lower by 0.17 cm^{-1} in our latest analysis. This is because our earlier analysis of $H_2{}^{18}O$ was perturbed by infrared energy levels for 6_{60} and 6_{61} which were high by 0.30 cm^{-1} compared to the $H_2{}^{18}O$

TABLE VI

Comparison of Observed Energy Levels with those Calculated from Eq. (2) (cm^{-1})

State	Observed	Calculated	Difference
1_{10}	42.1870	42.1870	0.0000
2_{20}	135.4312	135.4313	-0.0001
3_{30}	283.7677	283.7678	-0.0001
4_{40}	485.2361	485.2365	-0.0004
5_{50}	737.6225	737.6239	-0.0014
6_{60}	1038.7648	1038.7667	-0.0019
7_{70}	1386.4179	1386.4186	-0.0007
8_{80}	1778.2960	1778.3059	-0.0099

energy levels shown in Table III. For medium values of J_τ the energy levels of Refs. (*6*) and (*8*) differ from the levels of Table III by substantially more (typically 0.01 cm^{-1}) than do our earlier energy levels. The energy levels of Ref. (*6*), which extend to higher J_τ than those of Ref. (*8*), deteriorate somewhat relative to the values of Table III, but all agree to within 0.05 cm^{-1} or better.

It is to be expected that our latest analysis is better than previous analyses because it contains the earlier data sets as subsets and because our analysis technique makes possible rather sensitive tests for bad data points and substantially reduces the degrees of freedom. It is perhaps somewhat surprising that our earlier analysis was so good.

Since all of the energy levels of the three isotopes were calculated independently, one check of their accuracy and also of the accuracy of Eq. (2) can be accomplished by the use of the $H_2{}^{16}O$ and $H_2{}^{18}O$ energy levels in this equation to calculate the energy levels of $H_2{}^{17}O$. Since it is most difficult to get good energy levels at high K_{-1} and since the isotopic splittings of the energy levels are also greatest there, the most stringent test would be the J_{J0} levels. The close argument shown in Table VI between the energy levels calculated directly from the $H_2{}^{17}O$ data and the levels calculated via Eq. (2) confirms both the accuracy of this relation and the quality of the energy levels for all three species.

RECEIVED: November 18, 1977

Note added in proof. The problems in our earlier analysis of $H_2{}^{18}O$ have recently been attributed (J.-M. Flaud, C. Camy-Peyret, and R. A. Toth, *J. Mol. Spectrosc.* **65**, 219 (1977)) to the heavy weights assigned the microwave data in that analysis. In fact, as shown above, the errors in the literature of 0.30 cm^{-1} in the infrared energies of 6_{60} and 6_{61} perturbed several of the higher order distortion constants and some of the energy levels closely associated with 6_{60} and 6_{61}. All analyses reported in this paper contain heavily weighted microwave data, and, as demonstrated above, excellent agreement among the isotopes result. All checks of isotopic agreement were performed after each isotopic analysis was final, and no adjustments at subjective points in the data analysis were carried out with isotopic agreement as an objective.

REFERENCES

1. F. C. De Lucia, P. Helminger, R. L. Cook, and W. Gordy, *Phys. Rev. A* **5**, 487 (1972).
2. F. C. De Lucia and P. Helminger, *J. Mol. Spectrosc.* **56**, 138 (1975).
3. F. C. De Lucia, P. Helminger, R. L. Cook, and W. Gordy, *Phys. Rev. A* **6**, 1324 (1972).
4. P. E. Fraley, K. Narahari Rao, and L. H. Jones, *J. Mol. Spectrosc.* **29**, 312 (1969).
5. J. G. Williamson, K. Narahari Rao, and L. H. Jones, *J. Mol. Spectrosc.* **40**, 372 (1971).
6. F. Winther, *J. Mol. Spectrosc.* **65**, 405 (1977).
7. F. J. Anscombe and W. Tukey, *Technometrics* **5**, 141 (1963).
8. R. A. Toth, J. M. Flaud, and C. Camy-Peyret, *J. Mol. Spectrosc.* **67**, 185 (1977).
9. C. Camy-Peyret, J. M. Flaud, G. Guelachvili, and C. Amiot, *Mol. Physics* **26**, 825 (1973).
10. J. M. Flaud, C. Camy-Peyret, and J. P. Maillard, *Mol. Physics* **32**, 499 (1976).
11. J. Bellet, W. J. Lafferty, and G. Steenbeckeliers, *J. Mol. Spectrosc.* **47**, 388 (1973).

JOURNAL OF MOLECULAR SPECTROSCOPY 76, 131–141 (1979)

Millimeter-Wave Spectrum, Centrifugal Distortion Analysis, and Energy Levels of HNO_3[1]

GABRIELE CAZZOLI[2,3] AND FRANK C. DE LUCIA

Department of Physics, Duke University, Durham, North Carolina 27706

One hundred and eleven new rotational transitions of HNO_3 have been measured in the millimeter-microwave region. This data set is the basis for a centrifugal distortion analysis and for the calculation of a complete set of energy levels through $J = 50$. The constants which result from this analysis are (in megahertz): $A = 13\,011.0287 \pm 0.0057$, $B = 12\,099.8611 \pm 0.0057$, $C = 6260.6391 \pm 0.0006$, $\Delta_J = (14.038 \pm 0.026) \times 10^{-3}$, $\Delta_{JK} = (-20.1780 \pm 0.0037) \times 10^{-3}$, $\Delta_K = (7.4153 \pm 0.0108) \times 10^{-3}$, $\delta_J = (1.1828 \pm 0.00039) \times 10^{-3}$, $\delta_K = (-20.5648 \pm 0.0046) \times 10^{-3}$, $H_J = (-9.84 \pm 3.82) \times 10^{-8}$, $H_{JK} = (-9.933 \pm 0.367) \times 10^{-8}$, $H_{KJ} = (1.03 \pm 0.12) \times 10^{-7}$, $h_J = (-9.241 \pm 0.127) \times 10^{-9}$, $h_{JK} = (-1.398 \pm 0.032) \times 10^{-7}$, and $h_K = (1.135 \pm 0.027) \times 10^{-6}$.

INTRODUCTION

Nitric acid is a near-oblate asymmetric rotor with rotational constants of the order of 10 GHz and moderate centrifugal distortion. The presence of this species in the atmosphere and its basic role in chemistry have stimulated numerous spectroscopic studies. The rotational spectrum of HNO_3 has been studied in the centimeter-wave region (*1–3*), and Kaushik and Venkateswarlu (*4*) have performed a centrifugal distortion analysis of these data. They noted that the relatively large standard deviations of the resulting coefficients and the indeterminacy of τ_{cccc} must be ascribed to the data set available. Conventional infrared spectroscopy reveals only broad vibrational bands because of the dense rotational fine structure of HNO_3 (*5–8*). Recently, however, Brockman *et al.* (*9*) have published an unassigned diode laser spectrum of HNO_3 in the 11-μm region that clearly resolves the rotational fine structure. Several other diode laser studies of HNO_3 are also in progress (*10*).

In this paper we report the measurement of 111 rotational transitions in the region between 80 and 300 GHz. This spectral coverage results in a well-conditioned data set which makes possible an accurate centrifugal distortion analysis and calculation of energy levels through $J = 50$. These ground-vibrational-state energy levels can serve as a basis for the analysis of the complex rotation–vibration spectra which are now being recorded as well as for the study of

[1] This work was supported by Army Research Office Grant DAAG29-77-G-0007.

[2] Present address: Laboratorio di Spettroscopia Molecolare, Consiglio Nazionale delle Ricerche, Via de'Castagnoli, 1, 40126 Bologna, Italy.

[3] Nato Senior Postdoctoral Fellow.

0022-2852/79/070131-11$02.00/0

TABLE I

Observed Microwave Transitions of HNO_3 (MHz)

Transition	Observed frequency	Transition	Observed frequency
1(0 1)- 0(0 0)	16 380.530[a]	10(4 6)- 9(4 5)	181 789.200
1(1 1)- 0(0 0)	19 271.800[a]	11(0 11)-10(1 10)	144 004.240
2(1 2)- 2(1 1)	-17 617.490[a]	11(9 3)-11(8 4)	-12 817.450[a]
2(0 2)- 2(1 1)	-17 616.080[a]	11(3 8)-10(3 7)	181 676.130
2(1 2)- 1(0 1)	31 782.800[a]	12(3 10)-11(2 9)	181 830.780
3(1 3)- 3(3 1)	-22 161.000[a]	12(10 3)-12(10 2)	-9 245.560[a]
3(2 1)- 3(3 0)	-9 447.970[a]	12(1 12)-12(1 11)	-144 339.740
3(1 2)- 3(2 1)	-16 700.740[a]	12(2 10)-12(2 11)	181 564.580
4(3 2)- 4(3 1)	-14 534.280[a]	14(2 12)-14(3 11)	-144 198.690
5(4 2)- 5(4 1)	-12 840.980[a]	14(0 14)-13(1 13)	181 560.980
5(3 3)- 5(3 2)	-29 175.380[a]	14(2 12)-14(4 11)	-144 196.940
6(5 2)- 6(5 1)	-10 344.230[a]	15(1 15)-15(2 14)	-181 995.690
6(4 3)- 6(4 2)	-27 369.470[a]	15(8 8)-15(9 6)	-105 887.150
6(3 4)- 5(3 3)	106 481.320	15(7 9)-15(8 8)	-105 885.880
6(2 4)- 5(2 3)	106 846.550	16(2 15)-16(3 14)	-181 927.420
7(6 2)- 7(6 1)	-8 097.580[a]	17(6 12)-17(7 11)	-143 887.520
7(5 3)- 7(5 2)	-24 893.510[a]	17(2 16)-17(3 14)	-181 848.630
7(1 6)- 6(1 5)	106 483.440	17(3 14)-16(3 13)	268 757.190
8(6 3)- 8(6 2)	-22 147.000[a]	18(4 15)-18(5 14)	-181 788.230
8(7 1)- 7(7 0)	174 944.800	18(6 12)-18(8 11)	-143 715.920
8(7 2)- 7(7 1)	169 702.230	18(2 16)-17(2 15)	268 723.390
8(6 2)- 7(6 1)	180 101.520	19(5 15)-19(6 14)	-181 684.810
8(4 5)- 7(4 4)	144 146.640	19(1 18)-18(1 17)	268 691.080
8(3 5)- 7(3 4)	144 201.880	20(6 15)-20(7 14)	-181 537.350
8(0 8)- 7(0 7)	106 445.510	20(0 20)-19(0 19)	268 657.760
9(7 3)- 8(7 2)	-18 986.580[a]	22(21 1)-22(22 0)	-103 748.060
9(2 7)- 8(2 6)	144 081.960	22(21 2)-22(22 1)	-103 750.640
10(4 6)- 9(5 5)	181 770.440	22(9 14)-22(9 13)	-186 514.460
10(5 6)- 9(4 5)	181 780.820	23(22 1)-23(23 0)	-103 757.340
10(1 9)- 9(2 8)	144 039.780	23(22 2)-23(23 1)	-103 758.550
10(8 3)-10(8 2)	-15 826.180[a]	24(23 1)-24(24 0)	-113 768.890
10(9 1)- 9(9 0)	215 606.940	24(23 2)-24(24 1)	-113 767.810
10(5 6)- 9(5 5)	181 772.040	24(15 9)-24(16 8)	-100 631.870

Transition	Observed frequency	Transition	Observed frequency
25(22 3)-25(23 2)	-100 637.760	34(31 4)-34(32 3)	-146 765.060
25(22 4)-25(23 3)	-100 642.920	34(22 12)-34(24 11)	-135 253.230
25(17 9)-25(18 8)	-100 559.340	35(23 12)-35(25 11)	-134 140.390
25(14 12)-25(15 11)	-141 778.890	35(24 12)-35(24 11)	-133 340.120
25(14 12)-25(14 11)	-141 776.510	36(32 4)-36(33 3)	-147 571.300
26(11 15)-26(13 14)	-160 446.060	36(32 5)-36(33 4)	-147 577.120
27(24 3)-27(25 2)	-111 014.200	36(27 9)-36(28 8)	-141 140.440
27(24 4)-27(25 3)	-111 051.200	36(24 12)-36(28 11)	-132 963.830
28(24 4)-28(25 3)	-105 628.560	36(25 12)-36(25 11)	-131 562.380
28(24 5)-28(25 4)	-106 141.810	37(36 1)-37(37 0)	-179 104.130
30(29 1)-30(30 0)	-143 880.370	37(32 5)-37(33 4)	-142 564.470
30(25 5)-30(26 4)	-103 954.590	37(32 6)-37(33 5)	-142 616.350
30(25 6)-30(26 5)	-105 807.140	37(25 12)-37(27 11)	-131 830.240
30(19 12)-30(20 11)	-138 917.330	37(26 12)-37(28 11)	-129 372.980
30(18 12)-30(19 11)	-138 890.960	38(37 1)-38(38 0)	-184 164.560
30(23 7)-30(25 6)	-144 855.990	38(28 12)-38(28 11)	-130 765.270
30(22 8)-30(24 7)	-106 777.580	38(25 13)-38(27 12)	-145 659.170
30(21 10)-30(21 9)	-107 041.060	38(26 13)-38(26 12)	-145 131.960
30(18 12)-30(20 11)	-138 919.210	38(23 15)-38(25 14)	-174 774.640
30(19 12)-30(19 11)	-138 889.080	38(24 15)-38(24 14)	-174 771.630
30(13 18)-30(13 17)	-217 946.740	38(21 18)-38(21 17)	-215 282.120
31(20 12)-31(21 11)	-138 125.640	38(18 21)-38(18 20)	-254 275.010
31(19 12)-31(20 11)	-138 072.320	40(38 2)-40(39 1)	-185 972.720
31(19 12)-31(21 11)	-138 129.630	40(20 21)-40(20 20)	-263 611.710
31(20 12)-31(20 11)	-138 066.360	42(32 10)-42(34 9)	-182 748.840
32(30 3)-32(31 2)	-145 533.760	43(39 5)-43(40 4)	-183 519.240
32(20 12)-32(22 11)	-137 256.360	44(23 21)-44(24 20)	-251 991.840
32(21 12)-32(21 11)	-137 134.290	45(40 6)-45(41 5)	-184 280.130
33(30 3)-33(31 2)	-141 695.530	46(28 21)-46(28 20)	-251 011.760
33(30 4)-33(31 3)	-141 697.210	47(36 11)-47(35 10)	-212 777.870
33(21 12)-33(23 11)	-136 295.940	48(26 21)-48(28 20)	-249 900.660
33(22 12)-33(22 11)	-136 061.540	50(48 3)-50(47 4)	-214 426.320
34(31 3)-34(32 2)	-146 765.070		

a. See Refs. 1 and 2.

HNO_3 by direct microwave techniques. A preliminary report of this work has been given recently (*11*).

II. EXPERIMENTAL DETAILS

We have previously detailed our general experimental technique (*12*, *13*). A brief description of the specific configuration for this work follows. Millimeter-wave energy was produced by King and Gordy (*14*) crystal harmonic generators driven by OKI klystrons in the 35-GHz range. This energy was focused by quasi-optical techniques through a 4-m-long absorption cell made of 10-cm-diameter KIMAX glass pipe and detected by a 1.6-K InSb photoconduction detector. The HNO_3 vapor was taken directly from a standard laboratory mixture of concentrated nitric acid.

Although most of the lines reported here are strong video oscilloscope lines, source modulation and lock-in techniques were used to record the weaker high-J lines. For this work the 35-GHz klystron was phase locked, via a phased-locked X-13 Varian klystron and transfer oscillator, to a crystal oscillator whose phase was continuously monitored against WWVB.

III. RESULTS AND DISCUSSION

We have used Watson's reduced centrifugal distortion Hamiltonian (*15*) and the computational and statistical techniques that we have previously discussed (*16*, *17*) for the analysis of the rotational spectrum of HNO_3. A "bootstrap" assignment–analysis procedure was used. At each step lines that would provide a balance between a maximum of new, independent information for the analysis and a minimum risk of assignment error were selected for measurement. In practice this amounted to the selection of lines whose prediction uncertainties were several megahertz. This procedure was iterated until all of the approximately 5000 lines of significant strength below $J = 50$ were predicted with an uncertainty of 1 MHz or less.

Table I shows the 131 rotational transitions included in our analysis and Table II shows the spectral constants which result. In our analysis H_K was found to be only marginally determined and was subsequently eliminated from the constant set. The rms deviation of the analysis was 0.124 MHz with or without

TABLE II

Spectroscopic Constants of HNO_3 (MHz)

$A = 13\,011.0287 \pm 0.0057$	$B = 12\,099.8611 \pm 0.0057$	$C = 6\,260.6391 \pm 0.0006$
$\Delta_J = (14.038 \pm 0.026) \cdot 10^{-3}$	$\Delta_{JK} = (-20.1780 \pm 0.0037) \cdot 10^{-3}$	$\Delta_K = (7.4153 \pm 0.0108) \cdot 10^{-3}$
$\delta_J = (1.1828 \pm 0.00039) \cdot 10^{-3}$	$\delta_K = (-20.5648 \pm 0.0046) \cdot 10^{-3}$	
$H_J = (-9.84 \pm 3.82) \cdot 10^{-8}$	$H_{JK} = (-9.333 \pm 0.367) \cdot 10^{-8}$	$H_{KJ} = (1.03 \pm 0.12) \cdot 10^{-7}$
$h_J = (-9.241 \pm 0.127) \cdot 10^{-9}$	$h_{JK} = (-1.398 \pm 0.032) \cdot 10^{-7}$	$h_K = (1.135 \pm 0.027) \cdot 10^{-6}$

TABLE III

Energy Levels of HNO_3 (cm^{-1})

J										
J= 1	0.837507	0.642832	0.612441							
J= 2	2.516396	2.341425	2.257255	1.672934	1.669643					
J= 3	5.041769	4.908752	4.726621	4.165727	4.169544	3.133938	3.133714			
J= 4	8.422871	8.325816	8.023434	7.538624	7.491669	6.478352	6.475797	5.013942	5.013929	
J= 5	12.667310 7.311672	12.621561	12.152571	11.733748	11.630264	10.657031	10.650942	9.194574	9.194461	7.311673
J= 6	17.7[illegible]457 12.328878	17.739572 10.027046	17.114729 10.027046	16.773683	16.582349	15.669893	15.651503	14.208918	14.208358	12.328885
J= 7	23.764381 18.179990	23.739761 15.660789	22.931406 15.660789	22.661330 13.160053	22.350913 13.160053	21.517220	21.473954	20.055866	20.053836	18.180032
J= 8	30.[illegible] 24.363899	30.[illegible] 22.568645	29.[illegible] 22.568643	29.600015 19.850272	28.939326 19.850272	28.200280 16.710689	28.110601 16.710689	26.734396	26.728415	24.864079
J= 9	38.347725 [illegible]	37.334767 [illegible]	37.131911 [illegible]	36.992798 27.374699	36.353828 27.374699	35.721072 24.237338	35.556339 24.237338	34.243766 20.678945	34.228630 20.678945	32.379882
J= 10	[illegible] 40.724387 25.[illegible]	[illegible] 39.443141	[illegible] 39.443087	45.442768 35.732597	44.603583 35.732596	44.032283 32.598234	43.308766 32.598234	42.583721 29.041987	42.549760 29.041987	40.726232 25.064812
J= 11	56.297605 49.897130 34.264210	56.295355 47.627726 [illegible]	54.810485 47.627542 [illegible]	54.752607 44.923142	53.697983 44.923139	53.287121 41.792724	52.969660 41.792724	51.754681 38.239273	51.685821 38.239273	49.901946 34.264210

J= 12	[illegible] 59.894629 44.297821	[illegible] 57.642228 39.[illegible]	[illegible] 57.641734 39.[illegible]	64.[illegible] 54.945421 35.089336	63.647507 54.945405 35.089336	63.[illegible] 51.320085	62.744470 51.820085	61.757852 48.270210	61.630233 48.270210	59.905989 44.297821
J= 13	77.924391 70.713051 55.165094	77.923742 68.485658 50.773874	75.930871 68.484249 50.773874	75.960158 65.798423 45.961337	74.461941 65.798370 45.961337	74.241853 62.679525 40.727966	73.441211 62.679524 40.727966	72.595253 59.134147	72.377420 59.134147	70.737642 55.165094
J= 14	89.988321 82.347354 66.865423	89.988435 80.156566 62.477283	87.872638 80.153028 62.477288	87.860716 77.481049 57.667423	86.148477 77.480893 57.667423	85.998816 74.370177 52.436214	84.969656 74.370172 52.436214	84.269641 70.830377 46.784158	83.924868 70.830377 46.784158	82.396683 66.885428
J= 15	102.920344 94.791304 79.398177 53.257893	102.920172 92.653721 75.013578	100.633667 92.645710 75.013579	100.626937 89.992108 70.207096	98.710624 89.991688 70.207096	93.613116 86.891094 64.978455	97.340874 86.891079 64.978455	96.784356 83.358129 59.328611	96.274415 83.358128 59.328611	94.883554 79.398177 53.257893
J= 16	116.718775 106.[illegible] 92.762640 66.638513	116.718687 105.976130 88.383039 60.149156	114.262988 105.959163 88.383039 60.149155	114.259249 103.330334 83.579820	112.148670 103.329231 83.579820	112.087379 100.241250 78.354208	110.566531 100.241207 78.354208	110.143111 96.716571 72.706954	109.432042 96.716570 72.706954	108.199481 92.762640 66.638513
J= 17	131.383335 124.081956 106.958065 80.852901	131.383391 120.123091 102.583920 74.365899	128.759896 120.089273 102.583920 74.365898	128.757847 117.494411 97.785022 67.457928	126.461081 117.491946 97.785022 67.457928	126.423665 114.419537 92.562959	124.657483 114.419418 92.562959	124.349757 110.904806 86.918714	123.406764 110.904802 86.918714	122.346505 106.958065 80.852901
J= 18	146.915649 136.920150 121.983647 95.900597	146.915627 135.054401 117.615930 89.416277	144.123879 13[illegible] 11[illegible]5930 [illegible]6277	144.122770 132.483024 112.822091 82.510748	141.645788 132.477590 112.822091 82.510748	141.623492 129.424760 107.604157 75.184189	139.621929 129.424456 107.604157 75.184189	139.408040 125.921868 101.963393	139.209597 125.921856 101.963393	137.327429 121.983647 95.900597
J= 19	163.213725 152.554305 137.838522 111.781109	163.213724 150.850516 133.478328 105.299836	160.354547 150.777021 133.478328 105.299836	160.353952 148.284939 128.690375 98.397060	157.700385 148.283598 128.690375 98.397060	[illegible]687859 [illegible]255648 [illegible]477219 [illegible]073039	155.464159 145.254918 123.477219 91.073039	155.321388 141.766716 117.840456 83.327919	153.852863 141.766683 117.840456 83.327919	153.145683 137.838523 111.781109
J= 20	180.578337 168.950737 164.521768 128.493913 91.889094	180.578302 167.512665 150.170324 122.016091	177.451540 167.321128 150.170325 122.016091	177.451264 164.929116 145.389183 115.116410	174.624361 164.706606 145.389193 115.116410	[illegible]617378 [illegible]910863 [illegible]181525 [illegible]795225	172.184753 161.909203 140.181525 107.795225	172.092745 158.438236 134.549342 100.052749	170.349394 158.438151 134.549342 100.052749	169.805113 154.521771 128.493918 91.889094

TABLE III—*Continued*

J= 21	198.708270	198.708267	195.414702	195.414536	192.416591	.412353	189.782134	189.724479	187.711162	187.309754
	186.236227	184.962913	184.656918	182.384852	182.342256	.389035	179.385444	175.935234	175.935024	172.032407
	172.032358	167.651086	167.651085	162.917782	162.917782	.716419	157.716419	152.089454	152.089454	146.038475
	146.038475	139.564532	139.564532	132.668319	132.668319	.350293	125.350293	117.610747	117.610747	109.449851
	109.449851	100.867690	100.867690							
J= 22	217.704320	217.704319	214.243656	214.243569	211.075244	.072875	208.253622	208.218364	205.947422	205.663573
	204.311861	203.244085	202.781238	200.661946	200.584973	7.688304	197.681387	194.256437	194.255947	190.369378
	190.269354	186.039719	186.039713	181.275396	181.275396	.081209	176.081209	170.460163	170.460163	164.414203
	164.414203	157.944620	157.944620	151.052282	151.052282	3.737768	143.737768	136.001460	136.001460	127.843599
	127.843599	119.264321	119.264321	110.263683	110.263683					
J= 23	237.565945	237.565944	233.938193	233.938148	230.600199	10.598889	227.596761	227.575626	225.063334	224.870249
	223.222127	222.359678	221.695563	219.760850	219.628008	16.808905	216.794229	213.400501	213.399409	209.531563
	209.531504	205.215280	205.215277	200.461203	200.461203	95.275165	195.275165	189.660807	189.660807	183.620491
	183.620491	177.155791	177.155791	170.267768	170.267768	62.957146	162.957146	155.224410	155.224410	147.069881
	147.069881	138.493752	138.493752	129.496129	129.496129	20.077045	120.077045			
J= 24	258.292922	258.292922	254.498066	254.498043	250.990963	250.990246	247.809484	247.797030	245.059964	244.932990
	242.984011	242.213649	241.406314	239.682794	239.464023	236.748279	236.720404	233.346023	233.363694	229.517768
	225.517626	225.216767	225.216760	220.474338	220.474338	215.297516	215.297516	209.690690	209.690690	203.656702
	203.656702	197.197449	197.197449	190.314220	190.314220	183.007901	183.007901	175.279097	175.279097	167.128217
	167.128217	158.555524	158.555524	149.561175	149.561175	140.145246	140.145246	130.307746	130.307746	
								⋮		
J= 25	279.885019	279.885019	275.923024	275.923012	272.247128	272.246739	268.890207	268.882977	265.935571	265.854424
	263.610620	262.110178	261.923850	260.429836	260.086522	257.506207	257.455321	254.151575	254.146801	250.326719
	250.326357	246.043115	246.043099	241.313884	241.313884	236.147454	236.147454	230.549081	230.549081	224.522165
	224.522165	218.068974	218.068974	211.191057	211.191057	203.889484	203.889484	196.164998	196.164998	188.018108
	188.018108	179.449155	179.449155	170.458358	170.458358	161.045836	161.045836	151.211640	151.211640	140.955758
	140.955758									
J= 26	302.341956	302.341956	298.212812	298.212806	294.368332	294.368123	290.837746	290.833603	287.687195	287.636558
	285.112316	284.753426	283.261201	282.004833	281.491922	279.092474	278.993164	275.755750	275.746324	271.957071
	271.956925	267.693155	267.693155	262.978975	262.978873	257.824125	257.824125	252.235212	252.235212	246.216176
	246.216176	239.769713	239.769713	232.897666	232.897666	225.601318	225.601318	217.881564	217.881564	209.739029
	209.739029	201.174144	201.174144	192.187191	192.187191	182.778347	182.778347	172.947701	172.947701	162.695277
	162.695277	152.021047	152.021047							
J= 27	325.663601	325.663601	321.267165	321.267161	317.354240	317.354128	313.651205	313.648858	310.311780	310.280811
	307.495189	307.247263	305.432955	304.411330	303.631363	301.477518	301.326913	298.177246	298.159289	294.407408
	294.405918	290.165808	290.165715	285.468288	285.468283	280.326634	280.326634	274.748279	274.748279	268.738001
	268.738001	262.298986	262.298986	255.433413	255.433413	248.142802	248.142802	240.428225	240.428225	232.290436
	232.290436	223.729964	223.729964	214.747170	214.747170	205.342287	205.342287	195.515454	195.515454	185.266732
	185.266732	174.596123	174.596123	163.503580	163.503580					

J= 28

349.849572	349.849572	345.385811	345.385810	341.204529	341.204469	337.329389	337.328574	333.806705	333.788089
330.760858	330.595208	328.454240	327.653374	326.661270	324.692557	324.448917	321.414970	321.381933	317.676263
317.673225	313.459680	313.459472	308.781045	308.781034	303.654038	303.654038	298.087437	298.087437	292.086871
292.086871	285.656081	285.656081	278.797631	278.797631	271.513310	271.513310	263.804386	263.804386	255.671760
255.671760	247.116072	247.116072	238.137767	238.137767	228.737147	228.737147	218.914404	218.914404	208.669640
208.669640	198.002893	198.002893	186.914141	186.914141	175.403321	175.403321			

J= 29

374.899638	374.899636	370.268471	370.268471	365.918880	365.918849	361.873230	361.872500	358.169907	358.158882
354.907646	354.800046	352.339311	351.735280	350.442464	348.729642	348.352279	345.468176	345.409445	341.762145
341.756156	337.573465	337.573014	332.916005	332.915979	327.805348	327.805347	322.251804	322.251804	316.261981
316.261981	309.640259	309.640258	302.989628	302.989628	295.712188	295.712188	298.009426	288.009426	279.882408
279.882408	271.331897	271.331897	262.358435	262.358435	252.962398	252.962398	243.144036	243.144036	232.903500
232.903500	222.240965	222.240965	211.156142	211.156142	199.649292	199.649292	187.720233	187.720233	

J= 30

400.813519	400.813519	396.014855	396.014854	391.496977	391.496960	387.280741	387.280340	383.359813	383.393371
379.932269	379.864021	377.099665	376.661376	375.038816	373.591647	373.032948	370.336625	370.235767	366.663597
366.652160	362.505742	362.504799	357.871962	357.871902	352.779521	352.779518	347.240454	347.240454	341.262492
341.262492	334.850741	334.850741	328.008683	328.008683	320.738758	320.738758	313.042702	313.042702	304.921765
304.921765	296.376850	296.376850	287.408604	287.408604	278.017487	278.017487	268.203815	268.203815	257.967791
257.967791	247.309533	247.309533	236.229086	236.229086	224.726439	224.726439	212.801535	212.801535	200.454276
200.454276									

J= 31

427.590422	427.590922	422.624663	422.624663	417.938495	417.938487	413.551983	413.551764	409.495232	409.491512
405.831154	405.738730	402.742380	402.435758	400.465958	399.282161	398.491676	396.020731	395.853608	392.379268
392.379268	388.253126	388.253125	383.647641	383.647503	378.575461	378.575454	373.052418	373.052418	367.087528
367.087528	360.686724	360.686724	353.854043	353.854043	346.592312	346.592312	338.903543	338.903543	330.789193
330.789193	322.250317	322.250317	313.287683	313.287683	303.901843	303.901843	254.093185	294.093185	283.861972
283.861972	273.208367	273.208367	262.132455	262.132455	250.634256	250.634256	238.713738	238.713738	226.370826
226.370826	213.605408	213.605408							

J= 32

455.231546	455.231547	450.097586	450.097586	445.243107	445.243103	440.686545	440.686426	436.455237	436.453112
432.601133	432.575214	429.262703	429.262084	426.740145	425.805314	424.734787	422.521691	422.254986	418.908025
418.908025	414.815770	414.814000	410.241692	410.241406	405.192014	405.191797	399.686681	399.686680	393.736173
393.736173	387.347368	387.347362	380.524929	380.524927	373.272116	373.272116	365.591255	365.591255	357.484027
357.484027	348.951663	348.951663	339.995060	339.995060	330.614874	330.614874	320.811573	320.811573	310.585484
310.585484	299.936823	299.936823	288.865716	288.865716	277.372219	277.372219	265.456329	265.456329	253.117994
253.117994	240.357121	240.357121	227.173585	227.173585					

J= 33

483.735078	483.735078	478.433306	478.433306	473.410479	473.410476	468.684030	468.683966	464.279081	464.277879
460.239547	460.224049	456.680113	456.543427	453.876793	453.165540	451.773480	449.841551	449.432588	446.249086
446.182864	442.198441	442.191218	437.652691	437.652097	432.627963	432.627925	427.142178	427.142176	421.207472
421.207471	414.831797	414.831797	408.020527	408.020527	400.777409	400.777409	393.105114	393.105114	385.005580
385.005580	376.480227	376.480227	367.530099	367.530099	358.155964	358.155964	348.358380	348.358380	338.137745
338.137745	327.494332	327.494332	316.428315	316.428315	304.939786	304.939786	293.028774	293.028774	280.695254
280.695254	267.939157	267.939157	254.760373	254.760373	241.158763	241.158763			

J= 34

513.101158	513.101193	507.631495	507.631495	502.440265	502.440264	497.544048	497.544014	492.966133	492.965459
488.744721	488.735459	484.970079	484.882207	481.888548	481.367325	479.622381	477.983195	477.381875	474.402179
474.250369	470.289506	470.376063	465.879142	465.877941	460.882026	460.831941	455.417793	455.417788	449.500425
449.500425	443.139100	443.139100	436.339994	436.339994	429.107398	429.107398	421.444374	421.444374	413.353140
413.353140	404.835323	404.835323	395.892144	395.892144	386.524479	386.524479	376.732992	376.732992	366.518157
366.518157	355.880311	355.880311	344.819678	344.819678	333.336394	333.336394	321.430522	321.430522	309.102066
309.102066	296.350980	296.350980	283.177177	283.177177	269.580532	269.580532	255.560892	255.560892	

TABLE III—*Continued*

J= 35	543.325571	543.325571	537.691812	537.691812	532.332116	532.332116	527.266211	527.266193	522.515837	522.515462
	518.114841	518.109408	514.135550	514.080190	510.783511	510.414949	508.298125	506.950254	506.103174	503.367688
	503.184945	499.351564	499.367227	494.515485	494.917120	489.352848	489.552669	484.512355	484.512344	478.613993
	478.613992	472.268331	472.268331	465.482452	465.482452	458.261264	458.261264	450.608258	450.608258	442.525968
	442.525968	434.016258	434.016258	425.080513	425.080513	415.719762	415.719762	405.934769	405.934769	395.726098
	395.726098	385.094153	385.094153	374.039215	374.039215	362.561465	362.561465	350.661005	350.661005	338.337870
	338.337870	325.592041	325.592041	312.423452	312.423452	298.831999	298.831999	284.817545	284.817545	270.379922
	270.379922									

J= 36	574.419856	574.419856	568.613909	568.613909	563.085670	563.085670	557.850127	557.850118	552.927681	552.927475
	548.348830	548.345477	544.172821	544.138543	540.564619	540.312271	537.818084	536.746932	535.602666	533.146788
	532.858281	529.203436	529.160561	524.772110	524.767575	519.839004	519.838632	514.424633	514.424608	508.547085
	508.547083	502.218501	502.218501	495.446992	495.446992	488.238156	488.238156	480.595964	480.595964	472.523300
	472.523300	464.022287	464.022287	455.094503	455.094503	445.741131	445.741131	435.963054	435.963054	425.760928
	425.760928	415.135233	415.135233	404.086313	404.086313	392.614398	392.614398	380.719633	380.719633	368.402086
	368.402086	355.661769	355.661769	342.498638	342.498638	328.912612	328.912612	314.903570	314.903570	300.471359
	300.471359	285.615801	285.615801							

J= 37	606.371697	606.371697	600.347427	600.347427	594.700557	594.700557	589.295401	589.295396	584.201182	584.201069
	579.443743	579.443532	575.078834	575.057930	571.230582	571.062567	568.198835	567.377779	565.891840	563.741516
	563.332623	559.324256	559.750821	555.435397	555.426922	550.538991	550.538241	545.153334	545.153281	539.298563
	539.298559	532.988582	532.988582	526.232667	526.232667	519.037190	519.037190	511.406660	511.406660	503.344347
	503.344347	[illegible]	494.652659	485.933389	485.933389	476.587887	476.587887	466.817165	466.817165	456.621984
	456.621984	446.002906	446.002906	434.960341	434.960341	423.494576	423.494576	411.605800	411.605800	399.294120
	399.294120	386.559577	386.559577	373.402157	373.402157	359.821798	359.821798	345.818401	345.818401	331.391828
	331.391828	316.541916	316.541916	301.268472	301.268472					

J= 38	639.184732	639.184732	633.041995	633.041995	627.176393	627.176378	621.601631	621.601628	616.335870	616.335809
	611.404793	611.403762	606.651193	606.838615	602.777681	602.666447	599.454186	598.847429	596.986022	595.154766
	594.512950	591.252823	591.131453	586.907764	586.892310	582.051235	582.049759	576.697098	576.696986	570.867235
	570.867228	564.577503	564.577503	557.838495	557.338495	550.657453	550.657453	543.039486	543.039486	534.988291
	534.988291	526.526501	526.506591	517.596419	517.596419	508.259303	508.259303	498.496401	498.496401	488.308584
	488.308584	477.656506	477.696506	466.660649	466.660649	455.201362	455.201362	443.318880	443.318880	431.013355
	431.013355	418.284860	418.284860	405.133410	405.133410	391.558969	391.558969	377.561457	377.561457	363.140756
	363.140756	348.256715	348.256715	333.029157	333.029157	317.337879	317.337379			

J= 39	672.858585	672.858585	666.547234	666.547234	660.512802	660.512802	654.768407	654.768406	649.331284	649.331251
	644.225294	644.224712	639.488046	639.480570	635.201430	635.131835	631.593276	631.160337	628.902820	627.390210
	626.469162	623.692430	623.294596	619.187748	619.160265	614.374097	614.371261	609.054491	609.054259	603.251855
	603.251839	596.984150	596.984149	590.263456	590.263456	583.097997	583.097997	575.493550	575.493550	567.454288
	567.454288	558.982280	558.982280	550.082818	550.082818	540.754634	540.754634	531.000037	531.000037	520.820024
	520.820024	510.215346	510.215346	499.186566	499.186566	487.734097	487.734097	475.858230	475.858230	463.559157
	463.559157	450.836994	450.836994	437.691784	437.691784	424.123518	424.123518	410.132139	410.132139	395.717548
	395.717548	380.879611	380.879611	365.618165	365.618165	349.933019	349.933019	333.823960	333.823960	

J= 40	707.352870	707.352870	700.912751	700.912751	694.709370	694.709370	688.795313	688.795312	683.186962	683.186944
	677.906625	677.906303	672.987950	672.987555	668.497598	668.454024	664.619770	664.320553	661.660713	660.452127
	659.237243	656.541147	656.231576	652.274114	652.226441	647.505393	647.500572	642.224006	642.223539	636.451113
	636.451080	630.207357	630.207355	623.506490	623.506490	616.357840	616.357340	608.767932	608.767932	600.741465
	600.741465	592.281890	592.281890	583.391788	583.391788	574.073106	574.073106	564.327326	564.327326	554.155577
	554.155577	543.558719	543.558719	532.537401	532.537401	521.092106	521.092106	509.223183	509.223183	496.930875
	496.930875	484.215336	484.215336	471.076644	471.076644	457.514820	457.514820	443.529829	443.529829	429.121594
	429.121594	414.290000	414.290000	399.034899	399.034899	383.356112	383.356112	367.253438	367.253438	350.726652
	350.726652									

J= 41

742.787151	742.787151	736.138146	736.138146	729.765692	729.765692	723.681923	723.681923	717.902443	717.902433
712.443236	712.446026	707.349749	707.347192	702.662629	702.635759	698.592663	698.331546	695.277442	694.345177
692.769951	650.402104	689.934226	686.165989	686.085367	681.444925	681.435171	676.204060	676.203141	670.463638
670.463568	664.245911	664.245907	657.566495	657.566495	650.435964	650.435964	642.861679	642.861679	634.848921
634.848921	626.401565	626.401565	617.522504	617.522504	608.213927	608.213927	598.477499	598.477499	588.314497
588.314497	577.725897	577.725897	566.712441	566.712441	555.274690	555.274690	543.413057	543.413057	531.127837
531.127337	518.419225	518.419225	505.287340	505.287340	491.732231	491.732231	477.753892	477.753892	463.352268
463.352268	448.527262	448.527262	433.278742	433.278742	417.606547	417.606547	401.510486	401.510486	384.990345
384.990345	368.045890	368.045890							

J= 42

779.041140	779.041140	772.223005	772.223005	765.681348	765.681348	759.427803	759.427803	753.477262	753.477257
747.[illegible]	747.[illegible]	742.572455	742.571012	737.693695	737.677350	733.328103	733.196134	729.767974	729.074137
727.[illegible]	725.078179	724.397030	720.852221	720.730233	716.189554	716.172061	710.592997	710.991229	705.287988
705.287988	[illegible]	[illegible]	692.442327	692.442326	685.331315	685.331315	677.773804	677.773804	669.775724
669.775724	661.341415	661.341415	652.474116	652.474116	643.176276	643.176276	633.449764	633.449764	623.296014
623.296014	612.716129	612.716129	601.710955	601.710955	590.281134	590.281134	578.427149	578.427149	566.149350
566.149350	553.447982	553.447982	540.323201	540.323201	526.775092	526.775092	512.803675	512.803675	498.408922
498.408922	483.590756	483.590756	468.349064	468.349064	452.683698	452.683698	436.594482	436.594482	420.081214
420.081214	403.143670	403.143670	385.781603	385.781603					

J= 43

816.154299	816.154293	809.166905	809.166935	802.455907	802.455907	796.032509	796.032508	789.910947	789.910944
784.109010	784.109856	778.655336	778.654493	773.588595	773.578772	769.001200	768.916306	765.142489	764.643631
762.249725	760.573387	759.610450	756.365528	756.152860	751.738242	751.707587	746.589096	746.585767	740.922648
740.922648	734.763528	734.763907	729.132793	728.132792	721.042798	721.042798	713.503288	713.503288	705.520913
705.520913	697.130525	697.130528	688.245749	688.245749	678.959311	678.959311	669.243304	669.243304	659.099336
659.099336	648.528645	648.523645	637.532189	637.532189	626.110700	626.110700	614.264735	614.264735	601.994704
601.994704	589.300905	589.300905	576.183538	576.183538	562.642720	562.642720	548.678507	548.678507	534.290893
534.290893	519.479326	519.479326	504.245212	504.245212	488.586920	488.586920	472.504788	472.504788	455.998626
455.998626	439.068221	439.068221	421.713337	421.713337	403.933721	403.933721			

J= 44

854.126238	854.126238	846.969410	846.969410	840.088926	840.088926	833.495586	833.495586	827.203022	827.203020
821.228957	821.228927	815.597559	815.537081	810.345604	810.339766	805.547215	805.493563	801.405400	801.057891
798.236546	796.851181	795.607317	792.674642	792.344225	788.089699	788.037200	782.990596	782.984458	777.366027
777.365457	771.240676	771.240633	764.636654	754.636551	757.569280	757.569280	750.049077	750.049077	742.083495
742.083495	733.677958	733.677958	724.836499	724.836499	715.562163	715.562163	705.857280	705.857280	695.723646
695.723646	685.162650	685.162650	674.175369	674.175368	662.762630	662.762630	650.925071	650.925071	638.663170
638.663170	625.977278	625.977278	612.867642	612.867642	599.334419	599.334419	585.377697	585.377697	570.997500
570.997500	556.193798	556.193798	540.966519	540.966519	525.315551	525.315551	509.240746	509.240746	492.741930
492.741930	475.818896	475.818899	458.471427	458.471427	440.699271	440.699271	422.502166	422.502166	

J= 45

892.956517	892.956517	885.630077	885.630077	878.579954	878.579954	871.816571	871.816571	865.353001	865.353000
859.206389	859.206673	853.398472	853.398204	847.963344	847.959910	842.962396	842.928302	838.556018	838.320571
835.080814	834.037234	832.372556	829.792385	829.295726	825.243002	825.155193	820.195724	820.184643	814.616458
814.616458	808.527344	808.527244	801.952617	801.952611	794.909583	794.909583	787.410078	787.410078	779.462446
779.462446	771.072735	771.072735	762.245436	762.245436	752.983937	752.983937	743.290828	743.290828	733.168109
733.168109	722.617330	722.617330	711.639696	711.639696	700.236143	700.236143	688.407394	688.407394	676.153996
676.153996	663.476362	663.476362	650.374787	650.374787	636.849471	636.849471	622.900538	622.900538	608.528041
608.528041	593.721978	593.731978	578.512300	578.512300	562.869911	562.869911	546.801684	546.801684	530.310456
530.310456	513.395037	513.395037	496.055214	496.055214	478.290749	478.290749	460.101390	460.101390	441.486863
441.486863									

TABLE III—*Continued*

J= 46

932.644684	932.644684	925.148447	925.148447	917.928526	917.928526	910.994991	910.994991	904.360391	904.360391
898.040774	898.040765	892.057428	892.057276	886.440678	886.438678	881.242576	881.222073	876.590394	876.434628
872.757454	872.016160	869.921917	867.721687	867.001376	863.197754	863.054474	858.202755	858.183165	852.672199
852.670120	846.622375	846.622195	840.079334	840.079321	833.062486	833.062485	825.585163	825.585163	817.656705
817.656705	809.293855	809.293855	800.471603	800.471603	791.223713	791.223713	781.543059	781.543059	771.431861
771.431861	760.851844	760.851844	749.924355	749.924355	738.530441	738.530441	726.710918	726.710918	714.466413
714.466413	701.737398	701.737398	688.704225	688.704225	675.187139	675.187139	661.246301	661.246301	646.881798
646.881798	632.093656	632.093656	616.881849	616.881849	601.246304	601.246304	585.186909	585.186909	568.703518
568.703518	551.795556	551.795556	534.464020	534.464020	516.707434	516.707484	498.526102	498.526102	479.919610
475.515610	460.887727	460.887727							

J= 47

973.150275	973.150273	965.524052	965.524052	958.134169	958.134169	951.030361	951.030361	944.224691	944.224691
937.732474	937.732469	931.573830	931.573717	925.775633	925.775478	920.386394	920.373659	915.503263	915.402289
911.398073	910.832748	908.304785	906.466309	905.460236	901.754245	901.726553	897.010094	896.976186	891.531445
891.527597	885.824261	885.573967	879.015396	879.015369	872.026720	872.026718	864.573163	864.573163	856.665179
856.665179	848.310283	848.310283	839.514014	839.514014	830.280545	830.280545	820.613058	820.613058	810.514016
810.514016	799.365332	799.365332	789.028504	789.028504	777.644701	777.644701	765.834839	765.834839	753.599628
753.599628	740.539609	740.539609	727.855191	727.855191	714.346667	714.346667	700.414241	700.414241	686.058033
686.058032	671.276102	671.276102	656.074444	656.074444	640.447012	640.447012	624.395711	624.395711	607.920414
607.920414	591.020958	591.020958	573.597154	573.597154	555.948736	555.948786	537.775619	537.775619	519.177396
519.177396	500.153844	500.153844	480.704675	480.704675					

J= 48

1014.592316	1014.592316	1006.756412	1006.756412	999.196396	999.196396	991.922185	991.922185	984.945390	984.945390
978.280648	973.280645	971.946575	971.946929	965.970345	965.969684	960.390636	960.383178	955.289396	955.225079
955.887327	950.491407	947.511888	946.030686	944.677985	941.513588	941.162020	936.616388	936.558939	931.192348
931.185350	925.231133	925.230449	918.759334	918.759278	911.800964	911.800960	904.372865	904.372865	896.486740
896.436740	883.150953	883.150953	879.371653	879.371653	870.153457	870.153457	860.499888	860.499888	850.413666
850.413666	839.896910	839.896910	828.951280	828.951280	817.578079	817.578079	805.778330	805.778330	793.552830
793.552830	780.902196	780.902176	767.826897	767.826897	754.327281	754.327281	740.403592	740.403592	726.055991
726.055991	711.284566	711.284566	696.089345	696.089345	680.470302	680.470302	664.427364	664.427364	647.960420
647.960420	631.069325	631.069325	613.753902	613.753902	596.013949	596.013949	577.849238	577.849238	559.259522
559.259522	540.244537	540.244537	520.804000	520.804000	500.937617	500.937617			

J= 49

1056.851820	1056.851820	1048.845037	1048.845037	1041.114710	1041.114710	1033.669957	1033.669957	1026.521966	1026.521966
1019.684747	1019.684745	1013.176344	1013.176319	1007.021022	1007.020646	1001.254551	1001.250165	995.944244	995.903899
991.266343	990.905965	987.573294	986.415700	984.666824	981.877807	981.351847	977.020660	976.925465	971.653056
971.640589	965.741614	965.740116	959.309607	959.309495	952.383845	952.383837	944.983017	944.983016	937.120219
937.120219	928.804766	928.804766	920.043474	920.043474	910.841445	910.841449	901.202581	901.202581	891.129874
891.129874	880.625669	880.625669	869.691798	869.691798	858.329710	858.329710	846.540542	846.540542	834.325187
834.325187	821.684341	821.684341	808.619539	808.618539	795.128184	795.128184	781.213569	781.213569	766.874894
766.874894	752.112282	752.112282	736.925793	736.925793	721.315421	721.315421	705.281120	705.281120	688.822798
688.822798	671.940324	671.940324	654.633537	654.633537	636.902247	636.902247	618.746238	618.746238	600.165273
600.165273	581.155094	581.159094	561.727428	561.727428	541.869984	541.869984	521.586462	521.586462	

J= 50

1099.966790	1099.966790	1091.789424	1091.789424	1083.888602	1083.888602	1076.273161	1076.273161	1068.953889	1068.953889
1061.944218	1061.944217	1055.261303	1055.261290	1048.927917	1048.927705	1042.976636	1042.974034	1037.464103	1037.439139
1032.525610	1032.365842	1028.506261	1027.538407	1025.444035	1023.049860	1022.289599	1018.222472	1018.068375	1012.911765
1012.390784	1007.053213	1007.050793	1000.664602	1000.664382	993.773932	993.773915	986.402316	986.402315	978.564411
978.564411	970.270567	970.270587	961.528399	961.528399	952.343489	952.343489	942.720146	942.720146	932.661681
932.661681	922.170673	922.170673	911.249149	911.249149	899.898706	899.898706	888.120606	888.120606	875.915845
875.915845	863.285204	863.285204	850.229289	850.229289	836.748562	836.748562	822.843368	822.843368	808.513949
808.513949	793.760466	793.760466	778.583007	778.583007	762.981600	762.981600	746.956217	746.956217	730.506788
730.506788	713.622201	713.623201	696.335311	696.335311	678.612939	678.612939	660.465883	660.465883	641.893916
641.893916	622.896787	622.896787	603.474232	603.474232	583.625967	583.625967	563.351697	563.351697	542.651112
542.651112									

H_K as a variable. The spectral constants have been used to generate the energy levels shown in Table III. Because of the large number of rotational lines, the calculated spectrum is not reproduced here. It is available either from the Editorial Office of this Journal or from the second author.

An important point should be made about the use of these data in conjunction with other data sets, especially infrared rotation–vibration data sets. Although accurate ground-state energy levels are a convenient starting point for spectra assignments, from a statistical point of view it is preferable to use the observed microwave data directly in the final spectral analysis. The appropriate weightings for data are then reasonably straightforward. On the other hand, if energy levels or spectral constants are used, the appropriate statistical treatment requires the consideration of both the uncertainties in the spectral constants and in the correlation matrix (*18*). This is especially important in large centrifugal distortion analyses because of the significant correlations among the constants.

RECEIVED: August 14, 1978

REFERENCES

1. D. J. MILLEN AND J. R. MORTON, *Chem. Ind. (N. Y.)*, 954–954 (1956).
2. D. J. MILLEN AND J. R. MORTON, *J. Chem. Soc.*, 1523–1528 (1960).
3. A. P. COX AND J. M. RIVEROS, *J. Chem. Phys.* **42**, 3106–3112 (1965).
4. V. K. KAUSHIK AND P. VENKATESWARLU, *Chem. Phys. Lett.* **48**, 115–118 (1977).
5. G. E. MCGRAW, D. L. BERNITT, AND I. C. HISATSUNE, *J. Chem. Phys.* **42**, 237–244 (1965).
6. A. GOLDMAN, F. S. BONOMO, W. J. WILLIAMS, AND D. G. MURCRAY, *J. Opt. Soc. Amer.* **65**, 10–12 (1975).
7. D. G. MURCRAY, T. G. KYLE, F. H. MURCRAY, AND W. J. WILLIAMS, *J. Opt. Soc. Amer.* **59**, 1131–1134 (1969).
8. H. COHN, C. K. INGOLD, AND H. G. POOLE, *J. Chem. Soc.* 4272–4282 (1952).
9. P. BROCKMAN, C. H. BAIR, AND F. ALLARIO, *Appl. Opt.* **17**, 91–100 (1978).
10. A. MAIK, private communication.
11. G. CAZZOLI AND F. C. DE LUCIA, Thirty-Third Symposium on Molecular Spectroscopy, 1978, Abstract WH 3.
12. P. HELMINGER, F. C. DE LUCIA, AND W. GORDY, *Phys. Rev. Lett.* **25**, 1397–1399 (1970).
13. F. C. DE LUCIA, *J. Mol. Spectrosc.* **55**, 271–277 (1975).
14. W. C. KING AND W. GORDY, *Phys. Rev.* **90**, 319–320 (1953).
15. J. K. G. WATSON, *J. Chem. Phys.* **45**, 1360–1361 (1966).
16. P. HELMINGER, R. L. COOK, AND F. C. DE LUCIA, *J. Mol. Spectrosc.* **40**, 125–136 (1971).
17. R. L. COOK, F. C. DE LUCIA, AND P. HELMINGER, *J. Mol. Spectrosc.* **41**, 123–136 (1972).
18. D. L. ALBRITTON, A. L. SCHMELTEKOPF, AND R. N. ZARE, *in* "Molecular Spectroscopy, Modern Research" (K. Narahari Rao, Ed.), Academic Press, New York, 1972.

Millimeter wave measurements of the rotational spectra of ClF, BrF, BrCl, ICl, and IBr

Robert E. Willis, Jr.[a] and William W. Clark, III[b]

Department of Physics, Duke University, Durham, North Carolina 27706
(Received 7 December 1979; accepted 18 January 1980)

The rotational spectra of all twelve stable isotopic species of ClF, BrF, BrCl, ICl, and IBr were observed and measured in the millimeter wave region by means of a sensitive microwave spectrometer. Transitions were detected over a wide range of frequencies for molecules in both the ground vibrational state and several excited states. The rotational spectrum of each molecule was split by the nuclear quadrupole interaction. Altogether, 250 new lines were measured. These correspond to 136 pure rotational transitions. Values of the Dunham coefficients Y_{01}, Y_{11}, Y_{21}, Y_{31}, Y_{02}, Y_{12}, and Y_{03} were obtained from a computer analysis of the measured frequencies. From these coefficients a number of equilibrium constants were derived to significantly greater accuracy than in previous work. In particular, the equilibrium distance, r_e, was found to two or three more significant figures.

INTRODUCTION

The mixed halide diatomic molecules described in this report have all been studied previously through techniques of microwave spectroscopy by various workers[1-8] whose results are presented in the N.B.S. tables of diatomic molecules.[9] However, most of their work was confined to the centimeter wave region and was concerned with nuclear quadrupole splittings of a few, low, rotational levels. Consequently, only a small number of rotational constants have been reported. The present work in the millimeter wave region has generated measurements of 136 new rotational transitions for molecules in a number of excited vibrational states. This has increased both the quantity and the accuracy of the rotational/vibrational constants which, in turn, has permitted the derivation of the equilibrium constants B_e, ω_e, $\omega_e x_e$, and r_e as well as the Dunham potential constants a_0, a_1, a_2, and a_3. In addition, this work has yielded rotational constants which are significantly different from previously reported values for six out of the 12 isotopic species studied.

THE SPECTROMETER

The spectrometer used for this study was similar in many respects to the ones used in other investigations of this laboratory.[10,11] Briefly, it consisted of a klystron-driven crystal harmonic generator, a quasi-free-space absorption cell, and a helium-cooled InSb photodetector. Most of the transitions were measured in real time on an oscilloscope screen, although a few were observed on a chart recorder with a lock-in amplifier and a phase-locked, slow-sweep klystron.[12]

For these experiments the absorption cell was a continuously evacuated 2 in. × 4 ft. nickel pipe with Teflon end plates to permit entry of the microwave radiation. The cell was encased by two 1400 W Linberg 2724-KSP semicircular heating elements. This arrangement allowed the temperature of the cell to be raised so that excited vibrational states could be populated. The flanges and end plates were sealed with neoprene O rings. Because of reactions with the halogens, these rings had to be regreased or replaced frequently. A nitrogen cold trap was used to protect the forepump from the gases; nevertheless, the oil had to be changed occasionally, especially during the use of iodine compounds.

CHEMICAL PREPARATIONS

ClF and BrF

Chlorine trifluoride ClF_3 was used in the preparation of ClF and BrF. This is an extremely reactive gas[13] even at the pressures used in the experiment ($\sim 5\times10^{-2}$ Torr); therefore, a few special precautions were taken for the fluorine compounds: (1) The neoprene O rings were wrapped with Teflon tape and (2) copper tubing and brass fittings were used for connectors in place of rubber or glass tubing.

Chlorine monofluoride ClF was observed as a decay product of ClF_3 as the latter was was simply allowed to flow through the cell. This method was chosen over the use of ClF gas directly because ClF_3 is less expensive, easier to handle, and somewhat safer than ClF gas. However, the reaction $ClF_3 \rightarrow ClF + F_2$ proceeds very slowly at the low pressures of the absorption cell. As a result, the ClF lines were relatively weak. Adding chlorine gas to the stream caused the line strength to go down rather than up. Warming the cell to about 100 °C increased the reaction rate, but above 100 °C, the line strength decayed, dropping to 1/4 of the maximum strength at only 200 °C. The rapid signal decay at elevated temperatures made it difficult to observe higher vibrational states. This problem was common to all the molecules in this study but was most severe for ClF because of its small molecular weight.

Bromine monofluoride BrF has been found only in the gaseous state in equilibrium with Br_2 and BrF_3. For this reason BrF was made by simultaneously pumping room-temperature quantities of Br_2 and ClF_3 through a cell that varied in temperature from 25 to 450 °C. Optimum line strength occurred with the cell at 200 °C, and the lines disappeared at 500 °C. Temperatures as high as 450 °C were used to populate excited vibrational states. Often strong lines were observed when the bro-

[a] Present address: Department of Physics, Mississippi State University, Mississippi State, Miss. 39762.
[b] Present address: Night Vision Electro-optic Laboratory, Fort Belvoir, Va. 22060.

 0021-9606/80/094946-05$01.00

mine flow was off. This agrees with the fact that in an equilibrium mixture of Br_2, BrF_3, and BrF, the relative fraction of BrF drops off sharply at Br_2 is added.

BrCl, ICl, and BrI

The compounds not involving fluorine were all easier to make and handle than the above two. Bromine monochloride, BrCl, was made when one-third mole each of bromine and chlorine were combined in a 22 l Pyrex flask. At room temperature such a mixture will be 57% BrCl. The BrCl, which boils at 20 °C, was then allowed to flow through the cell. The ground-state lines were strongest at room temperature and 200 °C was the highest temperature used to populate excited vibrational states.

Since the vapor pressure of iodine is too high for it to be placed directly in the cell, the iodine compounds were also made in the 22 l flask. Addition of one-third mole of chlorine to excess iodine resulted in a rapid exothermic reaction producing ICl, a red liquid or gas (melting point 27 °C), as well as ICl_3, a dark yellow solid. The ICl was then allowed to flow through the cell. All measurements were made at room temperature because ICl decomposes at 97 °C.

Iodine monobromide IBr was made in a similar manner from a mixture of iodine and bromine in the 22 l flask. This produced IBr, dark grey crystals that melt at 41 °C and sublime at 50 °C, as well as IBr_3, a brown liquid. The flask was heated slightly with an infrared lamp to produce flow rate sufficient for measurement. The IBR lines did not appear until the IBR_3 was pumped out of the flask. Since IBR decomposes at 116 °C, the cell was not heated. This did not prevent observation of higher vibrational states, since in molecules as heavy as IBr, excited vibrational states are well populated at room temperature.

ANALYSIS OF ROTATIONAL SPECTRA

The most accurate formulas for analysis of the rotational spectra of diatomic molecules are provided by Dunham theory.[14] Dunham solved the Schrödinger wave equation for the diatomic vibrating rotor with a potential function of the form

$$V(\xi) = ch a_0 \xi^2 (1 + a_1 \xi + a_2 \xi^2 + \cdots) , \tag{1}$$

where $\xi = (r - r_e)/r_e$, and a_0, a_1, a_2, ... are the potential constants. His solution for the rotation–vibration energies is expressed by the series

$$E_{v,J} = h \sum_{l,m} Y_{l,m} (v + \tfrac{1}{2})^l [J(J+1)]^m , \tag{2}$$

in which the coefficients $Y_{l,m}$ are known as the Dunham coefficients. Each $Y_{l,m}$ is a function of the molecular parameters r_e, a_0, a_1, a_2, ... which appear in Eq. (1). In terms of the familiar spectroscopic constants,

$$Y_{10} \cong \omega_{e'} Y_{01} \cong B_{e'} Y_{11} \cong -\alpha_{e'} Y_{21} \cong \gamma_{e'} ,$$
$$Y_{20} \cong -\omega_e x_{e'} Y_{02} \cong -D_{e'} Y_{12} \cong -\beta_{e'} Y_{03} \cong H_e . \tag{3}$$

For pure rotational transitions the transition frequencies are given by

$$\nu_{v,J} - \nu_{v,J+1} = 2[Y_{01} + Y_{11}(v + \tfrac{1}{2}) + Y_{21}(v + \tfrac{1}{2})^2 + Y_{31}(v + \tfrac{1}{2})^3 + \cdots]$$
$$\times (J+1) + 4[Y_{02} + Y_{12}(v + \tfrac{1}{2}) + \cdots](J+1)^3$$
$$+ Y_{03}(J+1)^3 [(J+2)^3 - J^3] + \cdots , \tag{4}$$

where only terms which give a detectable contribution to the spectra of this report are retained.

The spectrum of each species was analyzed by substitution of each reduced experimental rotational frequency (see quadrupole analysis) and the appropriate J and v quantum numbers into Eq. (4). This produced a set of simultaneous equations which were solved by the method of least squares for the $Y_{l,m}$'s. Although it is possible to analyze each individual isotopic species independently, use of the Dunham isotope relationship

$$Y'_{l,m} = (\mu/\mu')^{(l+2m/2)} Y_{l,m} \tag{5}$$

allows all the isotopic data for each molecular species to be analyzed together. This results in significantly better values for the $Y_{l,m}$, especially in the case of less abundant species for which few transitions are observed. Equation (5) is accurate to within experimental error for all $Y_{l,m}$ except Y_{01}.

The Y_{03} was calculated from the Dunham relation

$$Y_{03} = \frac{Y_{11}}{3} \left(\frac{-Y_{02}}{Y_{01}} \right)^{3/2} + \frac{2Y_{02}^2}{Y_{01}} \tag{6}$$

and its contribution to the measured frequencies removed before the least-squares analysis. Although its value can be calculated directly from the spectra, the procedure used here results in a more accurate Y_{03} as well as improved values for the other constants.

After determination of the Dunham coefficients the first four potential constants of Eq. (1) can be found by the relations

$$a_0 \equiv \frac{\omega_e^2}{4B_e} = \frac{B_e^2}{D_e} \cong \frac{-Y_{01}^2}{Y_{02}} , \tag{7}$$

$$a_1 = \frac{Y_{11} Y_{10}}{6Y_{01}^2} - 1 = \frac{Y_{11}}{3(-Y_{02} Y_{01})^{1/2}} - 1 , \tag{8}$$

$$a_2 = \frac{Y_{12}}{6} \left(\frac{Y_{01}}{-Y_{02}^3} \right)^{1/2} + \tfrac{9}{8} a_1 (2 + a_1) + \tfrac{19}{8} , \tag{9}$$

$$a_3 = -\frac{2}{5} \frac{Y_{21}}{Y_{02}} + \frac{a_2}{5}(3 + 13a_1) - \frac{a_1}{2}[4 + 3a_1(1 + a_1)] - 1. \tag{10}$$

The relations given in Eq. (3) and subsequently used in Eqs. (7)–(10) are not exact. The exact relations are power series in $(B_e/\omega_e)^2$. Since for the mixed halides this ratio is of the order 10^{-6}, these relations may be considered accurate to the experimental uncertainty except for Y_{01}, which can be calculated to a higher accuracy from precision spectral data. The precise relationship between Y_{01} and B_e is

$$Y_{01} = B_e [1 + C_3 (B_e/\omega_e)^2] = B_e + \delta_3 . \tag{11}$$

This difference between B_e and Y_{01} is known as the Dunham correction (δ_3).

Two other small corrections to Y_{01} result from electronic effects which are not included in the Dunham theory. These arise from the nonspherical distribution

of the atomic electrons around their respective nuclei (δ_1) and the wobble–stretch effect (δ_2).[15,16] The first of these may be calculated from knowledge of the molecular g factor by

$$\delta_1 = -(m_e/m_p) g_J B_e \ . \tag{12}$$

Although δ_2 cannot be calculated directly from known molecular parameters, its reduced mass dependence of $(1/\mu)^2$ allows its calculation if two or more isotopic species are observable. Since δ_1 and δ_3 also have a $(1/\mu)^2$ dependence, the net effect of all three corrections may be calculated from the system of equations.

$$(B_e - Y_{01})_i - C/\mu_i^2 = 0 \ , \tag{13}$$

where $C = \delta_1 + \delta_2 + \delta_3$ and i is an isotopic species label.

The values of B_e thus calculated provide a very accurate determination of the equilibrium distance r_e by means of the definition of B_e:

$$B_e \equiv h/8\pi^2 \mu r_e^2 \ . \tag{14}$$

The zero-point vibration frequency ω_e can next be calculated from the relation

$$\omega_e = (4B_e^3/D_e)^{1/2} \cong [4B_e^3/(-Y_{02})]^{1/2} \tag{15}$$

and $\omega_e x_e$ is obtained from

$$\omega_e x_e = -3Y_{01}(a_2 - \tfrac{5}{4}a_1^2)/2 \ .$$

NUCLEAR QUADRUPOLE INTERACTIONS

Hyperfine structure which occurs in the diatomic halides causes the observed frequencies to deviate slightly from those given in Eq. (4). These deviations are caused by nuclear electric quadrupole interactions with the electric field gradient at the nucleus. This splits the rotational energy levels into $2I+1$ sublevels, where I is the nuclear spin. The actual energy levels are found from perturbation theory and to first order are given by[17]

$$E_{J,v,F} = E_{J,v} - eQq\,Y(J,I,F) \ , \tag{16}$$

where $E_{J,v}$ is the rotational energy given by Eq. (2), eqQ is the quadrupole coupling constant, and $Y(J,I,F)$ is Casimer's[18] function. The F in Eq. (16) is the total angular momentum quantum number which can assume the values $(J+1)$, $(J+I-1)$, ..., $|J-I|$. Each rotational transition is thus split into a number of hyperfine lines, some of which are doubly degenerate or nearly degenerate. Figure 1 shows a typical rotational transition which is split by the quadrupole interaction.

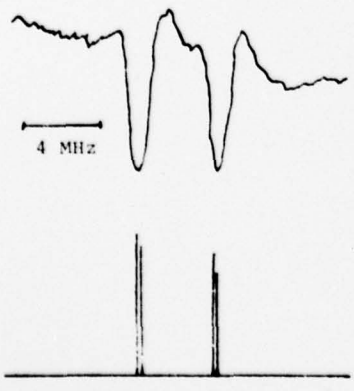

FIG. 1. Comparison of the theoretical and experimental quadrupole structure of ^{79}BrF, $J = 9 \rightarrow 10$, $v = 2$, at 209 379.84 MHz.

TABLE I. Dunham coefficients and equilibrium constants of chlorine monofluoride.

	$^{35}Cl^{19}F$	$^{37}Cl^{19}F$
Y_{01} (MHz)	15 483.2702(36)[a]	15 188.8247(30)
Y_{11} (MHz)	−129.6497(50)	−125.9687(49)
Y_{21} (kHz)	−520.3(1.7)	−500.7(1.6)
Y_{02} (kHz)	−26.91(2)	−25.90(2)
Y_{12} (kHz)	−0.14(2)	−0.13(2)
Y_{03} (Hz)	$-5.47(3)\times10^{-3}$	$-5.16(3)\times10^{-3}$
B_e (MHz)	15 484.4304(70)	15 189.9412(70)
r_e (Å)	1.628341(4)[b]	1.628341(4)[b]
ω_e (cm^{-1})	783.553(30)	776.067(30)
$\omega_e x_e$ (cm^{-1})	5.045(87)	5.026(84)

[a]Uncertainties represent one standard deviation.
[b]The uncertainty accrues from Planck's constant.

For $J \rightarrow J+1$ rotational transitions, the selection rules for quadrupole structure are $\Delta F = 0, \pm 1$. For the high J values observed in this report, the $\Delta F = +1$ transitions dominate in strength. Therefore, the deviation in line frequency from Eq. (4) is given by

$$\Delta\nu = -eqQ[Y(J+1,I,F+1) - Y(J,I,F)] \ . \tag{17}$$

Since the frequency shift given in Eq. (17) decreases as $1/J^2$, the quadrupole structure was unresolved at high values of J. Nevertheless, quadrupole structure was observed in lower J transitions for all of the molecules in this report and had to be considered before the rotational analysis was attempted.

The frequencies of the unsplit rotational lines were determined in two ways. First, through measurement of the hyperfine splitting in this work, a reduced frequency could be determined from Eq. (17). The second method was to use the eqQ's obtained by the earlier lower frequency work, which yielded values one to two orders of magnitude more accurate than the eqQ's calculated from this work. This latter method gave a slightly different center frequency for each hyperfine component; the average of these frequencies was then averaged with the frequency resulting from the first method to yield a final value for the reduced rotational frequency.

For the species in which both nuclei have a quadrupole moment, the weaker quadrupole moment produced no observable splittings or shifts but did cause considerable broadening in some cases. The effect was strongest for low-frequency transitions in IBr and BrCl. Severely broadened transitions which could not be resolved were avoided in most instances because of difficulty in determination of the center frequency.

SPECTRAL CONSTANTS

The actual transition frequencies are not listed here but are recorded in the Ph.D. thesis of R. E. Willis.[19]

TABLE II. Dunham coefficients and equilibrium constants of bromine monofluoride.

	$^{79}Br^{19}F$	$^{81}Br^{19}F$
Y_{01} (MHz)	10 667.4502(35)[a]	10 616.3476(36)
Y_{11} (MHz)	−77.8629(79)	−77.3040(78)
Y_{21} (kHz)	−201.6(45)	−199.7(45)
Y_{31} (kHz)	−6.2(8)	−6.1(8)
Y_{02} (kHz)	−12.049(10)	−11.934(10)
Y_{12} (Hz)	−66(1)	−66(11)
Y_{03} (Hz)	$-3.937(7)\times10^{-3}$	$-3.881(7)\times10^{-3}$
B_e (MHz)	10 668.0970(69)	10 616.9882(69)
r_e (Å)	1.758987(4)[b]	1.758987(4)[b]
ω_e (cm^{-1})	669.679(28)	668.67(28)
$\omega_e x_e$ (cm^{-1})	3.863(76)	3.844(78)

[a]Uncertainties listed are one standard deviation.
[b]The uncertainty accrues from Planck's constant.

TABLE IV. Dunham coefficients and equilibrium constants of iodine monochloride.

	$^{127}I^{35}Cl$	$^{127}I^{37}Cl$
Y_{01} (MHz)	3422.3638(20)[a]	3277.4173(19)
Y_{11} (MHz)	−15.9751(43)	−14.9710(40)
Y_{21} (MHz)	−35.2(26)	−32.3(24)
Y_{31} (kHz)	−0.6(4)	−0.5(3)
Y_{02} (kHz)	−1.2081(6)	−1.108(6)
Y_{12} (Hz)	−5.9(6)	−5.5(6)
Y_{03} (Hz)	$-2.639(3)\times10^{-4}$	$-2.318(3)\times10^{-4}$
B_e (MHz)	3422.4275(38)	3277.4758(36)
r_e (Å)	2.320962(6)[b]	2.320962(6)[b]
ω_e (cm^{-1})	384.290(96)	376.064(94)
$\omega_e x_e$ (cm^{-1})	1.501(26)	1.437(25)

[a]Uncertainties listed are one standard deviation.
[b]The uncertainty accrues from Planck's constant.

The molecular constants are given; they can be used for calculation of the frequencies to high accuracy (≤ 0.1 MHz).

ClF

Previous microwave measurements of ClF have been made by White[1] and Gilbert.[2] They measured a number of quadrupole lines of the $J = 0 \rightarrow 1$ rotational transition in the 0, 1 vibrational states. The current work has produced measurements of 42 new transitions: 32 of ^{35}ClF and 10 of the lesser abundant ^{37}ClF. These measurements yielded 22 reduced rotational frequencies covering the rotational states from $J = 2$ up to $J = 11$ in the 0, 1, 2 vibrational states. The frequencies ranged from 92 GHz at $J = 2 \rightarrow 3$ to 339 GHz at $J = 10 \rightarrow 11$.

The Dunham coefficients obtained from these measurements are shown in Table I along with the equilibrium constants. Comparison of calculated frequencies with the measured frequencies yields a root mean square deviation of 35 kHz for both isotopes combined.

From the previous measurements and an infrared measurement of ω_e,[20] three Dunham coefficients (Y_{01}, Y_{11}, Y_{02}) were obtained (calculated by Ref. 9). These values are in rough agreement with our values, except for Y_{01} of ^{37}ClF which differs by 5 MHz.

BrF

Previous microwave measurements of BrF have been made by Smith *et al.*[3] As in the case of ClF, only the lowest rotational transition in the 0, 1 vibrational states was measured. In the current work 56 new transitions have been measured: 20 of ^{79}BrF and 26 of ^{81}BrF. These measurements produced 28 reduced rotational frequencies covering the rotational states from $J = 3$ to $J = 13$ and the vibrational states 0, 1, 2, 3. The measured frequencies ranged from 85 to 276 GHz and the rms deviation of the fitting was 37 kHz.

Table II shows the Dunham coefficients and equilibrium constants obtained from this work. The earlier measurements gave values for Y_{01} and Y_{11} (calculated by Ref. 9). While our values of Y_{11} are in agreement, our values of Y_{01} differ by about 50 MHz for both isotopes.

BrCl

For BrCl, 63 new transitions were measured: 28 of $^{79}Br^{35}Cl$, 17 of $^{81}Br^{35}Cl$, 10 of $^{79}Br^{37}Cl$, and eight of $^{81}Br^{37}Cl$. The number of reduced rotational frequencies obtained was 33, covering rotational states from $J = 13$ to $J = 34$ and vibrational states $v = 0$ to $v = 3$. The frequencies of the measurements ranged from 122 to 309

TABLE III. Dunham coefficients and equilibrium constants of bromine monochloride.

	$^{79}Br^{35}Cl$	$^{81}Br^{35}Cl$	$^{79}Br^{37}Cl$	$^{81}Br^{37}Cl$
Y_{01} (MHz)	4570.9687(13)[a]	4536.3140(13)	4399.8516(13)	4365.1979(12)
Y_{11} (MHz)	−23.1426(29)	−22.8800(29)	−21.8553(27)	−21.5976(27)
Y_{21} (kHz)	−61.9(18)	−61.0(18)	−57.4(17)	−56.5(16)
Y_{31} (kHz)	−0.9(3)	−0.9(3)	−0.8(3)	−0.8(3)
Y_{02} (kHz)	−2.1527(7)	−2.1202(7)	−1.9945(7)	−1.9632(7)
Y_{12} (Hz)	−10.7(8)	−10.5(8)	−9.7(8)	−9.5(8)
Y_{03} (Hz)	$-4.656(3)\times10^{-4}$	$-4.551(3)\times10^{-4}$	$-4.152(3)\times10^{-4}$	$-4.055(3)\times10^{-4}$
B_e (MHz)	4571.0295(26)	4536.3793(25)	4399.9082(25)	4365.2527(25)
r_e (Å)	2.136124(5)[b]	2.136124(5)[b]	2.136124(5)[b]	2.136124(5)[b]
ω_e (cm^{-1})	444.322(62)	442.634(62)	435.926(61)	434.206(61)
$\omega_e x_e$ (cm^{-1})	1.856(20)	1.849(20)	1.787(19)	1.771(2)

[a]Uncertainties listed are one standard deviation.
[b]The uncertainty accrues from Planck's constant.

TABLE V. Dunham coefficients and equilibrium constants of iodine monobromide.

	$^{127}I^{79}Br$	$^{127}I^{81}Br$
Y_{01} (MHz)	1703.79826(30)[a]	1677.85957(30)
Y_{11} (MHz)	−5.90413(41)	−5.76982(40)
Y_{21} (kHz)	−13.66(15)	−13.25(15)
Y_{31} (kHz)	−0.14(2)	−0.13(2)
Y_{02} (Hz)	−304.91(2)	−295.70(2)
Y_{12} (Hz)	−1.50(2)	−1.44(2)
Y_{03} (Hz)	$-3.9868(11)\times10^{-5}$	$-3.8075(11)\times10^{-5}$
B_e (MHz)	1703.8172(6)	1677.8780(6)
r_e (Å)	2.479078(6)[b]	2.469078(6)[b]
ω_e (cm^{-1})	268.69(9)	266.64(9)
$\omega_e x_e$ (cm^{-1})	0.826(6)	0.814(6)

[a]Uncertainties listed are one standard deviation.
[b]The uncertainty accrues from Planck's constant.

GHz, and the rms deviation of the fitting was 36 kHz. The Dunham coefficients and equilibrium constants of BrCl are shown in Table III.

Smith *et al.*[4] did earlier work on BrCl as well as BrF. As for the previous molecule, they measured a number of quadrupole lines of the $J=0\rightarrow1$ rotational transition in two vibrational states (0, 1). This yielded two Dunham coefficients for each species Y_{01} and Y_{11} (calculated by Ref. 9). Except for one instance, their numbers are in good agreement with our more accurate values. Their value of Y_{01} for $^{79}Br^{37}Cl$ differs by 100 MHz from ours. This may be a misprint because it clearly violates the isotopic relationship of Eq. (5) although it does appear in both the original article and in the review work of Ref. 9.

ICl

Weidner,[5] Townes *et al.*,[6] and Herbst and Steinmetz[7] have all studied ICl. These earlier studies produced measurements of over 150 quadrupole lines in three rotational and two vibrational states. These measurements, in turn, have given very accurate values of Y_{01} and Y_{11}.[7,9] The current work on ICl has yielded five additional Dunham coefficients, as shown in Table IV. These were obtained from 50 new quadrupole lines (42 of $I^{35}Cl$ and eight of $I^{37}Cl$) of 23 new rotational frequencies. The current work covered the rotational states from $J=12$ to $J=44$ and vibrational states $v=0$ to $v=3$. The frequencies involved ranged from 85 to 300 GHz. The rms deviation of the fitting was higher for ICl (50 kHz) than for any other molecule in this study because of difficulty in resolution of the quadrupole structure.

IBr

Like ICl, IBr is a heavy diatomic with a complicated quadrupole structure at low J. Jaseta[8] has measured over 150 quadrupole lines of two rotational transitions ($J=4\rightarrow5$ and $J=5\rightarrow6$) in three vibrational states ($v=0$, 1, 2). In this study we have measured 40 new quadrupole lines (19 of $I^{79}Br$ and 21 of $I^{81}Br$) in 30 rotational states and five vibrational states (0, 1, 2, 3, 4). The rotational states covered the range from $J=43$ to $J=96$ and the frequencies, from 150 to 325 GHz. The transitions above $J=53\rightarrow54$ revealed no quadrupole structure.

TABLE VI. Dunham potential constants of the diatomic mixed halides.

	a_0 (cm^{-1})	a_1	a_2	a_3
ClF	$2.9712(25)[a]\times10^5$	−3.1171(9)	5.63(11)	−8.8(8)
BrF	$3.1503(26)\times10^5$	−3.2893(10)	6.29(15)	−9.5(11)
BrCl	$3.2369(9)\times10^5$	−3.4590(5)	6.85(8)	−11.2(7)
ICl	$3.2338(16)\times10^5$	−3.6188(5)	7.60(15)	−13.2(1.3)
IBr	$3.1755(26)\times10^5$	−3.7305(2)	7.70(3)	−12.6(3)

[a]Uncertainties represent one standard deviation.

In Table V are listed the Dunham coefficients obtained from this work. Jaseta[8] was able to obtain values for Y_{01} and Y_{11}, but our numbers are not in agreement with his.

POTENTIAL CONSTANTS

Shown in Table VI are the Dunham potential constants as calculated from Eqs. (7) through (10). To within experimental uncertainty, these constants are isotopically invariant, a result which confirms an initial assumption of Dunham theory. It is of interest to note that the values are similar for all the molecules, generally increasing slightly with increasing mass.

ACKNOWLEDGMENTS

This study was supported by the U. S. Army Research Office, Grant No. DAAG29-77-G-0007. The authors would like to express their appreciation to Dr. Walter Gordy, Mrs. Vida Gordy, and Dr. Frank C. DeLucia for continuing interest and guidance in this work.

[1]R. L. White, Rev. Mod. Phys. 27, 276 (1955).
[2]D. A. Gilbert, A. Roberts, and P. A. Griswald, Phys. Rev. 76, 1723 (1949).
[3]D. F. Smith, M. Tidwell, and D. V. P. Williams, Phys. Rev. 77, 420 (1950).
[4]D. F. Smith, M. Tidwell, and D. V. P. Williams, Phys. Rev. 79, 1007 (1950).
[5]R. T. Weidner, Phys. Rev. 72, 1268 (1947).
[6]C. H. Townes, B. D. Wright, and F. R. Merritt, Phys. Rev. 73, 1249A (1948).
[7]E. Herbst and W. Steinmetz, J. Chem. Phys. 56, 5342 (1972).
[8]T. S. Jaseta, J. Mol. Spectrosc. 5, 445 (1960).
[9]F. J. Lovas and E. Tiemann, J. Phys. Chem. Ref. Data 3 (1974).
[10]W. C. King and W. Gordy, Phys. Rev. 90, 319 (1953); 93, 407 (1954).
[11]E. Pearson and W. Gordy, Phys. Rev. 152, 42 (1966).
[12]F. C. De Lucia, J. Mol. Spectrosc. 55, 271 (1975).
[13]*The Merck Index of Chemicals and Drugs* (Merck, Rahway, 1960).
[14]J. L. Dunham, Phys. Rev. 41, 721 (1932).
[15]J. H. Van Vleck, J. Chem. Phys. 4, 327 (1936).
[16]B. Rosenblum, A. H. Nethercrot, and C. H. Townes, Phys. Rev. 109, 400 (1958).
[17]A general treatment of quadrupole interactions can be found in W. Gordy and R. Cook, *Microwave Molecular Spectra* (Wiley, New York, 1970).
[18]H. B. G. Casimer, "On the Interaction Between Atomic Nuclei and Electrons," Texler's Tweede Genootschap, E. F. Bohn, Haarlem, 1936.
[19]R. E. Willis, Jr., "Millimeter and Submillimeter Wave Spectra of the Mixed Diatomic Halides," unpublished Ph. D. dissertation, Duke University, 1979.
[20]A. L. Wahrhaftig, J. Chem. Phys. 10, 248 (1942).

Reprinted from
Proc. Natl. Acad. Sci. USA
Vol. 74, No. 1, pp. 216–220, January 1977
Biophysics

(15)

Nuclear coupling of ^{33}S and the nature of free radicals in irradiated crystals of *N*-acetyl-L-cysteine

(electron spin resonance/^{33}S hyperfine structure)

JOSEPH H. HADLEY, JR.* AND WALTER GORDY†‡

* Department of Physics, Georgia State University, Atlanta, Ga. 30303; and † Department of Physics, Duke University, Durham, North Carolina 27706

Contributed by Walter Gordy, October 26, 1976

ABSTRACT **Hyperfine structure due to ^{33}S in its natural abundance of 0.76% has been measured in the electron spin resonance of free radicals produced by x-irradiation of single crystals of *N*-acetyl-L-cysteine at 77 K. These measurements proved that the radicals produced at 77 K with principal *g* values of 1.990, 2.006, and 2.214 are monosulfide radicals with the 3*p* unpaired electron density of 0.70 on the S. They are believed to be negatively charged molecules RCH_2S^-H or neutral RCH_2SH_2 radicals in which 90% of the spin density of the captured electron is concentrated in a *d-p* hybrid orbital on the S. As the temperature is raised to 300 K, these, as well as the carbon-centered radicals produced at the lower temperature, are mostly converted to neutral disulfide radicals RCH_2SS like those observed in irradiated cystine.**

Free radicals with electron spin density concentrated on sulfur (sulfur-centered radicals) have now been detected with electron spin resonance (ESR) in many irradiated organic and biochemical compounds containing sulfur. Their principal *g* values are usually in the range of 2.003–2.065. However, a sulfur-centered radical with an exceptional *g* tensor having principal values ranging from 1.99 to 2.29 was observed by Akasaka (1) in single crystals of L-cysteine·HCL irradiated with 1.5 MeV at 77 K (one MeV equals 1.6×10^{-13} joule). The *g* tensor was found to have approximately axial symmetry about the larger value. In 1965, the structure of the crystal was unknown, and it was therefore impossible to relate the observed *g* tensor to the molecular structure. In the following year, Box *et al.* (2) observed radicals with principal *g* values of $g_u = 1.985$, $g_v = 2.004$, and $g_w = 2.251$ in single crystals of cysteine·HCl irradiated with UV at 77 K. The similarity in *g* tensors supported the conclusion that these radicals were probably of the same form as those observed by Akasaka. In the meantime, the structure of the cysteine·HCl crystals was obtained from x-ray diffraction by Ayyar and Srinivasan (3). This made it possible for Box *et al.* (2) to deduce that the largest *g* value had the direction of the CS bonds of the undamaged molecule. Later, this radical was also observed by Kayushin *et al.* (4). Recently Saxebøl and Herskedal (5) have observed sulfur radicals with principal *g* values of 1.990, 2.006, and 2.214 (denoted as "R_1" radicals) in single crystals of *N*-acetyl-L-cysteine irradiated at 77 K with 4.0 MeV electrons.

To distinguish between the different types of sulfur radicals and to gain more quantitative information about them, we initiated a program for measurement of the ^{33}S hyperfine structure in irradiated single crystals of sulfur compounds (6–8). Unlike the *g* tensor, the ^{33}S coupling gives a reliable distinction between disulfide and monosulfide radicals and provides quantitative values for the spin densities on particular S atoms. Because of the difficulty of obtaining sufficient quantities of compounds with enriched ^{33}S to grow the required single crystals, we decided to concentrate our efforts on improvement of our spectrometer sensitivity so that reliable measurement could be made on crystals with ^{33}S in its natural abundance of 0.76%. To our gratification, we found that we were able to detect the ^{33}S lines for the hyperfine components, with ample sensitivity (signal response about 25 times greater than background noise level) to make reliable measurements of the ^{33}S coupling for certain irradiated crystals. In some instances where the ^{33}S splitting is small or the spin-lattice relaxation time is unfavorable, the ^{33}S components are masked by wings of the much stronger absorption lines of the normal isotopic species. Other factors of importance to detectability of the ^{33}S lines are the degree of *g* anisotropy of the various species of radicals in the irradiated sample and the number of magnetically distinguishable orientations for each species. We have now succeeded in measuring the ^{33}S hyperfine structure of the radicals with the unusual *g* tensors in crystals of both cysteine·HCl (H_2O) and *N*-acetyl-L-cysteine. The measurements prove that both are monosulfide radicals with similar electronic structures. A description of the results for *N*-acetyl-L-cysteine is given below.

EXPERIMENTAL DETAILS

The *N*-acetyl-L-cysteine crystals were grown by slow evaporation from saturated H_2O solutions as was done by Saxebøl and Herskedal (5). They were given 200 Mrad dosages of 50 keV x-rays at 77 K and were observed with an X-band (9.3 GHz) spectrometer like that employed in our earlier work (6). One Mrad equals 10^4 J/Kg.

Samples were annealed at 300 K to destroy a carbon-centered radical (5). Because the linewidth was too great to permit observation of the R_1 sulfur-centered radical at room temperature, the ESR spectra were obtained at 77 K.

Although the detailed structure of acetyl cysteine is unknown, our preliminary x-ray diffraction shows that the crystal is triclinic with one molecule in unit cell. An orthogonal *uvw* coordinate system coinciding with the principal directions of the *g* tensor was chosen for the hyperfine measurements. Our *u* axis corresponds to the Z axis employed by Saxebøl and Herskedal and our *u* and *w* axes are about 28° from their Y and X axes, respectively.

THE MONOSULFIDE RADICAL

This is the sulfur radical (R_1) with the exceptional *g* tensor described above. It is produced by the irradiation at 77 K and is relatively stable to temperatures well above 77 K, having a room-temperature half-life of the order of 1 day. However, the radical decays rapidly at temperatures of 400 K and above. Our measurements confirm the unusual *g* tensor observed by Saxebøl and Herskedal. We did not improve their rather accurate values: $g_u = 1.990$, $g_v = 2.006$, and $g_w = 2.214$.

Abbreviation: ESR, electron spin resonance.
‡ To whom reprint requests should be addressed.

The ESR spectrum of this radical has an essentially isotropic proton hyperfine structure consisting of four lines arising from two protons with couplings of 22 G and 29 G. (One gauss equals 1×10^{-4} tesla.) This structure is superimposed on each ^{33}S hyperfine component and provides a ready identification for them. Fig. 1 shows a typical pattern observed. In the central region is the characteristic pattern for the abundant ^{32}S species, with the receiver gain reduced by a factor of 1/500. Beyond the breaks in the curve, on either side, where the gain is 500 times greater, are components of the ^{33}S species as indicated.

The ^{33}S hyperfine splitting was found to be maximum along the axis of g_u, the minimum principal g value, and to be very nearly axially symmetric about this axis. Fig. 2 shows plots of the observed displacements of the ^{33}S components as a function of angular deviation from the axis of g_u, as far as the components could be followed.

There is a small (3 MHz) low-field shift of the center of the ^{33}S patterns from the ^{32}S spectra due to a second-order Breit-Rabi type of interaction. However, this interaction did not measurably influence the component spacings which were fitted to the first-order formula expressed in the principal axes system as

$$A = (1/g)(g_u^2 A_u^2 l_u^2 + g_v^2 A_v^2 l_v^2 + g_w^2 A_w^2 l_w^2)^{1/2} \quad [1]$$

where

$$g = (g_u^2 l_u^2 + g_v^2 l_v^2 + g_w^2 l_w^2)^{1/2} \quad [2]$$

Here the l's are the cosines of the angles the external field makes with the orthogonal uvw coordinate system. A least-squares fitting of Eq. 1 to the observed hyperfine splittings with **H** in the uv and uw planes yielded (see Table 1) principal values of 199 ± 1, 38 ± 3, and 32 ± 6 MHz for the ^{33}S coupling. Note that the coupling is of approximately axial symmetry about the largest element. We therefore set

$$A_\parallel = A_u = 199 \text{ MHz}, \quad [3]$$

$$A_\perp \cong (A_v + A_w)/2 = 35 \text{ MHz}. \quad [4]$$

Substitution of these values in the axially symmetric coupling formulas,

$$A_\parallel = A_f + 2B \text{ and } A_\perp = A_f - B. \quad [5]$$

yields

$$A_f = 90 \text{ MHz and } B = 54.7 \text{ MHz}$$

where A_f is the isotropic component and B is the anisotropic component of the ^{33}S coupling. These results are summarized in Table 1.

We can safely assume that the anisotropic component B arises primarily from 3p orbital spin density on the S. Although the g tensor gives evidence for some contribution from the 3d orbital, the 3d spin density is probably not greater than 0.20, and the coupling by a 3d electron is an order of magnitude less than that of a 3p electron. With the known atomic 3p orbital coupling of 78 MHz, the 3p orbital spin density is thus found from the anisotropic coupling to be $\rho_{3p} = 54.7/78 = 0.70$. Similarly, the isotropic component with the known 3s orbital coupling indicates that $\rho_{3s} = 90/2700 = 0.03$ on the S. This 3s spin density is of the order of that expected from a σ–π configuration interaction.

Although the ^{33}S coupling proves that the spin density is concentrated mostly on a single sulfur, the g tensor of the monosulfide radical observed in acetyl cysteine indicates that this radical is not of the same type as the neutral radical RCH_2S observed at sub-room-temperatures in irradiated cystine (6). Akasaka (1) has proposed that the approximately axial symmetry in g and the anomalously large $g_w = 2.29$ which he observed for irradiated cysteine·HCl(H_2O) at 77 K might be attributed to a radical of the type RCH_2S in which there is a near degeneracy of the p_x and p_y orbitals. However, this model does not account for the fact that the minimum g is less than the free spin value nor for the large deviations of the other principal g values from those of the RCH_2S radical in cystine·HCl. We propose that the two observed monosulfide radicals are basically distinct, that the one observed in acetyl cysteine utilizes five valence orbitals of the S whereas the one found in irradiated cystine utilizes only four. The five-orbital S radical may be a negatively charged molecule $(RCH_2SX)^-$ or a neutral radical RCH_2SX_2 in which the X is H in the radicals discussed here.

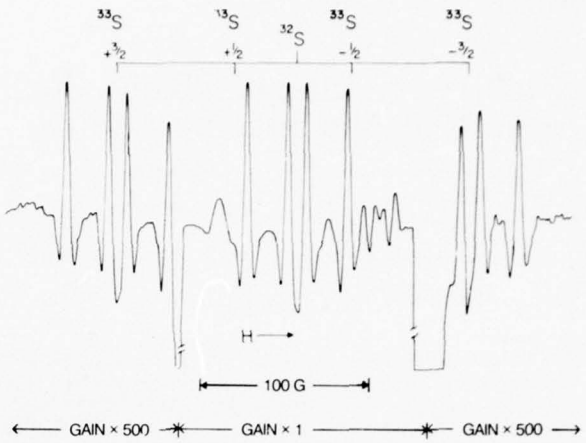

FIG. 1. Second-derivative ESR spectrum for the monosulfide radical R_1 observed with magnetic field in the uw plane 20° from the u axis (direction of minimum g). The four-line proton pattern for the unpaired spin localized in a ^{32}S atom is shown in the center of the spectrum at reduced gain. The $-3/2$ and $+3/2$ ^{33}S components can be seen to the right and left at high gain. The $\pm 1/2$ components are completely obscured by the stronger ^{32}S pattern and radicals stable at room temperature.

Probably the radical observed in L-cysteine·HCl(H_2O) at 77 K is the negatively charged molecule $(RCH_2SH)^-$ with the odd electron concentrated on the S. In *N*-acetyl-L-cysteine the sulfur radical is somewhat more stable than it is in cysteine and has a lower g_w (2.214 as compared with 2.29). Hydrogen bonding involving the S, as indicated in structure (I) may help to stabilize the negative charge on the S, or perhaps an internal shift of an H produces a more stable form (II),

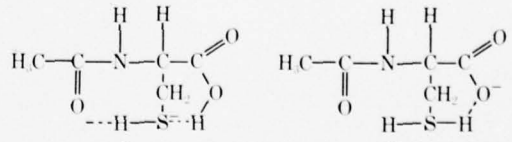

(I) (II)

in which the negative charge is on an oxygen. The dotted lines indicate hydrogen bonds. A possible alternative is transfer of a proton from the COOH of an adjacent molecule in the crystal to the negatively charged SH group of (I) to form the neutral radical (III)

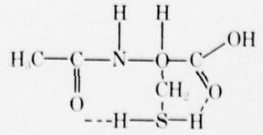

(III)

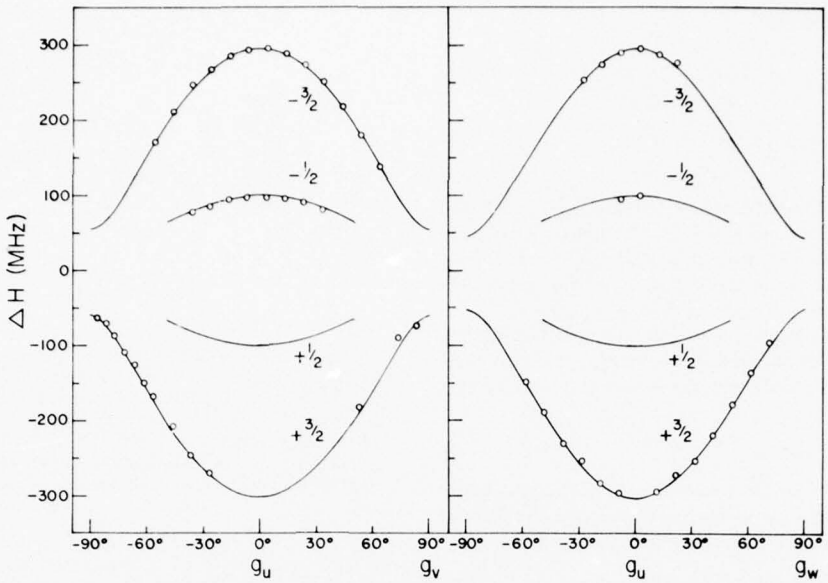

FIG. 2. Plots of the ^{33}S hyperfine splitting for the monosulfide radical with **H** imposed in the *uv* (left) and *uw* (right) planes. The splittings, plotted in MHz because of the large *g* variation in the *uw* plane, are measured from the center of the ^{32}S resonance. The circles are data points; the solid lines are computer fits to the splitting between the $-\frac{1}{2}$ and $+\frac{1}{2}$ components. The ^{33}S pattern is shifted about 3 MHz (downfield) from the center of the ^{32}S pattern by second-order effects.

Without specific knowledge of the locations of the atoms in the crystal one cannot predict which form is the more probable.

Although a radical of type (I), (II), or (III) would have anisotropic SH proton hyperfine interactions, approximate calculations indicate that these would not cause resolvable splitting and that the resulting spread would fall within the observed line widths. Furthermore, Saxebøl and Herskedal proved with deuterated crystals that the observed four-line spectrum was associated with the CH_2 protons rather than exchangeable hydrogens.

The important characteristic of the forms (I), (II), or (III) is the utilization of five orbitals of the S. It appears that an electron captured by RSH goes into a *p-d* hybridized orbital of the S, whereas one captured by RSSR goes into an antibonding σ^* orbital formed by a linear combination of *p* orbitals of the two sulfurs (7). Evidently a similar configuration utilizing an antibonding orbital of the CS or SH bond of cysteine has higher energy than one utilizing a fifth atomic orbital on the S formed by a hybridization of 3*d* and 3*p* orbitals. Thus, the "three-electron bond" does not appear to be involved in the formation of three bonds to the sulfur, but rather the 3*d* shell is employed to expand the number of bonding orbitals of the S to accommodate the additional bond.

The many unknown parameters prevent determination of the specific amounts or kinds of *d*-orbital hybridization that occur in the (RCH_2SH^-) or RCH_2SH_2 radical, but normalization of the unpaired electron density with the 3*p* spin density of 70% and the 10% positive spin density on CH_2 revealed by the proton coupling indicates that the 3*d* character of the unpaired electron orbital is approximately 20%. This amount is adequate to account for the observed reduction of g_u below the free-spin value and for the other unexplained features of the *g* tensor. The 3*s* spin density of 3% on the S is omitted from the normalization because it is likely due to spin polarization of the σ bonds and is hence counterbalanced by an equal and opposite spin density of these bonds.

Table 1. ^{33}S couplings and S spin densities of the monosulfide radical R1

Radical R1	^{33}S coupling (MHz)		S spin density*
RCH_2S^-H	$A_u = 199 \pm 3$		
		$A_f = 90$	$\rho_{3s} = 0.03$
or	$A_v = 38 \pm 3$		
		$B = 55$	$\rho_{3p} = 0.70$
RCH_2SH_2	$A_w = 32 \pm 6$		

* A 3*d* spin density of 0.20 is also predicted (see *text*).

The principal *g* values may be predicted from the second-order formula

$$g_j = g_f - 2\lambda \sum_n \frac{|\langle \phi_n | L_j | \phi_0 \rangle|^2}{E_n - E_0}, \qquad [6]$$

where ϕ_n includes all orbitals which are not orthogonal to $\phi_0' = L_j|\phi_0\rangle$, i.e., for which $\langle \phi_n | \phi_0' \rangle \neq 0$. Thus, in this problem ϕ_n must include the 3*d* orbitals on the S.

The ground molecular orbital of the unpaired electron may be expressed as

$$\phi_0 = \rho_S^{1/2}(\psi_S^0 + \sum_i a_i \psi_i), \qquad [7]$$

where ρ_S is the unpaired electron density on the S and $\Sigma a_i^2 = 1 - \rho_S$ is that on the other atoms. Because the interactions on the other atoms *i* do not contribute significantly to the anisotropy in *g*, they can be neglected in the evaluation of the last term of Eq. **6**. As an approximation based on the observed spin density and S model described above, we express

$$\psi_S^0 = (4/5)^{1/2}(3p_x) + (1/5)^{1/2}(3d_{xy}). \qquad [8]$$

Contributions of the 3*p* and 3*d* components of the hybrid can be calculated separately. Because $L_x|3p_x\rangle = 0$ and $L_x|3d_{xy}\rangle = i(3d_{xz})$, with ψ_i neglected, we can set

$$L_x|\phi_0\rangle = \rho_S^{1/2}(L_x|\psi_S^0\rangle = i\rho_S^{1/2}(1/5)^{1/2}(3d_{xz}). \qquad [9]$$

and from Eq. **6** can obtain

$$g_u = g_x = g_f - \frac{2\lambda_d \rho_S}{5} \sum_n \frac{|(\phi_n|3d_{xz})|^2}{E_n - E_1}$$

$$= g_f - \frac{2\lambda_d \rho_S}{5} \left(\frac{1}{E_d - E_0}\right). \quad [10]$$

The last form follows from the normalization $(d_{xz}|d_{xz}) = 1$ and from the orthogonality of all other combinations. Because the d shell is less than half-filled, the d spin-orbit coupling λ_d is here positive in sign. Thus, the contribution of the d character reduces g_u below the free-spin value of 2.0023, in agreement with observation. We do not know the specific value of the spin-orbit coupling constant for the $3d$ orbital of S nor $E_d - E_0$. However, with Eq. **10** we can evaluate experimentally the ratio $\lambda_d/(E_d - E_0)$ from

$$g_u - g_f = -2\lambda_d \rho_S/[5(E_d - E_0)] = -0.0123 \quad [11]$$

Although the bonding orbitals may have some s hybridization and perhaps also some d character, we suggest as a simplifying approximation that the other occupied orbitals of the S are:

$$\phi_1 = (1/2)^{1/2}[(1/2)^{1/2}(3p_y) + (1/10)^{1/2}(3p_y) + (2/5)^{1/2}(3d_{xy}) + \psi_{H_1}]. \quad [12]$$

$$\phi_2 = (1/2)^{1/2}[-(1/2)^{1/2}(3p_y) - (1/10)^{1/2}(3p_y) + (2/5)^{1/2}(3d_{xy}) + \psi_{H_2}]. \quad [13]$$

$$\phi_3 = (1/2)^{1/2}[(3p_z) + \psi_C]. \quad [14]$$

$$\phi_4 = (3s). \quad [15]$$

All these orbitals are assumed to have electron pairs. Orbitals ϕ_1 and ϕ_2 would bond the two H atoms of structure (II) or (III) while ϕ_3 would form the σ bond to the C and ϕ_4 would have an unshared pair.

Eq. **6** with the orbitals of Eqs. **7**, and **12–15** gives:

$$g_v = g_y = g_f - \left(\frac{8}{5}\right)\left(\frac{\lambda_p \rho_S}{E_3 - E_0}\right) - \left(\frac{2}{5}\right)\left(\frac{\lambda_d \rho_S}{E_d - E_0}\right). \quad [16]$$

$$g_w = g_z = g_f - \left(\frac{4}{5}\right)\left(\frac{\lambda_p \rho_S}{E_1 - E_0}\right) - \left(\frac{4}{5}\right)\frac{\lambda_p \rho_S}{E_2 - E_0} - \left(\frac{2}{5}\right)\left(\frac{\lambda_d \rho_S}{E_d - E_0}\right). \quad [17]$$

when it is assumed that, on the average, one electron of each bonding pair is on the S. With the term in λ_d given by Eq. **11**, with $\rho_S = \rho_{3p} + \rho_{3d} = 0.70 + 0.20$, $g_f = 2.0023$, $E_1 = E_2$, and $\lambda_p = -382$ cm^{-1}, these expressions reduce to:

$$g_v = 1.990 + 550/(E_3 - E_0), \quad [18]$$

$$g_u = 1.990 + 550/(E_1 - E_0). \quad [19]$$

With the measured values $g_v = 2.006$, $g_w = 2.214$, these equations give $E_3 - E_0 = 34{,}000$ cm^{-1} and $E_1 - E_0 = 2400$ cm^{-1} $= E_2 - E_0$. In addition to the other approximations, it is assumed that the spin density of 0.10 on the CH_2 group contributes nothing to the g anisotropy. Despite the small energy difference between E_1 or E_2, and E_0, the Boltzmann factor $\exp(-\Delta E/kT)$ is 0.00034 at 300 K, and the calculated spin density in orbital ϕ_1 or ϕ_2 is only 0.0003, not enough to give an observable SH proton splitting, nor a measurable deviation in the axial symmetry of the ^{33}S coupling.

In structure (I), the negative charge is on the S, and there are two electrons in the S orbital forming the S– – –H——O bridge.

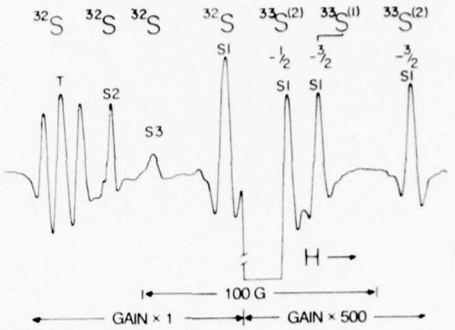

FIG. 3. ESR spectrum of stable disulfide radicals observed at room temperature. In the left-hand part of the spectrum are shown the ^{32}S patterns observed with low amplification. The crystal is oriented with the magnetic field in the direction of the minimum g-value for the S1 radical. A portion of the ^{33}S spectrum for S1 is shown at high gain in the right-hand portion of the spectrum. The spectrum reveals unequal coupling to two sulfur atoms, $S^{(1)}$ and $S^{(2)}$, within the radical.

If the same orbitals are assumed with ϕ_1 forming the SH bond and ϕ_2 having an unshared pair, and if the approximation $E_1 \approx E_2$ is made, then a similar calculation gives g_t the same as before but $g_w = 1.990 + 820/(E_1 - E_0)$. The observed g_u then indicates that $E_1 - E_0 = 3600$ cm^{-1}.

To eliminate unknown parameters in these solutions, we were forced to make rather severe simplifying assumptions. Whatever the nature of hybridization of the orbitals, $E_1 - E_0$ and $E_2 - E_0$ must be small and $E_3 - E_0$ must be large to account for the observed g_t and g_w values. Similar conditions are required for the model proposed by Akasaka (1), who assumed $E_{px} \approx E_{py} \ll E_{pz}$.

In the earlier work (6), we found that the isotropic CH_2 proton coupling A in the neutral RCH_2S and RCH_2SS radicals could be calculated with the relation

$$A = A_0 \rho_S \cos^2 \phi \quad [20]$$

with $A_0 = 31.5$ G. If one assumes the same HCH angle, 125°, for the present radical as for RCH_2S and a $\rho_S = 0.90$, the combined $3p$ and $3d$ density, Eq. **20**, requires a somewhat higher value, $A_0 = 36.6$ G, to account for the observed proton couplings of 22.1 G and 29.4 G. Perhaps this signifies a more effective hyperconjugation by the p-d hybrid orbital, but this conclusion

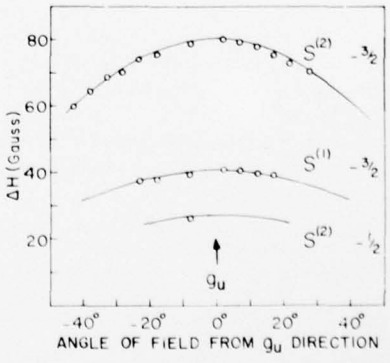

FIG. 4. Plot of the ^{33}S hyperfine splitting versus angle of the external field from the direction of the minimum principal g value for the disulfide radical S1. Circles represent measured splittings from the ^{32}S resonance; the curves are computer fits to the $-\frac{3}{2}$ components for each of the two sulfur sites. The splitting is axially symmetric about the g_u direction.

Table 2. ^{33}S couplings and S spin densities of the disulfide radical S1

Radical S1		^{33}S coupling (MHz)		S spin density	
		A_f	B	$3s$	$3p$
$RCH_2S^{(1)}S^{(2)}$	$S^{(1)}$	29.7	23.0	0.011	0.29
	$S^{(2)}$	59.6	44.8	0.022	0.57

is uncertain. Whatever the cause, the CH_2 couplings are significantly larger for the current radical than for the RCH_2S and RCH_2SS radicals.

THE DISULFIDE RADICALS

Fig. 3 shows the ESR spectrum for one orientation of an acetyl cysteine crystal which has been aged for 1 month after irradiation. In the low-gain region there are four distinct signals of sulfur-centered radicals of the normal isotopic species: a triplet indicated by T1 and three singlets indicated by S1, S2, and S3. The principal g values for T1 are 2.003, 2.024, 2.053; for S1, 2.002, 2.025, 2.064; for S2, 2.002, 2.025, 2.054; for S3, 2.003, 2.026, 2.054. They fall into the two sets of g values earlier observed for disulfide radicals (6–9), differing significantly only in the maximum value which is either close to 2.054 or to 2.064. For this reason, all four signals are presumed to arise from disulfide radicals although this structure could be verified by ^{33}S hyperfine structure only for the S1 signal.

The crystal orientation for Fig. 3 is such that the applied magnetic field is along the direction of g_u, the minimum g value for the S1 signal. The signals to the right, observed under high gain, are ^{33}S hyperfine components corresponding to the S1 species. We were able to observe these ^{33}S components over a sufficient range of crystal orientations (see Fig. 4) to obtain the principal values of the coupling as given in Table 2. The two different coupling values for ^{33}S prove the disulfide structure of the radicals as explained in the first paper of this series (6). The spin densities on the two sulfurs obtained from the coupling values are also listed in Table 2.

This research was supported in part by the Army Research Office through Grant no. DAAG29-77-G-0007 to Duke University.

1. Akasaka, K. (1965) *J. Chem. Phys.* **43,** 1182–1184.
2. Box, H. C., Freund, H. G. & Budzinski, E. E. (1966) *J. Chem. Phys.* **45,** 809–811.
3. Ayyar, R. R. & Srinivasan, R. (1965) *Curr. Sci.* **34,** 449–450.
4. Kayushin, L. P., Krivenko, V. G. & Pulatova, M. K. (1972) *Stud. Biophys.* **33,** no. 1, 59–66.
5. Saxebøl, G. & Herskedal, O. (1975) *Radiat. Res.* **62,** 395–405.
6. Hadley, J. H., Jr. & Gordy, W. (1974) *Proc. Natl. Acad. Sci. USA* **71,** 3106–3110.
7. Hadley, J. H., Jr. & Gordy, W. (1974) *Proc. Natl. Acad. Sci. USA* **71,** 4409–4412.
8. Hadley, J. H., Jr. & Gordy, W. (1975) *Proc. Natl. Acad. Sci. USA* **72,** 3486–3490.
9. Hadley, J. H., Jr. (1976) *Bull. Am. Phys. Soc.* **21,** 382.

Proc. Natl. Acad. Sci. USA
Vol. 77, No. 1, pp. 343–346, January 1980
Biophysics

Electron spin resonance of ^{17}O-labeled protein–peroxide radicals: Zein and edestin

(oxygenated free radicals/electron spin resonance spectra/^{17}O hyperfine structure)

LOUIS J. DIMMEY* AND WALTER GORDY

Department of Physics, Duke University, Durham, North Carolina 27706

Contributed by Walter Gordy, October 22, 1979

ABSTRACT **Hyperfine structure due to ^{17}O has been measured in irradiated zein and edestin after exposure to gaseous oxygen with ^{17}O concentrated to 24%. The observations prove that the free radicals produced by ionizing irradiation under vacuum at 300 K are converted by the oxygen to protein–peroxide free radicals $X—O^{(1)}—O^{(2)}$, with the unpaired electron density in a π-type orbital predominantly on the peroxide group. From the observed couplings, the $2p_\pi$ spin densities on zein–peroxide are found to be 0.29 and 0.45 for $O^{(1)}$ and $O^{(2)}$, respectively; those on edestin–peroxide are 0.26 and 0.48 for $O^{(1)}$ and $O^{(2)}$, respectively.**

In the first observations of electron spin resonance (ESR) signals in irradiated proteins (1), a proton hyperfine doublet produced from bone collagen was found to be converted to a singlet when the specimen irradiated in vacuum was exposed to oxygen. It was postulated that that O_2 combined with the free radicals in the irradiated sample to produce a protein–peroxide free radical. Since this initial finding, many examples of this oxygen effect have been observed for other proteins (2) as well as for biochemicals of other types (3). In certain proteins such as zein and edestin, chosen for the present ^{17}O study, the conversion of the proton multiplet to the oxygen singlet is rapid, with complete conversion to the singlet occurring within minutes after exposure of the sample to atmospheric oxygen. In others, most notably silk, the oxygen effect is slow, requiring days of exposure for partial conversion. This slower conversion is believed to result from steric factors that hinder or prevent the molecules of oxygen from reaching the free-radical centers in fibrous proteins such as silk. The oxygen effect is not observed for sulfur-centered radicals produced by irradiation of proteins, probably because molecular oxygen does not combine with the sulfide free radicals.

The earlier studies of the oxygen effect in irradiated proteins were made with ^{16}O, which has no hyperfine structure. Although there seems to be little doubt that the radicals formed upon admission of oxygen are peroxide radicals, the present study of ^{17}O-labeled radicals unquestionably confirms this interpretation and, in addition, provides new information about the electronic structure of the protein–peroxide radicals.

In many irradiated proteins, including edestin and zein, the free-radical site giving the ESR pattern in the absence of oxygen is believed to be the C_α—R group in structure **I**

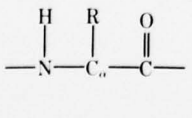

I

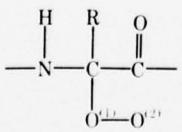

II

formed by loss of a H from a carbon of the polypeptide chain. For edestin under vacuum, a proton doublet like that for the $C_\alpha H$ fragment in irradiated polyglycine is formed (2), which indicates that R = H and that the radical is formed in the glycine unit. A similar doublet is observed for evacuated zein, but with a superimposed quartet like that for polyalanine (2). This indicates formation of radical sites in both glycine and alanine ($R = CH_3$) units of zein. Relative intensities of the superimposed patterns indicate that formation in the alanine unit is somewhat less than that in the glycine unit. Both patterns are converted to singlets when normal oxygen ($^{16}O_2$) is admitted to the irradiated sample.

Upon exposure of the irradiated samples to oxygen, peroxide radical **II** is evidently formed. When this occurs, as the present study confirms, the spin density of **I** is effectively transferred to the captured O_2, where its interaction with the protons of the R group is insufficient to produce a resolvable proton splitting. Although ^{16}O has no hyperfine structure, the substituted ^{17}O has nuclear spin $I = 5/2$, which gives rise to a sextet ESR splitting by each of the inequivalent oxygens in peroxide radical **II**.

Previously, ^{17}O hyperfine structure has been observed for randomly oriented peroxide radicals of irradiated polytetrafluoroethylene (4) and for oriented peroxide radicals $C_{10}H_{11}OO$ in single crystals (5). Also, the isotropic component of the ^{17}O hyperfine structure has been observed for some simpler peroxide free radicals in liquid solutions (6, 7). These earlier observations have been helpful to us in our analysis of the ^{17}O hyperfine structure for the protein–peroxide radicals.

EXPERIMENTAL PROCEDURES

A balanced-bridge, X-band ESR spectrometer operated at a frequency of 9000 MHz was used for these measurements. Evacuated tubes made of Spectrosil quartz held the protein powders, which were placed in a ^{60}Co γ-ray source for irradiation at 300 K. Doses were approximately 3×10^5 rads (300 grays). Afterward, the tubes were annealed in a gas/oxygen flame to eliminate any free radicals formed in the quartz.

Exposure of the irradiated samples to normal gaseous oxygen or to ^{17}O concentrated gas was accomplished in this way. The tube was connected to a flask of the oxygen gas, the glassware between them was evacuated, and the flask was immersed in liquid nitrogen. When the valve on the flask was opened, the oxygen at its vapor pressure at 77 K (about 130 torr) flowed into the sample tube. After the sample was disconnected from the flask, it was ready for observation in the spectrometer. Conversion of the radicals formed under vacuum to peroxides required 2–4 hr. The enriched oxygen gas contained 24% ^{17}O atoms.

Abbreviation: ESR, electron spin resonance.

* Present address: School of Engineering, Duke University, Durham, NC 27706.

OBSERVED SPECTRA

Fig. 1 shows a comparison of the second-derivative spectra of irradiated zein after exposure to normal oxygen gas and after similar exposure to gas with 24% substitution of ^{17}O atoms for ^{16}O atoms. The spectrometer amplification for the two curves was approximately the same. The stick diagrams at the base correspond to the theoretically expected ^{17}O hyperfine patterns of the two forms, X—^{16}O—^{17}O and X—^{17}O—^{16}O. Hyperfine components for the less-probable species, X—^{17}O—^{17}O, proved to be too weak for detection. The pattern with the wider span is that for X—^{16}O—^{17}O. Fig. 2 shows the curve obtained for irradiated edestin after exposure to the ^{17}O-substituted gas.

The nature of the ESR signals and of the free radicals formed upon irradiation in the absence of oxygen are described in the Introduction. For both proteins, the primary radicals are believed to have the general structure **I** and the peroxide radicals (secondary) to have structure **II**. The hyperfine structure and g values for these protein–peroxide radicals are explained in the following paragraphs.

HYPERFINE STRUCTURE

The analysis of ESR hyperfine structure for randomly oriented free radicals is now well known (ref. 8, pp. 353–441). The shapes of the observed absorption curves depend on several factors, the most important of which are the anisotropy in the **g** tensor and in the nuclear coupling tensors. In the protein–peroxide

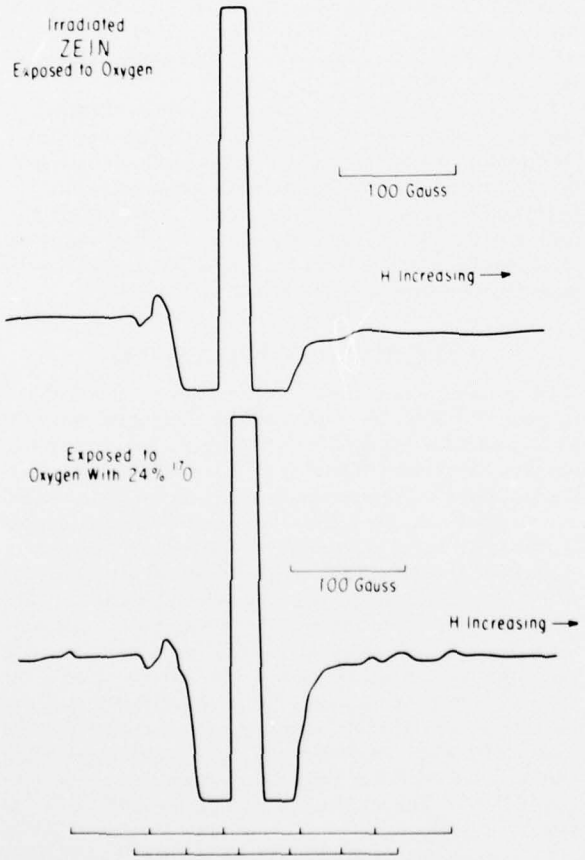

FIG. 1. Second-derivative ESR spectrum of γ-irradiated zein after exposure to gaseous $^{16}O_2$ (*Upper*) and after exposure to oxygen gas enriched with 24% ^{17}O (*Lower*).

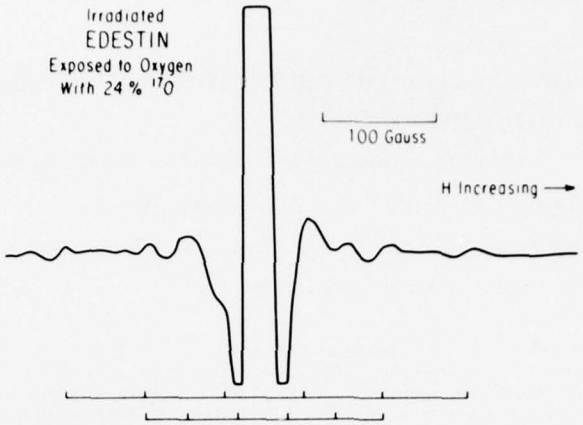

FIG. 2. Second-derivative ESR spectrum of γ-irradiated edestin after exposure to oxygen gas enriched with 24% ^{17}O.

radicals considered here, the isotropic component A_f of the ^{17}O coupling is of comparable magnitude to the anisotropic coupling B and is of like sign. Consequently, the resultant coupling $(A_f - B)$ for the magnetic field of orientations perpendicular to the p_π orbital of the unpaired electron is very small. As a result, the critical absorptions corresponding to the perpendicular-field orientation are not resolvable and are not separable from the strong ^{16}O singlet absorption. To obtain a value for B, one must observe the much weaker critical absorptions corresponding to orientation of the field approximately parallel to the coupling p_π orbital of the ^{17}O atoms.

The nature of the ^{17}O hyperfine spectra is illustrated by the idealized curves of Fig. 3, in which line-broadening factors are neglected except those of the anisotropy in the nuclear coupling and in **g**. Also, for simplification of the diagram, **g** as well as **A** is assumed to be axially symmetric about the directions of the coupling p_π orbital. The weak peaks in the observed derivative curves (Figs. 1 and 2) correspond to the outer terminations of the different ^{17}O component absorptions. If the coupling constant is expressed in magnetic-field units, these outer peaks occur at the critical field values,

$$H_\parallel = h\nu_0/(g_\parallel\beta) + A_\parallel M_I, \qquad [1]$$

where ν_0 is the operating frequency and $g_\parallel = g_u$ is the effective g value for **H** along the coupling p_π orbital, and

$$A_\parallel = A_f + 2B, \qquad [2]$$

where $A_\parallel$ is the effective coupling constant for **H** along the coupling p_π orbital. The much stronger unresolvable inside-component terminations occur at

$$H_\perp = h\nu_0/(g_\perp\beta) + A_\perp M_I, \qquad [3]$$

where $g_\perp$ is the effective g value for **H** imposed in the plane perpendicular to the p_π orbital, and

$$A_\perp = A_f - B. \qquad [4]$$

Although $g_\parallel$ has a fixed value, $g_\perp$ ranges in value from g_e to g_{uu}. However, for simplicity in Fig. 3, g_e was chosen as the particular value for $g_\perp$. The quantum numbers are $M_I = \pm 5/2$, $\pm 3/2$, $\pm 1/2$, corresponding to the spin $I = 5/2$ for ^{17}O. The coupling constants have the same sign and are both negative because the nuclear magnetic moment of ^{17}O is negative.

The fact that the $H_\perp$ components cannot be resolved or separated from the unsubstituted ^{16}O absorption indicates that $A_f \approx B$. With $A_f = B$, the observed component separation of

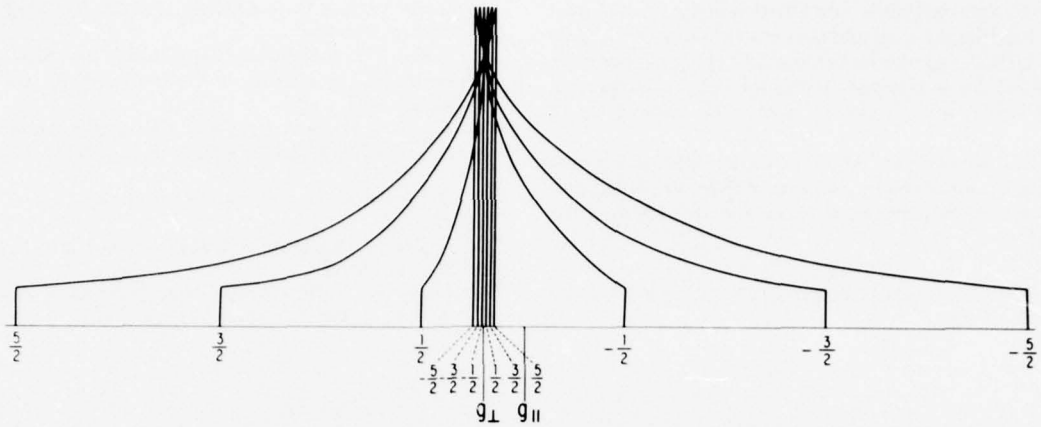

FIG. 3. Idealized theoretical pattern of ESR hyperfine structure for a coupling ^{17}O of randomly oriented peroxide radicals having axial symmetry in coupling with $A_\perp = A_f - B = 2.5$ G and with $A_\parallel = -71$ G, as for $^{17}O^{(2)}$ of edestin peroxide. For simplicity, the **g** tensor is also assumed to have axial symmetry about the coupling $2p$ orbital with $g_\parallel = g_u$ and $g_\perp = g_v$ for edestin. Line-broadening factors other than anisotropies in **g** and **A** are neglected.

71 G for $^{17}O^{(2)}$ in edestin-peroxide gives with Eq. **2** the value $A_f = B = 23.7$ G for the terminal oxygen; and the observed component separation of 42 G for $^{17}O^{(1)}$ gives $A_f = B = 14$ G for the central oxygen. However, we believe that more accurate values for B are obtained with the assumption that $A_f(^{17}O^{(1)}) = 16$ G and $A_f(^{17}O^{(2)}) = 22$ G, as measured for the radicals $(CH_3)_2COO$ and $C_6H_5(CH_3)_2COO$ in liquid solution (7). These values are close to the isotropic coupling observed in diverse peroxide radicals (5–7) in which the O_2 is bonded to a carbon. With these values assumed for A_f in both zein and edestin, the anisotropic coupling constants calculated with Eq. **2** are as listed in Table 1. The couplings $A_\parallel$ in MHz are related to the component separations in gauss by

$$A_\parallel(\text{MHz}) = 1.40 g_\parallel \Delta H(\text{G}). \qquad [5]$$

PRINCIPAL g VALUES

The principal g values of these protein–peroxide radicals cannot be accurately derived from the randomly oriented radicals, but approximated values have been deduced by the following procedure. The weak peak to the left of the strong central absorption in the unsubstituted ^{16}O peroxides, shown for zein in Fig. 1 *Upper*, evidently corresponds to the maximum g value, g_w. The value determined by this peak is $g_w = 2.044$ for the zein peroxide. The value similarly obtained for the edestin is 2.040. These values are in the range of those derived for the peroxide radical in single-crystal measurements (ref. 8, p. 602). For example, in the $C_{10}H_{11}OO$ radical, $g_w = 2.045$ and 2.039 for the two crystal sites (5). The g_u values are expected from theory to be directed approximately along the O—O bond axis. Peaks corresponding to the intermediate and minimum g values, g_v and g_u, respectively, cannot be separated for the unsubstituted ^{16}O radicals; both of them are evidently within the strong central absorption with the center corresponding to 2.007 for zein and to 2.006 for edestin. However, the minimum value g_u is expected from theory to have the direction of the p_π orbital, that for which the ^{17}O hyperfine components are measured. Thus, if slight second-order shifts are neglected, the g_u value corresponds to the center of the $A_\parallel M_I$ hyperfine pattern like that shown in Fig. 3. We have assumed that the intermediate values g_v correspond to those for the strong central absorption for the unsubstituted ^{16}O radicals. The unresolved $A_\perp M_I$ pattern is depicted as a closely spaced multiplet centered near g_v in Fig. 3. This multiplet evidently falls under the strong central $^{16}O_2$ absorption. For orientations of the magnetic field along or near g_w, the ^{17}O components are too weak for observation. The approximate g values derived by these procedures and assumptions are listed in Table 2. They are close to the values 2.0026, 2.0065, and 2.038 derived by Che and Tench (4) for the chain radicals —CF_2—CF(OO)—CF_2— at 77 K.

Table 1. ^{17}O coupling constants for protein peroxides, X—$O^{(1)}$—$O^{(2)}$

Parent protein	Coupling atom	Component separations $\Delta H_\parallel$(G)	Effective couplings,* MHz A_f‡	B	Spin densities† ρ_{2s}	ρ_{2p}
Zein	$^{17}O^{(1)}$	46 ± 2	(−)45	(−)42	0.010	0.29
	$^{17}O^{(2)}$	68 ± 2	(−)62	(−)65	0.013	0.45
Edestin	$^{17}O^{(1)}$	42 ± 2	(−)45	(−)37	0.010	0.26
	$^{17}O^{(2)}$	71 ± 2	(−)62	(−)69	0.013	0.48

* Signs are not measured but are theoretically negative.
† Calculated with atomic coupling values $A_{2s} = -4628$ MHz and $B_{2p} = -144$ MHz (ref. 8, pp. 337, 338).
‡ Values assumed from measurements of liquids (see text).

CONCLUSIONS

The combined spin densities on $O^{(1)}$ and $O^{(2)}$ derived for edestin and for zein, 0.74, are not unity, as would be expected for an unpaired electron entirely in a π orbital on the two oxygens for which orbital-overlap distortions are neglected. This discrepancy might be interpreted to indicate some spreading of the π orbital of the unpaired electron to the carbon or to another atom of the protein. Also, some reduction in the effective B values and derived p_π spin densities is expected to result from rather large torsional oscillations of the peroxide group about the C—O bond. Such oscillations would reduce the observed maximum coupling below that expected for a static, parallel alignment of the p orbital as was assumed in the derivations. If the entire reduction is attributed to these oscillations and the $2p_\pi$ spin

Table 2. Approximate g values of protein–peroxide radicals

Parent protein	g_u	g_v	g_w
Zein	2.001	2.007	2.044
Edestin	2.002	2.006	2.040

density on the two oxygens is normalized to unity, the indicated $2p_\pi$ spin densities are 0.39 and 0.61 for $O^{(1)}$ and $O^{(2)}$ of zein peroxide and 0.35 and 0.65 for $O^{(1)}$ and $O^{(2)}$ of edestin peroxide. The small 2*s* spin densities are attributed entirely to spin-polarization effects and do not influence the calculations of ρ_{2p}.

These measurements of ^{17}O hyperfine structure verify that the ESR signals produced by exposure of these irradiated proteins to molecular oxygen are due to peroxide radicals, as earlier postulated.

This work was supported by Grant DAAG 29-77-G-0007 from the Army Research Office.

1. Gordy, W., Ard, W. B. & Shields, H. (1955) *Proc. Natl. Acad. Sci. USA* **41**, 983–996.
2. Patten, R. A. & Gordy, W. (1964) *Radiat. Res.* **22**, 29–44.
3. Rexroad, H. N. & Gordy, W. (1959) *Proc. Natl. Acad. Sci. USA* **45**, 256–269.
4. Che, M. & Tench, A. J. (1976) *J. Chem. Phys.* **64**, 2370–2374.
5. Melamud, E., Schlick, S. & Silver, B. L. (1974) *J. Magn. Reson.* **14**, 104–111.
6. Fessenden, R. W. & Schuler, R. H. (1966) *J. Chem. Phys.* **44**, 434–437.
7. Adamic, K., Ingold, K. U. & Morton, J. R. (1970) *J. Am. Chem. Soc.* **92**, 922–923.
8. Gordy, W. (1979) *Theory and Applications of Electron Spin Resonance* (Wiley-Interscience, New York).

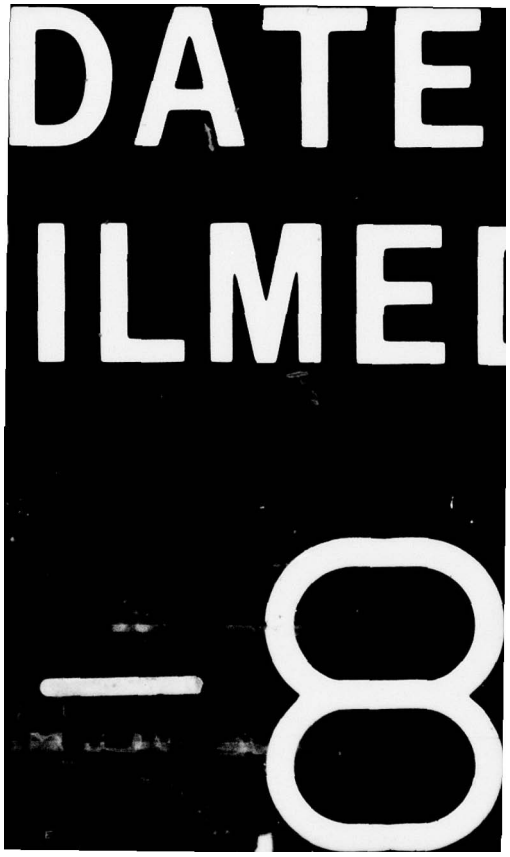
DATE
ILME
8